The Containment Trap:

How Efforts to Contain Epidemics Intensify Civil Conflict*

Mitsuru Mukaigawara†

May 18, 2026

Click Here for the Latest Draft

Abstract

Despite their strong implications for strategic interactions between states and non-state actors, epidemics remain underinvestigated as catalysts of civil conflict. This paper explains how, why, and when epidemics intensify civil conflict. I argue that *frontier plagues*, defined as severe epidemics in low-capacity regions, intensify civilian coercion in outbreak epicenters. During frontier plagues, states send healthcare professionals and deploy security forces to epicenters for protection. Insurgents respond by reallocating combatants to these areas to defend territorial control, but they shift from battles against the state toward coercive violence against civilians as direct confrontation becomes costly. Frontier plagues thus generate a *containment trap*: efforts to control epidemics intensify civil conflict. I test this argument using microlevel data on 44,331 Ebola patients in the Democratic Republic of the Congo and 922 epidemics across sub-Saharan Africa. Using a spatiotemporal causal inference design, I show that frontier plagues significantly increase civilian targeting in outbreak epicenters.

Keywords: Civil war; civil conflict; state capacity; epidemic; infectious disease; spatiotemporal causal inference; heterogeneous treatment effect; microlevel data

*I am grateful to Marcella Alsan, Dara Cohen, Kosuke Imai, and Joshua Kertzer for encouragement, support, and feedback. I thank Peter Buisseret, Melani Cammett, Stephen Chaudoin, Christina Davis, Jeff Frieden, Jeff Friedman, Scott Gates, Peter Hall, Iain Johnston, Gary King, Gabriella Levy, Jason Lyall, Christoph Mikulaschek, Megumi Naoi, Rich Nielsen, Lotem Bassan-Nygate, Yuri Zhukov, member of the Imai Research Group and Kertzer Research Group, an anonymous reviewer for IQSS rapidPeer, and participants at seminars at Harvard, IHME, ISA, JSQPS, MIT, Peace Science Society, PolMeth, and Suntory Foundation for their helpful comments on earlier versions of this manuscript/project. In addition, I thank the Weatherhead Center for International Affairs, Suntory Foundation (#2023-315), and Toyota Foundation (D24-HS-0049) for their partial financial support. This research was reviewed and approved by the Harvard University Institutional Review Board in accordance with regulations governing human subjects research (IRB 23-0440). I affirm that this article adheres to the principles concerning research with human participants laid out in American Political Science Association's Principles and Guidance on Human Subject Research. All errors are my own.

†Ph.D. Candidate, Department of Government, Harvard University, 1737 Cambridge Street, Cambridge MA, 02138. Email: mitsuru_mukaigawara@g.harvard.edu, Website: MitsuruMukaigawara.com. First Draft: June 11, 2025.

1 Introduction

Epidemics and civil conflict frequently co-occur. From Ebola in Central Africa to cholera in Yemen, epidemics concentrate in territories experiencing active civil conflict (Ghobarah, Huth and Russett, 2003; Price-Smith, 2008; Michaud et al., 2019). This co-occurrence is of direct policy importance: to contain epidemics, states and international organizations often deploy healthcare professionals and humanitarian agencies into active conflict zones (Mackenzie et al., 2014). Understanding when and why epidemics reshape conflict dynamics—and how containment efforts interact with ongoing conflict—is essential for the protection of civilian populations.

Political scientists have extensively studied how exogenous shocks reshape civil conflict (e.g., Bazzi and Blattman, 2014; Koubi, 2019; Powell, 2006; Nielsen et al., 2011). Yet epidemics have received surprisingly little theoretical attention, even though they necessitate the very strategic interactions between state and non-state actors that are at the center of civil conflict research (Fearon, 1995; Kalyvas, 2006; Blattman and Miguel, 2010). Infectious disease often demands state-led containment that insurgents can neither provide nor ignore, and international monitoring by humanitarian agencies and international organizations creates strong pressure for state intervention (Fazal, 2020; Ge, forthcoming). Epidemics are thus among the most consequential yet least studied shocks that reshape strategic interactions between states and insurgents during civil conflict: they confront states with a choice over how aggressively to project its capacity into contested territory, and insurgents with a choice over whether to accommodate or exploit that projection.

In this article, I offer an overarching framework to explain how epidemics intensify civil conflict. I argue that the consequences of epidemics depend on the interaction between disease characteristics and political geography. I define *frontier plagues* as severe epidemics in areas of weak state capacity. Because of their severity, frontier plagues generate domestic and international scrutiny, which prompts states to deploy healthcare professionals and security forces for their protection to outbreak epicenters. Since containment requires specialized training and equipment that insurgents do not possess, these interventions appear to insurgents as a hearts-and-minds strategy they cannot substitute for (Berman, Shapiro and Felter, 2011). Insurgents thus counter by concentrating forces in outbreak epicenters to resist state encroachment (e.g., Sexton, 2016; Lyall, 2019). Yet as state capacity rises in the epicenter, direct engagement with state forces becomes more costly. Insurgents therefore shift from direct battles against the state toward coercive violence against civilians, which deters civilian cooperation with state forces and containment efforts. This adaptive pattern emerges only under frontier plagues because the combination of high severity and frontier geography produces localized shifts in relative power. Frontier plagues thus generate a *containment trap*: efforts to control severe epidemics intensify conflict and endanger civilians.

To test my theory, I construct two datasets that provide an unprecedentedly detailed insight into epidemics and civil conflict in sub-Saharan Africa, the region with the world's highest infectious disease mortality (GBD 2021 Causes of Death Collaborators, 2024) and the majority of international emergency deployments (Mackenzie et al., 2014). The first is a microlevel, spatiotemporal dataset of 922 epidemics from 2011 to 2020, compiled from the most comprehensive academic, official, and public sources (e.g., Pigott et al., 2014; Cuomo-Dannenburg et al., 2024; Moore et al., 2017). The second is a patient-level dataset of all 44,331 cases from the 2018-2020 Ebola epidemic in the Democratic Republic of the Congo (DRC), an operational record known as a "line list" that is rarely used outside public health and contains more than a thousand clinical, geographic, laboratory, and exposure variables per patient (Gregg, 2008). Combined with high-resolution data on political violence (Raleigh et al., 2010), I develop exceptionally granular, microlevel data of epidemics and political violence.

I leverage the variation in severity across cholera epidemics (2011–2020) and the 2018–2020 Ebola epidemic in the DRC to test my theory. The contrast between highly severe Ebola and less severe cholera offers a valuable insight into how diseases with varying degrees of legibility, fatality, and uncertainty affect conflict dynamics. The patient-level data of the Ebola epidemic also offers a unique opportunity to examine the microlevel dynamics with unprecedented granularity. For identification, I exploit exogenous spatial variation in exposure to environmental and animal reservoirs, specifically fruit bat habitats for Ebola (Pigott et al., 2017) and major water bodies for cholera (Bompangue et al., 2008; Taty et al., 2024). These ecological features are time-invariant and predetermined with respect to short-term conflict dynamics. I incorporate them, together with spatiotemporal covariates, to model outbreak and patient locations and estimate propensity scores, which I then use to construct inverse probability weighting (IPW) estimators.

Methodologically, the spatial spillover and temporal carryover effects that epidemics generate pose a challenge. A single Ebola patient in a frontier area might trigger shifts in state capacity that influence conflict dynamics far beyond the outbreak's epicenter. The effects of a new patient might also appear only after the individual becomes infectious and symptomatic. These spatial spillovers and temporal carryovers can occur in countless combinations, and thus any structural assumptions about them are hard to defend. Classical panel data methods, however, require such assumptions to estimate causal effects, for example by adding lagged outcome variables in selected neighboring regions in the model, which can bias the estimates.

For these reasons, I move beyond traditional panel data approaches and employ a spatiotemporal causal inference framework (Mukaigawara et al., 2025; Papadogeorgou et al., 2022). Unlike classical panel approaches that aggregate microlevel variation and impose assumptions about spillovers and carryovers, the spatiotemporal causal inference framework models treatment patterns directly and

uses the distribution of outbreaks and patients as the intervention itself, without imposing any assumptions about spillovers and carryovers. This *map-as-treatment* approach allows me to examine average treatment effects while capturing spillovers and carryovers (Papadogeorgou et al., 2022), explore effect heterogeneity (Zhou et al., 2024), and probe causal mechanisms (Mukaigawara et al., 2025), all with flexible counterfactual designs and intuitive visualizations (Mukaigawara et al., 2023).

Consistent with my theory, I find that high severity and frontier political geography jointly intensify civil conflict. As frontier plagues intensify, battles decline in areas neighboring the outbreak epicenter while violence against civilians increases within the epicenter. Placebo outcome tests using satellite-detected fires (Schroeder et al., 2014) show null effects, and additional tests do not support alternative mechanisms, especially contagion avoidance by insurgents during frontier plagues.

This article makes four contributions to the literature. First, I offer a conceptual framework linking epidemics and civil conflict by bridging political science and medicine. Despite increased scholarly attention following COVID-19, we still lack a systematic account of how disease characteristics interact with political geography to shape conflict dynamics. Political scientists examine how epidemics influence violence through intergroup tensions (Dipoppa, Grossman and Zonszein, 2022; Brancati, Birnir and Idlbi, 2023), repression (Grasse et al., 2021), and aid allocation (Farzanegan and Gholipour, 2023), yet they rarely incorporate the medical properties of disease or their strategic implications and compare across epidemics to derive an overarching framework linking epidemics and civil conflict.[1] Public health scholars generate detailed insights into microlevel disease transmission, institutional response, and community trust (Ilunga Kalenga et al., 2019), but they remain largely agnostic about how political actors strategically adapt to epidemics. I bring these literatures together to develop a typology of epidemics based on disease characteristics and political geography, and from it derive a theory of epidemics and civil conflict.

Second, I contribute to the study of civil war by theorizing shocks as temporary and spatially uneven expansions of state reach. Existing work shows how commodity, climatic, and aid shocks alter state-insurgent interactions (e.g., Bazzi and Blattman, 2014; Dube and Vargas, 2013; Crost, Felter and Johnston, 2014; Koubi, 2019; Nielsen et al., 2011), but treats shocks primarily as changes in resources, grievances, or opportunity structures at national or provincial scales. I identify a different mechanism: shocks can redirect coercive and administrative capacity into specific localities and shift the local balance of power. Frontier plagues demonstrate that localized exogenous shocks can reshape

[1]Scholars tend to focus on one specific disease such as malaria (Bagozzi, 2016; Cervellati et al., 2018; Cervellati, Sunde and Valmori, 2017), zoonoses (Koren and Bukari, 2024; Koren and Weidmann, 2025), HIV/AIDS (Kustra, 2017), the Black Death (Voigtländer and Voth, 2012), Ebola virus disease (Gonzalez-Torres and Esposito, 2016), or COVID-19 (e.g., Brancati, Birnir and Idlbi, 2023; Dipoppa, Grossman and Zonszein, 2022; Grasse et al., 2021; Ide, 2021; Koehnlein and Koren, 2022; Wood et al., 2022; Berman et al., 2022; Bloem and Salemi, 2021; Farzanegan and Gholipour, 2023; Neumayer, Pfaff and Plümper, 2023).

civil war by relocating state power within contested territory.

Third, the theory advances the literature on civilian victimization during civil conflict. Research on civilian targeting shows that armed groups use violence to manage contested control, deter collaboration, and substitute coercion for direct fighting under military pressure (Kalyvas, 2006; Wood, 2014). Work on aid and conflict shows that external assistance can reshape violence when insurgents compete over, disrupt, or seek to capture the political benefits of service delivery (Sexton, 2016; Crost, Felter and Johnston, 2014; Narang, 2015). Frontier plagues identify a different pathway. Epidemic response expands what insurgents might treat as collaboration with the state. Seeking treatment or reporting symptoms can become politically consequential when those acts connect civilians to state-backed responders. The theory of frontier plagues therefore shifts attention from why armed groups punish collaboration to how shocks make ordinary civilian compliance punishable.

Finally, the empirical analyses in this paper provide unusually granular evidence by combining microlevel data with a spatiotemporal causal inference framework. Whereas geospatial data are now common in political science, most studies rely on aggregated panels, and even rare applications of spatial point processes (Harris and Posner, 2019; Monogan, Konisky and Woods, 2017) do not estimate causal effects or account for spillovers and carryovers. This article is among the few (Mukaigawara et al., 2025; Papadogeorgou et al., 2022; Zhou et al., 2024) to employ a *map-as-treatment* design, producing fine-grained estimates of combatant behavior during epidemics. I also introduce an underused data source, patient-level outbreak line lists (Gregg, 2008), and demonstrate how these data can be incorporated into political science to advance the study of conflict.

In Section 2, I develop a typology of epidemics, introduce the concept of frontier plagues, explain why they affect civil conflict dynamics, and present the testable hypotheses. Section 3 describes the empirical context, microlevel data, and descriptive evidence. Section 4 outlines the spatiotemporal causal inference framework. Section 5 presents the empirical findings. I conclude in Section 6.

2 Frontier Plagues

I first introduce a typology of epidemics and then explain why *frontier plagues* intensify civil conflict. Following CDC (2006), I define a disease epidemic as the occurrence of disease exceeding its normal or anticipated level in a specific area and time period. I focus on infectious disease epidemics (hereafter, epidemics), which are caused by pathogenic microorganisms including bacteria, viruses, and parasites. Following Gleditsch et al. (2002), I define civil conflict as "organized armed combat between the government and an internal opposition group, resulting in at least 25 battle-related deaths per year."

2.1 A Typology of Epidemics

Political science and public health scholarship identify two dimensions along which epidemics can be classified. The first is political geography, defined by the degree of state presence (e.g., Herbst, 2014; Boone, 2003), which shapes both outbreak progression and political actor responses. The second is severity, or more specifically *disease burden*, which captures the total impact of disease and is measured by mortality, morbidity, and various other indicators (Murray and Lopez, 2013).[2]

Political geography. Political geography shapes both the progression of outbreaks and the responses of political actors. I focus on the contrast between the *frontier*, which I define as an area of weak state capacity, and the *center*, an area of high state capacity.[3] In the context of epidemics, state capacity comprises coercive and administrative dimensions (e.g., Tilly, 1990; Hendrix, 2010) and an informational dimension (e.g., Lee and Zhang, 2017; Scott, 1998), which correspond respectively to the use of military and police forces, the provision of healthcare services, and disease surveillance.[4]

This definition thus emphasizes the spatial distribution of state capacity rather than topographical constraints alone. Whereas Herbst (2014) explains how physical geography shaped the territorial reach of states through the costs of power projection, I conceptualize the frontier and the center in terms of subnational variation in coercive, administrative, and informational capacities. Political geography therefore reflects spatial variation in state capacity rather than a fixed physical constraint. Uneven capacity shapes political responses to epidemics by shaping the state's deployment of security forces, healthcare, and surveillance.

Disease burden. Disease burden broadens the analysis beyond mortality to include morbidity, economic costs, and political consequences that can shape the microlevel dynamics of political violence.[5] Infectious diseases vary in causative organisms, mortality and transmission rates, incubation periods (the time between initial infection and symptom onset), clinical symptoms, transmission routes, and the availability of vaccines or treatment (see Table 1). Viral hemorrhagic diseases such as Ebola and Marburg virus diseases are highly fatal, legible viral infections that require initial animal-to-human transmission followed by secondary human-to-human transmission. In contrast, cholera is transmitted through contaminated water sources via fecal-oral transmission and generally results in lower mortality rates than viral hemorrhagic diseases.

[2] Commonly used metrics in public health include disability-adjusted life years (DALYs) and quality-adjusted life years (QALYs) (Murray and Lopez, 2013).

[3] I use the term political geography because I focus on *areas* of high and low state capacity.

[4] Whereas fiscal capacity (e.g., Tilly, 1990; Hendrix, 2010) is also an important dimension of state capacity, I focus on coercive, administrative, and informational capacity because they are more salient and undergo the most rapid adjustments during the initial phase of epidemic response.

[5] Political scientists have focused on mortality as the primary indicator of health impact (King and Mukaigawara, 2025). Focusing on disease burden can offer further leverage by capturing the total impact of disease on politics (e.g., Ghobarah, Huth and Russett, 2003; Mukaigawara, Smith and Murray, 2026).

Three clinical features, in particular, determine the political consequences of epidemics: *legibility* of clinical symptoms, *fatality*, and *uncertainty* regarding the trajectory of epidemics. The first two features, legibility and fatality, jointly trigger political attention. Viral hemorrhagic fevers such as Ebola and Marburg cause highly legible symptoms, including internal and external bleeding. Because of high fatality, clusters of patients with bleeding trigger state investigations, World Health Organization (WHO)-mandated reporting of suspected cases, and intensified surveillance by non-governmental organizations (NGOs) and the media. The third feature, uncertainty, is also essential because infected individuals initially show no symptoms (the incubation period), nor are they infectious (the latent period). This delay generates uncertainty about outbreak progression, complicates outbreak investigation, and shapes state capacity allocation and insurgent response.[6]

Whereas disease and disease burden are both multidimensional, we can map diseases onto their typical burden levels because diseases often cluster into stable profiles across those dimensions (Table 1). High-burden diseases exhibit a consistent combination of high legibility, high fatality, and longer incubation, whereas low-burden diseases exhibit the opposite configuration. Viral hemorrhagic diseases such as Ebola, Marburg, and Crimean-Congo hemorrhagic fever constitute high-burden diseases. In contrast, cholera, COVID-19, and seasonal influenza are low-burden diseases.

Physiologically, host-pathogen mismatch explains the stability of disease profiles. Host-pathogen mismatch is the maladaptation that occurs when a pathogen infects a novel host species that are not evolutionarily optimized (Antia et al., 2003). Mismatch between pathogen replication strategies and host immune defenses can produce systemic infection, severe clinical symptoms, and high fatality due to maladaptation of the new host species (Longdon et al., 2014). It also produces atypical infection dynamics, including altered timing of viral load peaks relative to symptom onset, which could delay detectability and complicate outbreak control (Antia et al., 2003; Longdon et al., 2014).

Host-pathogen mismatch offers a mechanism through which epidemics could differentially perturb conflict dynamics. Civil conflict research has shown that geography shapes conflict dynamics by structuring state reach and information flows (Fearon and Laitin, 2003; Kalyvas, 2006), the political status of ethnic groups (Carter, Shaver and Wright, 2019), and armed group mobility (e.g., Buhaug and Rød, 2006). Yet the role of geographically localized shocks in shaping conflict dynamics remains contested.[7] In epidemics, many pathogens to which humans are not evolutionarily adapted are maintained in animal reservoirs. High burden infections often emerge through ecological interfaces where humans and reservoir species interact, where environmental conditions support reservoir habitation,

[6]Epidemics generate greater uncertainty than other localized shocks, such as natural disasters. In their early stages, actors often cannot determine whether a cluster of suspected cases constitutes an epidemic, or whether it will escalate nationally or globally into a pandemic.

[7]See, for example, existing work on climate related shocks and conflict (e.g., Burke, Hsiang and Miguel, 2015).

Table 1: **Characteristics of key infectious diseases**. R_0 is the basic reproduction number (the number of people that one patient can infect). CCHF: Crimean–Congo Hemorrhagic Fever; MERS: Middle East Respiratory Syndrome; SARS: Severe Acute Respiratory Syndrome. *Sources:* Feldmann, Sprecher and Geisbert (2020); Cuomo-Dannenburg et al. (2024); Zumla, Hui and Perlman (2015); Ergönül (2006); Monath (2001); Prentice and Rahalison (2007); Stephens, Greenwood and Brandtzaeg (2007); Gessain, Nakoune and Yazdanpanah (2022); Racaniello (2006); Petersen et al. (2016); Clemens et al. (2017); Wiersinga et al. (2020); Bautista et al. (2010); Uyeki et al. (2022).

Disease	**Pathogen**	**Mortality (%)**	R_0	**Incubation (days)**	**Major Symptoms**	**Transmission**	**Treatment**	**Vaccine**	**Typical Burden**
Ebola Virus Disease	*Ebolavirus* (Filoviridae)	25–90	1.5–2.5	2–21	Fever, hemorrhage, multi-organ failure	Contact (body fluids)	Supportive; antivirals	Yes	High
Marburg Virus Disease	*Marburgvirus* (Filoviridae)	24–88	1.5–2.0	2–21	Fever, hemorrhage, shock	Contact (body fluids)	Supportive	No	High
MERS	*MERS-CoV* (Coronavirus)	30–35	0.5–1.0	2–14	Fever, cough, pneumonia	Droplets; contact	Supportive	No	High
CCHF	*CCHFV* (Nairovirus)	10–40	0.8–1.2	1–9	Fever, hemorrhage, liver failure	Tick bites; contact	Supportive	No	High
Yellow Fever	*Yellow fever virus* (Flavivirus)	20–50	2.0–5.0	3–6	Fever, jaundice, hemorrhage	Mosquito bites	Supportive	Yes	High
Bubonic Plague	*Yersinia pestis* (bacterium)	30–60	1.0–1.3	1–7	Fever, lymphadenitis, sepsis	Flea bites	Antibiotics	No	High
Meningococcal Meningitis	*Neisseria meningitidis* (bacterium)	10–15	1.2–1.5	2–10	Fever, neck stiffness, confusion	Droplets	Antibiotics	Yes	Moderate-High
Mpox	*Monkeypox virus* (Orthopoxvirus)	1–10	1.1–2.4	5–21	Fever, rash, lymphadenopathy	Contact, droplets	Supportive; antivirals	Yes	Low
Poliomyelitis	*Poliovirus* (Picornaviridae)	2–10	5–7	3–35	Fever, paralysis, muscle weakness	Fecal–oral; droplets	Supportive	Yes	Low
Zika Virus Disease	*Zika virus* (Flavivirus)	0.01	1.4–3.0	3–14	Fever, rash, arthralgia	Mosquito bites; sexual	Supportive	No	Low
Cholera	*Vibrio cholerae* (bacterium)	1–50	1.2–2.0	0.5–5	Watery diarrhea, dehydration	Fecal–oral	Rehydration; antibiotics	Yes	Low
COVID-19	*SARS-CoV-2* (Coronavirus)	0.5–1	2.0–3.5	2–14	Fever, cough, fatigue, dyspnea	Droplets	Supportive; antivirals	Yes	Low
H1N1 Influenza	*Influenza A/H1N1* virus	0.1	1.4–1.6	1–4	Fever, cough, myalgia	Droplets	Antivirals; supportive	Yes	Low
Seasonal Influenza	*Influenza A/B* viruses	0.01–0.1	1.2–1.5	1–4	Fever, cough, myalgia	Droplets	Antivirals; supportive	Yes	Low

Table 2: **A typology of epidemics**. Epidemics can be classified along both disease burden and political geography. The combination of a high-burden disease and frontier (frontier plagues, top left in bold) results in intensification and reconfiguration of civil conflicts during epidemics.

		Disease Burden	
		High	Low
Political Geography	Frontier	Frontier plague (e.g., Ebola × Low-capacity)	Silent frontier (e.g., Cholera × Low-capacity)
	Central	Central plague (e.g., Ebola × High-capacity)	Routine epidemic (e.g., Cholera × High-capacity)

and where limited surveillance and early treatment capacity allow infections to progress until they become systemic and severe. These conditions are most common in frontiers. State responses to such epidemics become fragmented because of low baseline capacity, remain poorly targeted and ineffective because of uncertainty, and generate insurgent responses that alter conflict dynamics.[8]

A typology of epidemics. The interaction between political geography and disease burden yields four ideal types of epidemics (Table 2): *frontier plagues* (high-burden epidemics in frontier regions), *central plagues* (high-burden epidemics in central regions), *silent frontier* (low-burden epidemics in frontier regions), and *routine epidemics* (low-burden epidemics in central regions). For example, Ebola outbreaks in frontier regions constitute frontier plagues, whereas outbreaks in central regions constitute central plagues. Similarly, cholera outbreaks in frontier regions constitute either silent frontiers or routine epidemics.

2.2 The Containment Trap: Frontier Plagues and Insurgent Violence

Among the four ideal types of epidemics (see Table 2), frontier plagues create a *containment trap* for states and international actors. The effort to control severe epidemics requires the concentration of aid and security forces in affected areas, yet this very response can provoke insurgent adaptation, intensify civil conflict, and increase civilian targeting. The trap stems from the three features of frontier plagues: their legibility and fatality limit who can credibly carry out containment, while their uncertainty shapes both the targets and effectiveness of containment efforts.

Legibility and fatality determine the agents responsible for medical care and containment. Severe diseases such as Ebola require specialized equipment and expertise that insurgents do not possess, and this capacity is often supplied by external agencies such as the WHO and NGOs. Because these agencies depend on government authorization, aid provision during frontier plagues remains under state

[8]The distinctiveness of outbreak progression in frontier regions has also been documented in public health scholarship on the Amazon frontier. See for example Sawyer (1987) and Caldas de Castro et al. (2006).

control. Insurgents resist these efforts because state-led containment can undermine their legitimacy, reduce civilian support, expose sensitive information about insurgent capacity and infection among combatants, and expand the state's security presence in contested territory. These dynamics are consistent with research on insurgent resistance to government aid in contested areas (e.g., Sexton, 2016), the political effects of government-channeled humanitarian assistance (Sexton, 2016), aid perceived as penetration into insurgent governance (Lyall, 2019), and grievance-inducing state actions (e.g., Huff, 2024; Balcells, 2017; Gurr, 2010; Petersen, 2002; Post, 2005).

Uncertainty about the progression of frontier plagues affects the targeting and effectiveness of containment efforts. High uncertainty and long incubation periods make it difficult for states to target surveillance or care with precision.[9] As a result, states often intervene intensively only after transmission is already widespread and concentrate containment and security deployments in the outbreak epicenter. The surge in state capacity in the outbreak's epicenter produces sharp local shifts in the distribution of power, a key determinant of combatant strategy (Wood, 2014). Insurgents therefore adjust to the surge in state capacity in the outbreak's epicenter.

To illustrate the behavioral implications of frontier plagues, consider a localized, high-burden outbreak such as Ebola in a peripheral territory characterized by limited coercive, administrative, and informational state capacity. Shifts in conflict dynamics occur in three stages: state capacity surge, insurgent adaptation, and strategic restraint and substitution.

Stage 1. State capacity surge. State response to frontier plagues involves two objectives: containing frontier plagues and consolidating territorial control. Domestically, containment signals competence and helps secure civilian support. Internationally, high-burden diseases invite scrutiny by media, humanitarian organizations, and the WHO under the International Health Regulations. Perceived failure imposes reputational costs (Goldfien, Joseph and McManus, 2023) that threaten leaders' political and physical security. To mitigate these risks, the state deploys healthcare personnel, often in collaboration with international agencies, and expands administrative and informational capacity through service provision and disease surveillance. The state also strengthens coercive capacity through the deployment of military or police units to protect healthcare professionals (Michaud et al., 2019). As is often the case with the clinical management of outbreaks, uncertainty about who is infected or exposed, combined with resource constraints, produces an acute and spatially concentrated surge of state capacity in the epicenter.

Stage 2. Insurgent adaptation. Insurgents also seek to contain the epidemic and consolidate territorial control, but they face competing pressures. Accepting state-led containment might improve

[9]While scholars show that aid flows shape uncertainty about commitment (Savun and Tirone, 2011) or capability (Narang, 2015), epidemics generate uncertainty directly by obscuring infection status and transmission chains, which complicates the information environment.

public health but risks exposing their limited administrative capacity and weakening their authority because state-led containment efforts function as a strategy to improve civilian welfare (Galula, 1964; Trinquier, 1964; Berman, Shapiro and Felter, 2011). Such efforts can shift civilian support toward the state and risk information breaches about insurgent capacity. Insurgents also lack the resources needed to contain high burden disease outbreaks. Moreover, concentrated state coercive presence in the outbreak's epicenter increases the risk of territorial control. The rational insurgent response is therefore to reallocate combatants from neighboring areas into the outbreak's epicenter to counter the state's inflow of capacity, which results in *spatial* substitution of violence from neighboring regions in the frontier toward the outbreak's epicenter.[10]

Stage 3. Strategic restraint and substitution. Once in the outbreak's epicenter, intensified state coercive presence makes direct confrontation costly. Insurgents therefore align their tactics with the local balance of power and strategically refrain from battles against state forces. Because insurgents lack the capacity to provide care to civilians or directly confront state forces, they seek to undermine the state by demonstrating its inability to protect the population. Insurgents attack civilians to demonstrate state incapacity to protect them, target healthcare professionals to undermine state-led containment efforts, and use violence to terrorize and coerce civilians to deter engagement with state forces and containment efforts. Another substitution dynamic thus emerges at the *tactical* level, in which insurgents shift from open battles against state forces to violence against civilians. This dynamic parallels theories of selective violence in contested territories (Kalyvas, 2006), coercion under resource scarcity (Weinstein, 2007), and civilian targeting when opportunities for battle diminish (Stanton, 2016).[11]

The consequences of frontier plagues are driven primarily by elite decision-making rather than civilian behavior. Both the surge in state capacity and subsequent insurgent adaptation reflect strategic choices by state and non-state elites. This contrasts with arguments that emphasize civilian misattribution of epidemics to state forces or healthcare workers as a driver of grievances and resistance.[12] More broadly, it differs from much of the existing research on political responses to exoge-

[10] Here I make two assumptions. First, I assume that insurgents project power across the frontier, rather than only within a narrow locality, and can shift this power projection (Boulding, 1962; Buhaug, 2010). The mechanism should still operate, however, when insurgent reach is more limited. Local insurgents near outbreak epicenters face the same increase in state presence, competitive pressure, and risk of losing civilian support. Second, I assume that insurgent presence is associated with the incidence of violence. This assumption is plausible because insurgent violence often requires territorial access, local intelligence, or local networks (Kalyvas, 2006; Zhukov, 2012; Buhaug and Gates, 2002). Even indirect tactics, such as explosive devices, require some prior access to the target area and the ability to operate without immediate detection.

[11] Thus, whereas states might also exploit epidemics for repression (Grasse et al., 2021), in the case of frontier plagues, the main perpetrators are insurgents, since states lack incentives to repress specific groups because of international monitoring and scrutiny.

[12] Additionally, my argument differs from explanations that emphasize civilian reactions to state actions under condi-

nous shocks, which focuses on bottom-up mechanisms driven by civilian beliefs and attribution.[13]

Further, the theory of frontier plagues challenges two prominent claims in political science about how capacity shocks shape civil war. The first holds that adverse economic, climatic, and epidemiological shocks weaken livelihoods, strain state institutions, and expand opportunities for rebellion (e.g., Burke, Hsiang and Miguel, 2015; Koubi, 2019; Price-Smith, 2008). This logic implies state retreat from affected peripheries and insurgent expansion around them. Frontier plagues predict the opposite. When a shock requires non-substitutable state capacity and triggers international scrutiny, the state pushes capacity into the periphery and prompts insurgent adaptation.[14] The second claim is that state inputs in contested territory either strengthen insurgents when they can divert those inputs (Sexton, 2016) or reduce violence by inducing civilians to share intelligence (Berman, Shapiro and Felter, 2011). Both arguments imply a single directional effect near state inputs. Frontier plagues instead reorganize violence across space and tactics as insurgents adapt to the surge in state capacity.

2.3 Disease Burden and Political Geography as Natural Cleavages

The intensification and reconfiguration of violence occur only under frontier plagues because the necessary conditions include a shift in state capacity triggered by uncontainable infectious disease. The remaining three types of epidemics lack these conditions.

Silent frontier. In silent frontiers, low-burden diseases such as cholera require primarily supportive care rather than specialized equipment, which allows both the state and insurgents to provide basic treatment even in frontier regions. The state therefore has limited incentive to surge its capacity into the frontier, and insurgents can instead shift toward service provision, improve civilian welfare, and cultivate local support rather than resorting to violence.[15]

Central plague. Due to the high burden of disease, central plagues can induce a surge in state capacity. However, this surge takes place in the center, not in the frontier. Because state capacity is already concentrated in the center, states can expand their response without reallocation. As a result,

tions of limited state presence. Nathan (2023) argues that where the state is weakly embedded in local society, isolated state interventions can generate outsized political reactions. In Nathan (2023)'s framework, limited state presence amplifies grievances through civilian misinterpretation. By contrast, my argument emphasizes how epidemics alter the strategic environment faced by state and insurgent elites.

[13]For example, research on economic voting during income shocks focuses on the role of misattribution among civilians on voting behavior (e.g., Novaes and Schiumerini, 2022; Ashworth, Bueno de Mesquita and Friedenberg, 2018).

[14]Another distinctive feature of frontier plagues is the high uncertainty surrounding their progression. Other shocks, such as natural disasters, may share some of the four features that induce the three-stage mechanism: legibility, lethality, uncertainty, and the state's comparative advantage in service provision. Yet frontier plagues generate much greater uncertainty than other localized shocks because they can escalate into national or global pandemics.

[15]When a silent frontier outbreak escalates into a large-scale epidemic, however, the government is more likely to intensify its capacity surge. In such cases, silent frontiers could induce constrained insurgent adaptation, though the resulting effects on conflict dynamics remain weaker than those observed during frontier plagues.

the spatial distribution of state capacity remains unchanged, insurgent adaptation becomes unlikely, and the effects of central plagues on civil conflict are limited.

Routine epidemic. For routine epidemics, the state does not need to surge its capacity in the core regions because such outbreaks can be contained with existing resources. Unlike the other three types, routine epidemics therefore do not induce a state capacity surge.

2.4 Testable Hypotheses

The dynamics of frontier plagues and comparisons across four types of epidemics generate three testable hypotheses. The first hypothesis states the effects of frontier plagues in comparison with the other three ideal types.

> *H1 (Frontier Plagues).* Frontier plagues intensify civil conflict more than central plagues, silent frontiers, and routine epidemics.

The first hypothesis captures the core prediction that the interaction of high disease burden and frontier political geography drives the intensification of civil conflict. Because legibility, fatality, and uncertainty jointly trigger domestic and international scrutiny and prompt states to deploy health-care professionals and security forces to outbreak epicenters, the effect on civil conflict should be observed only for high-burden diseases in frontier regions. Empirically, this hypothesis implies a positive interaction between high disease burden and frontier location.

The second hypothesis examines the spatial substitution during frontier plagues.

> *H2 (Mechanism: Spatial Substitution).* During frontier plagues, insurgents reduce attacks in regions neighboring the outbreak's epicenter and increase violence within the epicenter.

Because the state concentrates its forces at the outbreak's epicenter, insurgents relocate to defend their territorial control in this area, which reduces violence in neighboring regions and increases it within the epicenter.

Finally, the third hypothesis captures the tactical substitution during frontier plagues.

> *H3 (Mechanism: Tactical Substitution).* During frontier plagues, insurgents shift from battles against state forces to violence against civilians.

The tactical substitution operates in conjunction with the spatial shift: as insurgents relocate to the epicenter, the form of violence changes from battles in neighboring areas to violence against civilians in the epicenter. Within the epicenter, direct confrontation with state forces is costly.

3 Context and Data

I draw on epidemics and civil conflicts in sub-Saharan Africa to test my theory. Sub-Saharan Africa has been central to research on epidemics and insurgent violence (e.g., Ide, 2021; Koren and Bukari, 2024). Mortality from infectious diseases remains higher here than in any other region (GBD 2021 Causes of Death Collaborators, 2024), and more than half of all emergency deployments by the Global Outbreak Alert and Response Network occur in sub-Saharan Africa (Mackenzie et al., 2014). The region also experiences a wide range of epidemics, from high-burden outbreaks such as Ebola, Marburg, and meningitis to lower-burden ones such as cholera, in both central and frontier settings. Combined with the region's high incidence of civil conflict (e.g., Fearon and Laitin, 2003), this variation provides a unique opportunity to examine how epidemics affect the dynamics of civil conflicts.

To probe the mechanisms linking frontier plagues and civil conflict, I leverage the 2018–2020 Ebola epidemic in northeast DRC. The DRC is among the most theoretically central cases of civil conflict in sub-Saharan Africa (e.g., Lindsey, 2022; Autesserre, 2010, 2014; Koos and Traunmüller, 2025). Its protracted civil conflict in the northeast, combined with recurrent outbreaks of Ebola and cholera, has made the region a focal point for research on epidemics and civil conflicts (e.g., Sauter, 2024). The 2018–2020 Ebola epidemic involved 3,481 confirmed cases with an estimated mortality rate of 66%. The outbreak period saw more than 450 violent incidents or threats against healthcare professionals and at least 42 attacks on healthcare facilities.[16] The 2018-20 Ebola epidemic in the DRC thus offers a valuable case for examining how frontier plagues shape patterns of violence.

I construct two microlevel datasets. The first is an outbreak-level dataset of 922 epidemics across sub-Saharan Africa (2011–2020), which enables cross-epidemic comparison. The second is a patient-level dataset of 44,331 Ebola and 42,597 non-Ebola clinical records from the 2018–2020 Ebola outbreak in northeast DRC, which captures the dynamics of frontier plagues. I then combine both with political violence event records (Raleigh et al., 2010) to construct a comprehensive epidemics-conflict dataset.

3.1 Outbreak-level Data

The outbreak-level dataset captures 922 epidemics in sub-Saharan Africa from 2011 to 2020, including cholera (867 epidemics), Ebola (15), Marburg (5), and meningococcal meningitis (35). I obtain the most comprehensive georeferenced datasets available, first using academic publications for Ebola (Pigott et al., 2014), Marburg (Cuomo-Dannenburg et al., 2024), and cholera (Moore et al., 2017) and the Emergency Events (EM-DAT) Database for meningitis, and then validating and supplementing all records

[16] See reliefweb.int/report/democratic-republic-congo.

with academic publications, official records by the CDC and WHO, and public databases.[17] For each epidemic, the dataset includes the disease name, confirmed cases and deaths, start and end dates, and a georeferenced location. I take the start date and location to be those of the index clinical case, since it determines the timing and place of the initial response by local health authorities.

The variation of the four diseases in the dataset makes them representative of disease burden and political geography. Viral hemorrhagic diseases (Ebola and Marburg) are characterized by high disease burden, whereas cholera has lower and more variable (but generally low) mortality. Meningococcal meningitis produces outbreaks in the Meningitis Belt from Senegal to Ethiopia and has moderate to high mortality without appropriate antibiotic treatment.[18] Spatially, these epidemics occur in both frontier and central regions (Figure 1, Panel A).

3.2 Individual-level Data

From mobile-phone traces to climatological data, spatiotemporal data are collected everyday but often remain underused for research or policy. In public health, outbreak-response teams routinely assemble "line lists," patient-level records documenting timing, location, clinical features, contacts, and test results (Gregg, 2008). Although indispensable during an outbreak, these datasets are rarely analyzed afterward or beyond epidemiology. By leveraging line-list data collected for operational purposes yet seldom used in political science, I test the link between epidemics and civil conflict.

The dataset contains 88,458 clinical records from the 2018–2020 Ebola epidemic. After excluding observations without spatiotemporal information and those reported before August 2018 (n = 86,298), 3,163 cases are classified as confirmed, 136 as probable, 41,032 as suspected, and 42,597 as not a case.[19] The dataset was originally curated by the DRC Ministry of Health, the WHO, and humanitarian medical organizations involved in the clinical response.[20]

For each patient, the dataset contains 1,175 variables, including demographic information (e.g., surname, age, gender, pregnancy status, history of Ebola infection, dates and locations of onset, and occupation); clinical signs and symptoms (indicators for 36 symptoms, including hemorrhage); hos-

[17] I address the potential underreporting in low-capacity regions by triangulating across academic compilations, EM-DAT, and WHO and CDC records, which rely on international surveillance rather than national reporting alone. See Appendix Section B.1.

[18] Diseases such as malaria and HIV/AIDS are excluded because they are endemic rather than epidemic.

[19] Use of these patient-level records was reviewed and approved by the Harvard University Institutional Review Board (IRB 23-0440), and the analyses follow the APSA *Principles and Guidance for Human Subjects Research*. See Appendix Section B.3 for full ethical considerations, including consent waiver justification, de-identification procedures, and replication policy.

[20] Surveillance and case reporting during the outbreak were conducted through a joint system involving the DRC Ministry of Health, the WHO, and humanitarian medical organizations involved in clinical response. Case data were therefore compiled by both domestic and international actors rather than a single government source, which mitigates concerns about systematic reporting bias.

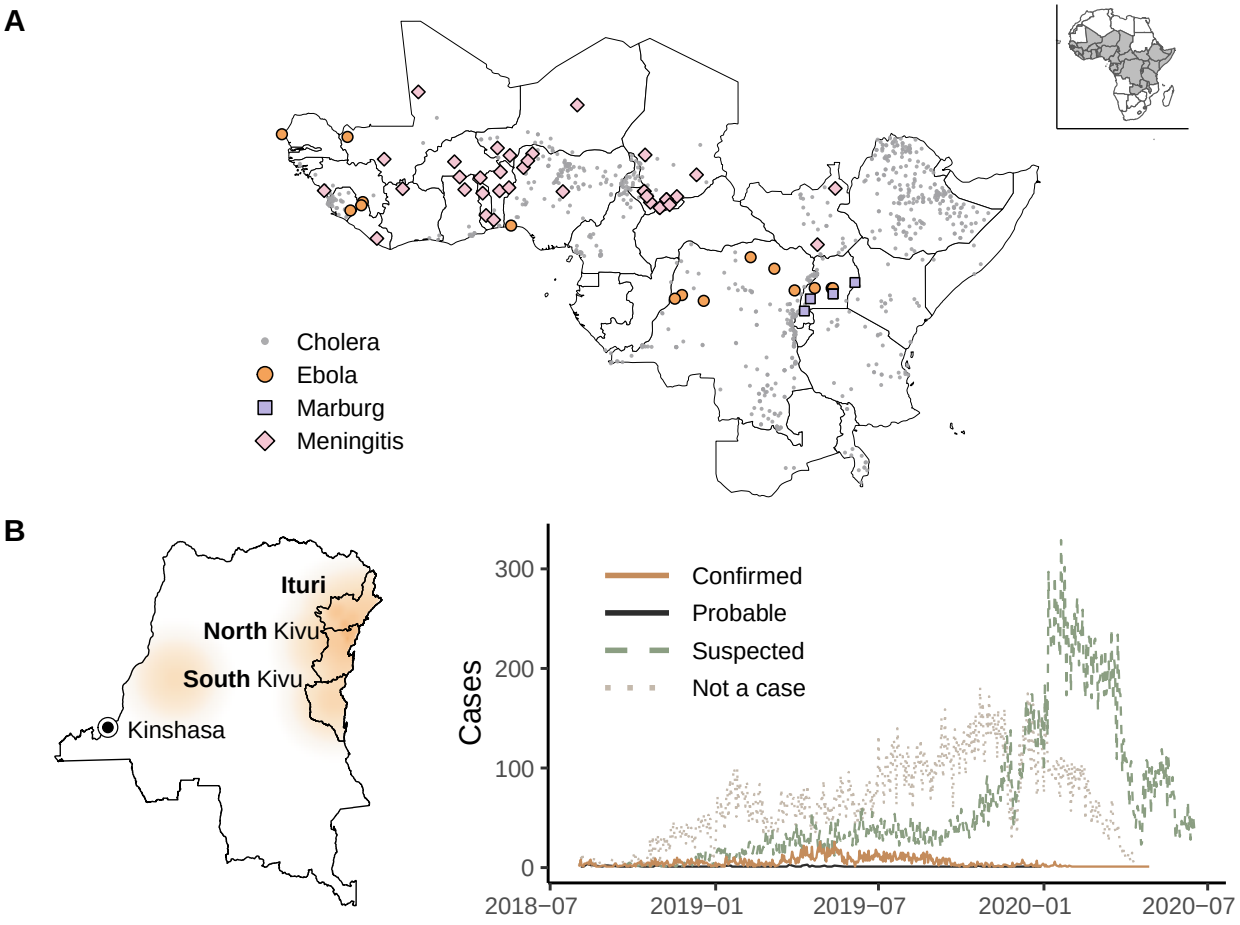

Figure 1: **Spatiotemporal trends of epidemics (2011-2020) and Ebola patients (2018-2020)**. Panel A shows epidemic locations in sub-Saharan Africa for both high- and low-burden diseases (Ebola, Marburg, meningococcal meningitis, and cholera). Cholera epidemics are displayed as dots for visualization purposes. Due to the limited sample sizes, all recorded cases beyond the 2011–2020 period are shown for Ebola and Marburg. Panel B shows the spatial distribution of confirmed Ebola patients (left; onset locations), where darker orange shading reflects higher case densities based on a smoothed, log-transformed surface. The right panel displays the temporal trajectory of patient counts during the 2018–2020 outbreak (August 1, 2018–June 25, 2020).

pitalization information (hospitalization status, facility names, and dates of admission); epidemiological risk factors (e.g., contact histories, attendance at funerals, travel history, hospital visits, and visits to traditional healers, as well as contact with animals); laboratory testing results (e.g., rapid diagnostic tests and PCR assays); information about interviewers; and patient outcomes (final clinical status, timing and location of death, and all symptoms recorded over the clinical course).[21] For location information, the dataset reports country, sous-coordination (SC), district, and village names, which I convert to geographic coordinates using a multi-stage geocoding pipeline that combines text

[21] See Appendix Section B.2 for a summary of patient characteristics.

normalization and fuzzy string matching against administrative boundary gazetteers.[22]

The spatiotemporal distribution of Ebola patients highlights how Ebola complicates the information environment. During the 2018–2020 outbreak, cases were heavily concentrated in northeast DRC (Ituri, North Kivu, and South Kivu), which also experiences protracted civil conflict (Figure 1, Panel B, left). Over time, most recorded patients were ultimately classified as not Ebola cases or as not meeting confirmatory case definitions (Figure 1, Panel B, right). The rise in such cases underscores the difficulty of distinguishing who is infected.

3.3 Political Violence Events

For dependent variables, I use the Armed Conflict Location and Event Data (ACLED) (Raleigh et al., 2010), which captures spatiotemporal information of political violence events. A key advantage of using the ACLED dataset is that it incorporates reports from the Kivu Security Tracker, a high-resolution spatiotemporal source based on local correspondents' accounts from northeastern DRC.[23]

The primary outcomes are expected frequencies of political violence events, measured as daily counts of battles, lethal violence against civilians, and non-lethal violence against civilians. I follow ACLED's typology, which defines battles as armed engagements between two organized actors and violence against civilians as the use of force by an organized actor against unarmed civilians. I classify violence against civilians as lethal when at least one fatality is reported and non-lethal otherwise.[24]

3.4 Descriptive Evidence

The descriptive analysis shows the spatiotemporal correlations between frontier plagues and civil conflict. High-burden epidemics cluster in frontier regions, whereas low-burden epidemics appear across both central and frontier areas. In the DRC (Figure 2, Panel A), Ebola outbreaks (orange) occur mainly in the conflict-affected north (gray shades displaying log-transformed mean annual event counts), while cholera outbreaks (blue) are more broadly distributed. Additionally, temporal patterns show the same frontier dynamic (Panel B). During the 2018–2020 DRC Ebola epidemic, spikes in Ebola cases (orange) coincide with surges in lethal violence against civilians (gray), which indicates that high-burden frontier epidemics and violence often escalate in tandem.

[22] See Appendix Section C.1 for full details.

[23] I use the ACLED dataset, which provides complete coverage of the Kivu Security Tracker dataset and was released on March 2, 2026. A potential concern of the ACLED dataset is that the time series of reported violence could itself be affected by exogenous shocks such as Ebola outbreaks, but inspection of temporal trends across years suggests that this is not a major issue. See Appendix Section B.4.

[24] Non-lethal violence against civilians typically involves robbery, abduction, assault, or sexual violence, whereas lethal violence against civilians capture intentional killing (Raleigh et al., 2010).

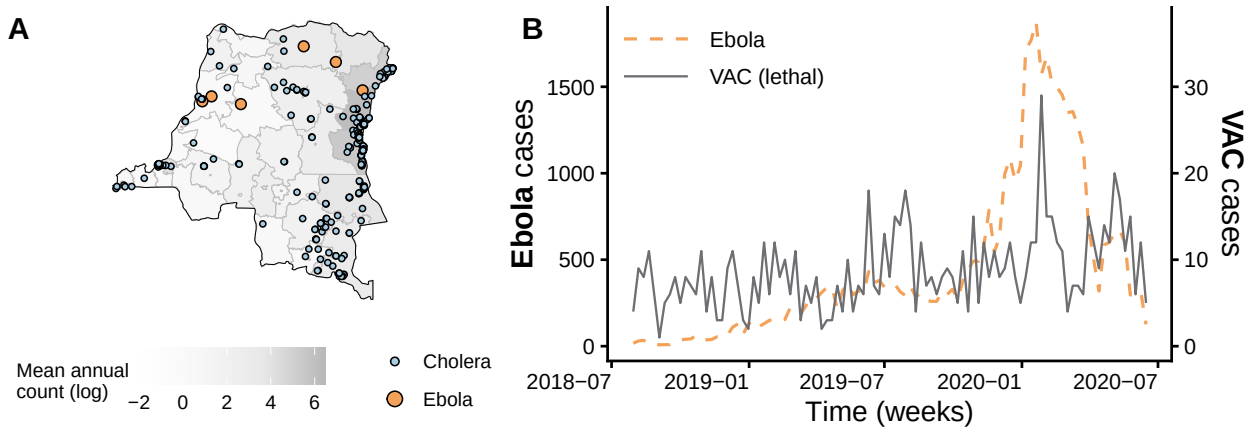

Figure 2: **Spatiotemporal correlations.** Panel A maps epidemic locations (points) and mean annual political-violence incidence (2011–2020, log scale; gray) in the DRC. Panel B shows weekly Ebola cases (orange) and lethal violence against civilians (gray). VAC: violence against civilians.

Additionally, a qualitative literature review suggests that state capacity shifts occur during frontier plagues (see Appendix Section D). I compare two epidemics in northeastern DRC (the 2018–2020 Ebola epidemic and the 2017–2018 cholera epidemic), which were among the largest Ebola (high-burden) and cholera (low-burden) outbreaks in the DRC's frontier region. Because the outbreaks were similar in geography and scale but differed sharply in disease burden,[25] this comparison provides a useful way to assess the impact of frontier plagues on shifts in state capacity. During Ebola, I find that the DRC government, with Doctors Without Borders (MSF) and WHO, established and directly managed eleven treatment centers across Ituri, North Kivu, and South Kivu, and expanded diagnostic laboratories. During cholera, however, only five new centers opened in North and South Kivu, all primarily operated by MSF, with minimal laboratory expansion.

4 Methods

Descriptive evidence shows spatial and temporal associations between frontier plagues and civil conflict, but these patterns remain correlations. Identifying causal effects requires methods that exploit the full granularity of the microlevel data. In this section, I outline the spatiotemporal causal inference framework, explain the identification strategies, and describe the research design.

4.1 Overview

Methodologically, spatial spillovers and temporal carryovers that epidemics might generate pose a crucial challenge. A single Ebola patient in a frontier region might draw state resources from else-

[25] Cholera produced approximately 55,000 cases nationwide, many in the northeast, but had a mortality rate of 2%.

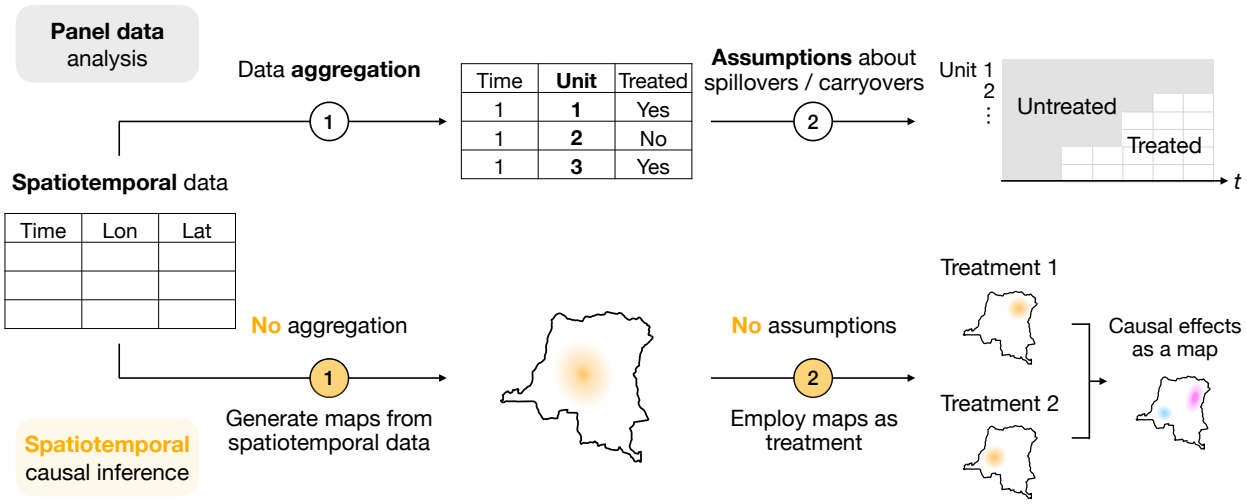

Figure 3: **Spatiotemporal causal inference framework**. Panel data methods (top) aggregate observations to regions or grid cells, impose assumptions about spillovers and carryovers, and estimate causal effects, which can bias estimates. The spatiotemporal causal inference framework (bottom) avoids aggregation and instead generates maps of treatment and outcome locations. It also permits flexible counterfactuals, such as shifting the location of outbreaks.

where and influence conflict dynamics far beyond the outbreak's epicenter, and these effects might appear only after several days after the patient becomes symptomatic. Because spillovers and carryovers can combine in many ways across continuous space, structural assumptions about them are difficult to justify.

I therefore employ a spatiotemporal causal inference framework (Mukaigawara et al., 2025). Figure 3 contrasts panel data methods with the spatiotemporal causal inference framework. Panel data methods (the top panel) aggregate microlevel coordinates and timing to administrative units or grid cells and impose assumptions about spillovers and carryovers, for example through lagged outcomes in selected neighboring areas, which can all introduce bias. Contrarily, the spatiotemporal framework (the bottom panel) avoids aggregation. It converts treatment and outcome locations into maps and uses the spatial distribution as the treatment. This *map-as-treatment* strategy allows estimation of average treatment effects, exploration of effect heterogeneity, and examination of mechanisms without assumptions about how spillovers or carryovers operate.[26] This framework is especially well suited to my setting, where spillovers and carryovers are likely, the data are highly granular in space and time, and the observation period is sufficiently long.

Substantively, the framework estimates how insurgent violence changes when the spatial distribution of treatment shifts from one distribution to another over a specified period (Figure 3, bottom

[26] Further details can be found in Appendix Section A. Readers interested in technical details should consult Mukaigawara et al. (2025), Papadogeorgou et al. (2022), and Zhou et al. (2024).

right). In Figure 3, Treatment 1 and Treatment 2 represent two distributions of outbreaks or patients (a more frontier-concentrated distribution versus a more center-concentrated one). The method compares the effects of one distribution against another (e.g., effects of shifting epidemics from the center to the frontier) over a specified duration (e.g., seven days) and estimates the resulting change in violence. Like the treatment, the causal effects are represented as a map (the blue-red map in Figure 3, with blue indicating negative expected violence and red indicating positive expected violence). Mathematically integrating the map over an area of interest, such as northeast DRC, yields the causal effect as a count (the expected change in the number of violent events in northeast DRC when outbreaks shift from the center to the frontier for seven days).[27]

4.2 Identification Strategy

The spatiotemporal causal inference framework rests on two causal assumptions (formally stated in Appendix Section A). The first is *unconfoundedness*. Conditional on the observed history of treatments, outcomes, and covariates, the treatment point pattern at each time period is independent of all potential outcomes. Substantively, this means that the locations and timing of disease cases are random once I account for spatiotemporal predictors of treatments. The second is *overlap*. The counterfactual treatment distributions that I construct should be realistic and have positive probability under the propensity score model. The overlap assumption ensures that the estimated effects reflect plausible scenarios rather than extrapolations.

Exogenous variation in exposure. For identification, I exploit exogenous variation in exposure to the environmental and animal reservoirs of cholera and Ebola. Cholera is initially transmitted through contaminated water sources containing *Vibrio cholerae*, and large lakes and rivers in the African Great Lakes region have been identified as potential environmental reservoirs (e.g., Bompangue et al., 2008; Taty et al., 2024). Environmental variation in access to these water bodies therefore offers a source of exogenous spatial variation. I model cholera outbreak locations using distances to major water sources, along with histories of cholera outbreaks and political violence, distances to major cities, population density and time splines.[28]

[27] Slightly more formally, the causal estimand is the average treatment effect of changing the spatial distribution or intensity of outbreaks or patients on violence counts. Each counterfactual is a *stochastic intervention*, defined as a probability distribution over outbreak or patient locations (Appendix Section A). Under the two causal assumptions of unconfoundedness and overlap, I estimate propensity scores and use inverse probability weighting (IPW) to estimate the average treatment effect as the difference in weighted violence outcomes between two counterfactual interventions.

[28] Because my theory centers on state response and insurgent adaptation, I focus on epidemic onset and examine whether newly emerging epidemics intensify civil conflict. Although I control for prior violence and prior outbreak or patient histories when estimating propensity scores, focusing on newly emerging epidemics further ensures that subsequent cases are treated as post-treatment dynamics.

Ebola initially spreads to humans through contact with infected wildlife, with fruit bats of the family *Pteropodidae* considered likely natural hosts. Variation in the distribution of reservoir animals thus provides a source of random treatment locations. I use existing fine-grained measures of index-case locations and outbreak potential at the lowest administrative level, derived from the spatial distribution of reservoir animals and previously reported human and animal Ebola cases (Pigott et al., 2017). I also include spatiotemporal covariates (histories of political violence and Ebola incidence, spatial and temporal indicators, and time splines) in the model so that, conditional on these factors, the observed patient locations can be treated as random.[29]

Threats to inference. The overlap assumption faces a specific threat in the context of Ebola. Because Ebola has a high case fatality rate, patients at affected locations might die or flee, and if no new cases arise there, the spatial support of the treatment process thins over time. This would reduce overlap between the observed and counterfactual treatment distributions. I assess this threat with a nearest-neighbor stationarity diagnostic (see Appendix Section H.1 for methodological details).

To examine the plausibility of the unconfoundedness assumption, I employ two strategies. First, I conduct placebo outcome tests using satellite-detected fires (Schroeder et al., 2014), which share the same spatial confounding structure as political violence but have no plausible link to Ebola (Appendix Section H.2). Second, I perform a sensitivity analysis that generalizes the bounds approach of Rosenbaum (2002) to the spatiotemporal setting (Papadogeorgou et al., 2022), which quantifies how much the inverse probability weights would need to deviate from their assumed values before the estimated effects become indistinguishable from zero.

4.3 Counterfactual Design

To test my hypotheses, I employ both cross- and within-epidemic analyses. In the cross-epidemic analysis, I estimate the interaction effects of disease burden and political geography on weekly incidence of violence. I then conduct within-epidemic analyses using Ebola patient records to estimate the causal effects of intensifying frontier plagues.

Cross-epidemic analysis. I begin by testing *H1* through an analysis of how disease burden interacts with political geography (Table 3, the first row). Using the Ebola patient line list, I construct counterfactual outbreak distributions in frontier and central regions by taking the out-of-sample density

[29] I provide the model specification for cholera in Appendix Section E and for Ebola in Appendix Section F, where I also present a set of model verification tests, including inspections of average residual fields (Baddeley et al., 2005), results from the superthinning residual tests (Schoenberg, 2003; Clements, Schoenberg and Veen, 2012), out-of-sample prediction performance, and visual assessments of the propensity score model (Papadogeorgou et al., 2022; Mukaigawara et al., 2025). I confirm that, after controlling for a set of covariates, the spatiotemporal patterns of cholera outbreak locations and Ebola patient locations can be treated as random.

Table 3: **Summary of counterfactual designs.** The outcomes (violence) include battles, lethal violence against civilians, and non-lethal violence against civilians.

Analysis	Quantities of Interest	Counterfactuals
Cross-epidemic	Interaction effects (disease burden × political geography) on weekly incidence of violence: `(A – B) – (C – D)`	`A`. Ebola (frontier), 1 outbreak / week `B`. Ebola (center), 1 outbreak / week `C`. Cholera (frontier), 1 outbreak / week `D`. Cholera (center), 1 outbreak / week
Within-epidemic	Effects of intensifying frontier plagues on weekly incidence of violence: `E – F`	`E`. Ebola (frontier), 2–7 patients / day `F`. Ebola (frontier), 1 patient / day

of Ebola cases and reweighting it with the density of healthcare facilities. Public hospitals and clinics shift the distribution toward central regions, and private hospitals, which in the DRC are largely complementary to public facilities, shift it toward frontier regions.[30]

I then estimate the average treatment effect of a shift from central to frontier regions (Table 3, the first row: `A - B` for Ebola and `C - D` for cholera), measured by the change in weekly violence incidences in northeastern DRC and in the DRC and adjacent areas of Rwanda and Uganda. I include these neighboring areas because porous borders allow spatial spillover. For cholera, using the outbreak-level data, I construct counterfactual distributions in frontier and central regions and set weekly outbreaks to one to simulate the onset of a new outbreak.[31] For Ebola, due to the small sample size in the outbreak-level data, I turn to the patient-level data. To simulate the onset of a new outbreak, I set the intensity to be 4 cases per week, based on the average daily incidence during the first four months of the 2018–20 outbreak. Finally, I compare the average treatment effects for Ebola and cholera and examine the interaction effects (corresponding to `(A - B) - (C - D)` in the first row of Table 3).

Within-epidemic analysis. To test *H2* and *H3*, I employ the Ebola patient-level data (Table 3, the second row). I maintain the spatial distribution of patients the same and examine the effects of intensifying frontier plagues by increasing the daily number of patients from 1 to 2–7 cases, which reflects the actual number of daily cases during the 2018–20 Ebola epidemic (corresponding to `E - F`). To further probe heterogeneity and mechanisms, I estimate heterogeneous treatment effects within the epicenter and conduct causal mediation analyses.

[30] See Appendix Section F. I also vary prioritization parameters as a robustness check.
[31] See Appendix Section E.

5 Results

To preview the main findings, the cross-epidemic analyses show that high disease burden and frontier locations jointly intensify civil conflict. Direct analysis of frontier plagues reveals that battles decline in the outbreak's epicenter as the epidemic intensifies. With a series of heterogeneity analyses, I find patterns consistent with the spatial and tactical substitution hypotheses.

5.1 Interaction Effects of Disease Burden and Political Geography

To test *H1 (Frontier Plagues)*, I examine the interaction effects of disease burden and political geography (Figure 4, top left) and obtain the interaction effects as a map (Figure 4, right), which shows positive interaction effects throughout northeastern DRC. The estimated interaction effects obtained by mathematically integrating the map (bottom left) are an additional 0.87 attacks per week in northeastern DRC (95% CI: 0.068–1.672) in the case of lethal violence against civilians. This effect corresponds to a 14.6% increase (1.14–28.13) compared with the 2018 baseline.[32] These findings are robust across a range of counterfactual specifications. The findings become statistically insignificant when non-Ebola cases, rather than Ebola cases, are used as the intervention.[33]

Two points are worth noting. First, the comparison between Ebola and non-Ebola cases as treatments shows that legibility, fatality, and uncertainty jointly intensify civil conflict. Non-Ebola cases are clinical cases that presented to hospitals or clinics but were ultimately ruled out as Ebola. Their clinical profiles differ sharply from those of confirmed Ebola cases (see Table B.2). Confirmed Ebola cases display more legible symptoms, such as bleeding (19% among confirmed Ebola cases versus 8.6% among non-Ebola cases), much higher fatality (64% versus 19%), and greater uncertainty because of Ebola's incubation period. Because only Ebola combines these three features, the difference in interaction effects between Ebola and non-Ebola cases indicates that this triad jointly intensifies civil conflict.

Second, the cross-epidemic results indicate the presence of heterogeneity. Although the pattern of interaction effects is consistent across alternative counterfactual specifications (see Appendix Section G.1), the magnitude and precision of the estimates vary across outcomes, with the effects on lethal violence against civilians being the most robust. To further probe this heterogeneity, I next perform the within-epidemic analysis.

[32] For the DRC and neighboring regions, the effect is 1.099 attacks per week (95% CI: 0.105–2.092). This finding implies that approximately 20.8% of the interaction effect occurs outside northeastern DRC, which justifies the use of the spatiotemporal causal inference method.

[33] See Appendix Section G.1 for the full results.

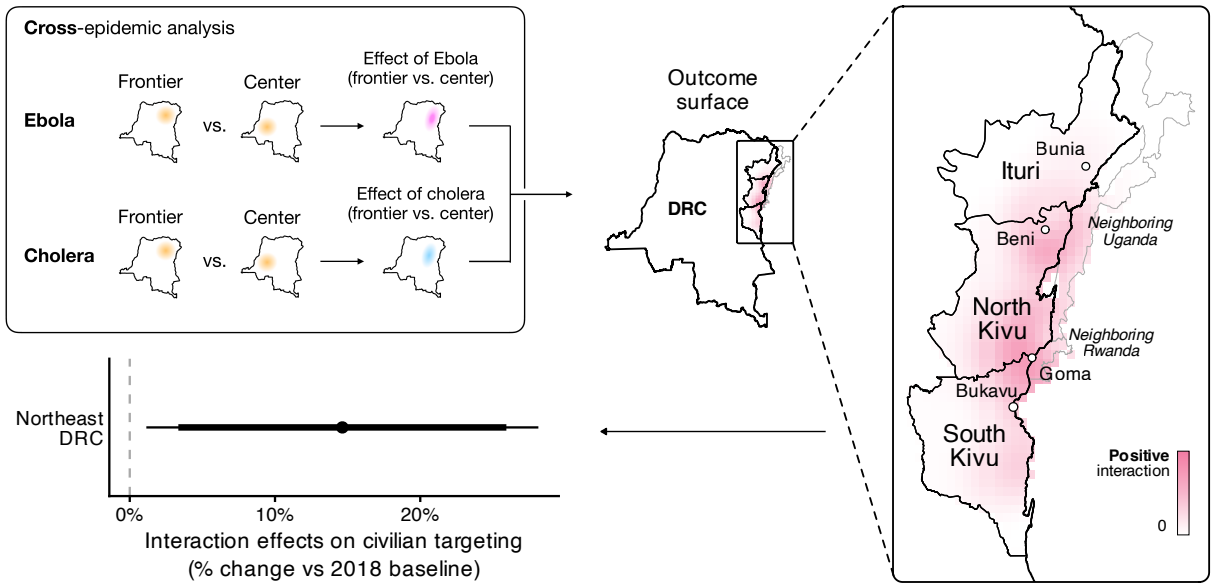

Figure 4: **Disease burden and political geography jointly intensify civil conflict**. The cross-epidemic design (top left) compares the effects of shifting Ebola from the center to the frontier for one week against the corresponding effects of cholera. The outcome surface (right) shows locations with positive (red) interaction effects on lethal violence against civilians in northeastern DRC. Mathematically integrating the map over northeast DRC generates the interaction effects (bottom left), expressed as percentage change relative to the January–July 2018 pre-outbreak baseline. Thick and thin lines show the 90% and 95% confidence intervals, respectively.

5.2 Spatial and Tactical Substitutions

Within-epidemic analyses provide direct evidence for the spatial (*H2*) and tactical (*H3*) substitution hypotheses. Figure 5 summarizes the average treatment effects of intensifying frontier plagues on violence across northeastern DRC. The overall effects on violence are positive and statistically significant and demonstrate a dose-response pattern (Panel A). Further, battles between insurgents and the state decline in Ituri, a neighboring area of the outbreak epicenter (Panel B, left), whereas violence against civilians increases in North Kivu, the outbreak epicenter (Panel B, right).[34] These findings imply that insurgents shift the locus of violence from neighboring regions toward the outbreak epicenter (*H2*) and shift tactics from battles toward violence against civilians (*H3*).[35]

[34]A series of diagnostic and sensitivity checks lends support to the identifying assumptions. The spatial support of patient locations remains stable across specifications, the placebo test yields no detectable effect, and the sensitivity analysis indicates that an unmeasured confounder would need to change the IPW weights by a factor of approximately 1.7 to attenuate the estimated effects to zero. Given that the analysis already conditions on a rich set of spatiotemporal covariates, the sensitivity analysis suggests that the main findings are robust to substantial departures from the unconfoundedness assumption. See Appendix Sections H.1 and H.2.

[35]The effects on lethal violence against civilians are more uncertain because of greater heterogeneity in lethal attacks. The point estimates follow a similar pattern. See Appendix Section G.2 for the full results.

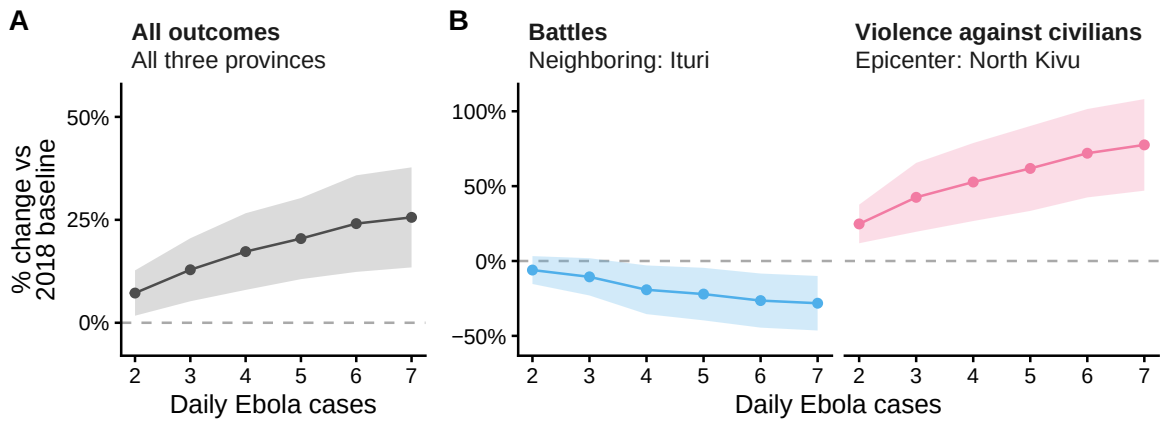

Figure 5: **Frontier plagues reduce battles in neighboring areas and intensify violence against civilians in the epicenter.** Frontier plagues intensify violence during civil conflict (Panel A), while reducing battles in neighboring Ituri (specifically Djugu, since the Ituri territoires south of Djugu fall within the epicenter case area, Panel B, left) and intensifying violence against civilians in the epicenter, North Kivu (Panel B, right). Effects are shown as percentage change relative to the January–July 2018 pre-outbreak baseline. Shaded ribbons denote 95% confidence intervals. The treatment contrast compares 1 versus 2–7 daily Ebola cases.

Observable implications of frontier plagues. I now move beyond the aggregate pattern in Figure 5 to test three observable implications of the frontier-plague theory. First, insurgents should project power beyond their bases. Because armed groups' ability to project power declines with distance from their strongholds (Boulding, 1962; Buhaug, 2010), insurgent operations usually remain near their bases. Frontier plagues should disrupt this pattern: state redeployment to the epicenter pulls insurgents outward and spreads violence across a wider area. Second, insurgents should avoid direct confrontation where state forces are concentrated. Since Ebola treatment centers served as focal points of state deployment during the 2018–2020 outbreak, battles should decline near these facilities.[36] Third, insurgents should act strategically rather than in response to grievances. Preexisting grievances should therefore not moderate the effect of frontier plagues on violence. I test each implication in turn.

To examine whether insurgents operate beyond their bases, I infer insurgent base locations from pre-outbreak data and estimate the cumulative effects of frontier plagues on violence as a function of distance from those locations.[37] I find that violence disperses well beyond pre-outbreak areas of

[36] Although the spatial and tactical substitution hypotheses state this prediction at the regional level, the same logic applies within the epicenter.

[37] I first identify locations of insurgent-perpetrated violence against civilians in the year before the outbreak (August 2017–July 2018) and infer base locations using Gaussian mixture model clustering. I use violence against civilians because these events are unilateral and directly reflect perpetrators' areas of control. I select the number of clusters using the Bayesian Information Criterion. I then compute the distance from each location in the study area to the nearest inferred base and examine how the cumulative effects of frontier plagues on violence vary with distance from those bases.

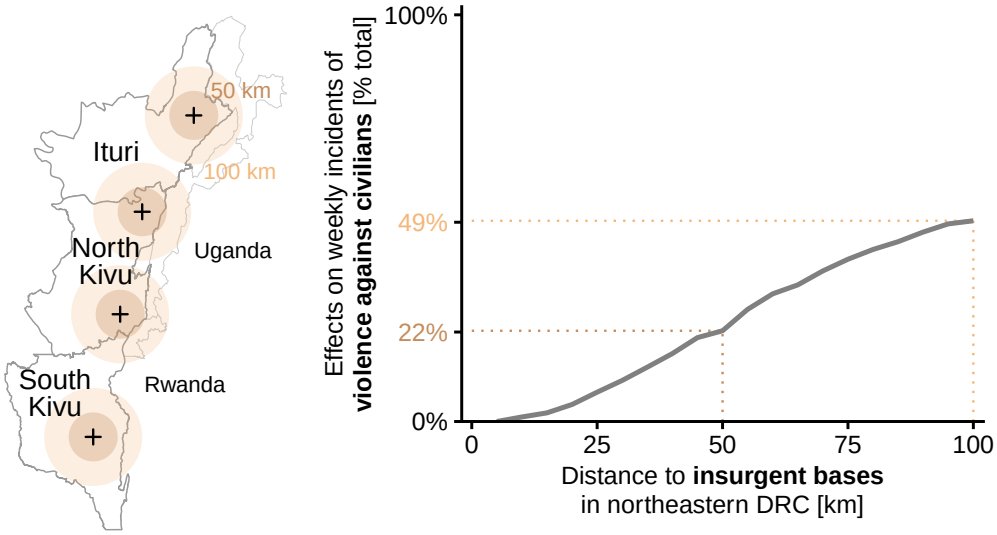

Figure 6: **Frontier plagues push insurgent activity beyond pre-outbreak areas of operation.** The map (left) shows the locations of insurgent bases in northeastern DRC with 50 and 100 km rings. The line plot (right) shows the cumulative share of weekly violence against civilians by distance to the nearest base. Only 49% of the effect occurs within 100 km of pre-outbreak bases. The treatment contrast compares 1 versus 6 daily Ebola cases.

operation (Figure 6). Under the treatment contrast of 1 versus 6 daily Ebola cases, only 22% and 49% of violence against civilians occurs within 50 and 100 km of the nearest pre-outbreak insurgent base, respectively. This geographic displacement suggests that epidemic response alters the local balance of territorial control. The influx of state capacity challenges rebel control in the epicenter by forcing insurgents to project power beyond their original areas of operation. Frontier plagues thus disrupt the loss-of-strength gradient emphasized by Boulding (1962) and Buhaug (2010).

Further, insurgents avoid areas where the state concentrates its forces.[38] The effect of intensifying frontier plagues on battles is negative and statistically significant near Ebola treatment centers, but indistinguishable from zero farther away (Figure 7, Panel A). The lines in Panel A trace the conditional average treatment effects for treatment contrasts of 2, 4, and 6 daily Ebola cases relative to 1, and the shaded bands denote confidence intervals for the 6-case contrast. Areas closer to treatment centers, captured by higher proximity measures near 1, exhibit significantly more negative conditional average treatment effects than areas farther away. The dose-response relationship suggests that as frontier plagues intensify, insurgents increasingly avoid zones of concentrated state capacity.

Moreover, preexisting grievances do not affect insurgent strategies.[39] I find that neither poverty

[38] I estimate heterogeneous treatment effects by proximity to Ebola treatment centers. I construct a time-varying proximity measure that assigns values near 1 to locations at a treatment center and values near 0 to distant locations. I then estimate conditional average treatment effects of intensified frontier plagues on battles as a function of this proximity measure. See Appendix Section C.2 for details.

[39] I use the 2013–14 DRC Demographic and Health Survey (DHS) to construct two moderators: the proportion of house-

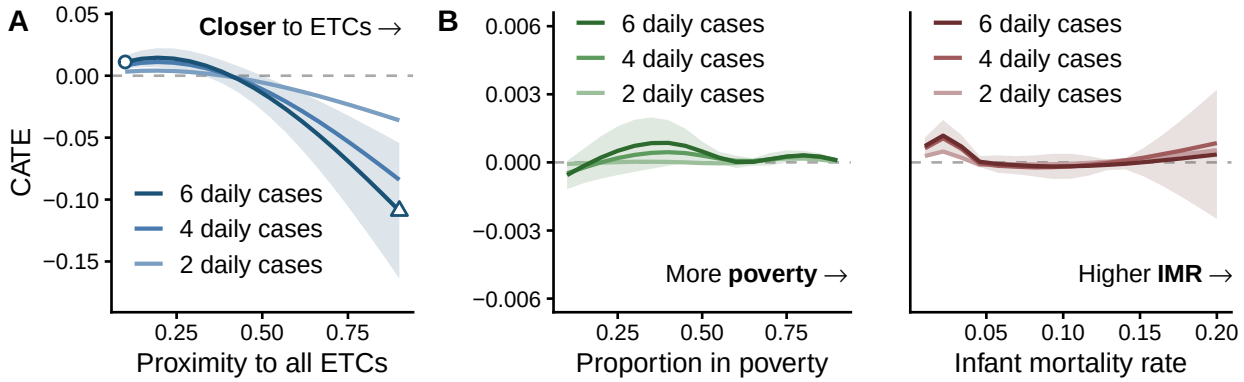

Figure 7: **Insurgents strategically avoid areas of state capacity expansion.** Panel A shows that battles decrease in areas closer to ETCs, with a clear dose-response relationship by daily Ebola case counts. Panel B shows that poverty (left) and infant mortality (right) do not moderate the effect on battles. Shaded bands denote 95% confidence intervals for 6 daily cases. CATE: conditional average treatment effects; ETC: Ebola treatment centers; IMR: infant mortality rate.

nor infant mortality moderates the effect of intensifying frontier plagues (Figure 7, Panel B). Poverty captures material deprivation, and infant mortality captures weak public health infrastructure. If the effect were grievance driven, areas with higher poverty or worse infant mortality should exhibit stronger treatment effects. Yet the estimated conditional average treatment effects are flat across both moderators. The conflict-inducing effect of frontier plagues therefore does not appear to depend on baseline deprivation. These null moderation results support the theory's third implication: insurgent elites adapt strategically to shifts in state presence and territorial control, not because preexisting grievances amplify mobilization.

An alternative mechanism: contagion avoidance. The empirical findings so far support the theory of frontier plagues, but they could also follow from an alternative mechanism: insurgents avoid direct contact during frontier plagues to reduce the risk of infection. The decline in battles would reflect delayed confrontation until the state contains the epidemic, after which insurgents reengage. The avoidance of Ebola treatment centers would stem from efforts to avoid areas with high infection risk. The rise in violence against civilians would indicate a shift toward indirect tactics, such as shooting from a distance, that allow insurgents to continue extracting from civilians (e.g., Weinstein, 2007) while limiting their exposure to patients.

I test this alternative mechanism in three ways. First, I estimate the effects of intensifying frontier plagues on forms of violence that require direct contact with targets, which directly examines

holds in poverty and the infant mortality rate (IMR), both aggregated to the admin-2 level. Poverty is defined as households with a DHS wealth index in the bottom two quintiles. The IMR is computed from the DHS birth history module. I employ the DHS because Afrobarometer data are not available for the DRC. See Appendix Section C.3 for the spatial distribution of these moderators.

whether insurgents shift from direct to indirect tactics when the risk of infection increases. Second, I de-intensify Ebola from the median number of cases and estimate the subsequent effects on violence. If insurgents wait for the state to contain the epidemic before reemerging, then violence should increase as the number of Ebola patients decreases. Third, I conduct a causal mediation analysis that increases the proportion of patients with bleeding while holding the number of Ebola cases constant.[40] If insurgents avoid violence because they fear contagion, the indirect effect through visible disease severity should be statistically significant.

None of the three tests, however, supports the alternative mechanism (see Appendix G.3). Intensifying frontier plagues neither reduces direct tactics nor increases indirect tactics. Deescalating Ebola cases does not increase violence. Clinical symptoms also do not mediate the effects, which suggests that insurgents respond not to the risk of infection but to state-capacity surges under uncertainty about epidemic progression.

Taken together, the empirical results presented in this section demonstrate that frontier plagues intensify civil conflict and induce spatial and tactical substitutions of violence. The cross-epidemic comparison shows that this effect depends on the combination of high disease burden and frontier political geography (*H1*). The within-epidemic analysis identifies the mechanism: as frontier plagues intensify, state-capacity deployment to the epicenter triggers insurgent adaptation (*H2* and *H3*). Insurgents withdraw from neighboring regions, avoid direct confrontation where state presence is concentrated, and shift strategically to violence against civilians. These shifts are not well explained by contagion avoidance.

6 Conclusion

Despite the large, influential body of literature on exogenous shocks and civil conflict, political scientists have paid surprisingly little attention to the role of epidemics in civil conflict. The existing literature mostly focuses on a single disease outbreak and is thus agnostic to how medical aspects of the shock affect civil conflict. I argue here that the combination of high disease burden and frontier political geography intensifies civil conflict and produces spatial and tactical substitutions of violence. Frontier plagues thus create a *containment trap*, in which efforts to contain a severe epidemic put the civilians they aim to protect at greater risk.

The findings broaden how civil war scholarship theorizes exogenous shocks and civilian victimization. Existing accounts emphasize how shocks alter resources, grievances, opportunity costs, or fiscal capacity at national or provincial scales (e.g., Bazzi and Blattman, 2014; Dube and Vargas, 2013;

[40] See Appendix A.3 for methodological details and Appendix F.6 for model validation.

Koubi, 2019; Nielsen et al., 2011). Frontier plagues operate differently: they relocate state power at a local and temporary scale through specialized containment capacity that insurgents cannot capture or credibly provide. The implication for theories of civilian victimization (e.g., Kalyvas, 2006; Wood, 2014; Sexton, 2016; Crost, Felter and Johnston, 2014) is that collaboration is not a fixed category. Crisis response can make ordinary acts of civilian compliance, such as seeking treatment or reporting symptoms, politically consequential in contested territory.

These findings carry direct implications for outbreak response and civil-military coordination. Response strategies should anticipate insurgent adaptation from the outset, rather than focus only on epidemiological containment and security around treatment centers. When protection concentrates around healthcare facilities, insurgents may shift violence toward less protected civilians nearby. Outbreak response should therefore extend civilian protection beyond treatment facilities, integrate conflict monitoring with epidemiological surveillance, and align humanitarian access with patterns of territorial control as well as disease spread. The implication is not to demilitarize healthcare in every setting. Rather, it is to treat the population of the outbreak epicenter, not only the treatment centers, as the protected unit.

The theory also suggests several directions for future research. First, future work should examine how the strategic logic changes when localized epidemics become pandemics. Pandemics cover larger territories, often produce more uniform state responses, and may weaken the localized power shifts that drive the frontier-plague mechanism. Second, the framework points to longer-run effects on state-society relations and insurgent organization in contested frontier regions. Crisis-driven state reach may recede after containment, but the political consequences of surveillance, coercion, and service provision may persist. Third, cross-border contagion risk and weak host capacity may create openings for foreign subversion, especially where neighboring states can exploit public health emergencies to undermine host authority (Lee, 2020). Future research should examine how contagion risk, neighbor capacity, and border permeability shape these forms of intervention.

Frontier plagues show that epidemics are not merely background conditions for civil war. They are political shocks that can relocate state power, alter insurgent strategy, and transform civilian compliance into a target of coercion. For populations exposed to both infection and insurgent violence, containment is therefore not only a medical challenge. It is also a problem of civilian protection in contested territory.

References

ALIMA. 2019. "Ebola DRC: Operational Update on ALIMA's Activities.". April 2019.
URL: *https://alima.ngo/en/news/ebola-drc-operational-update-alima-activities/*

Antia, Rustom, Roland R. Regoes, Jacob C. Koella and Carl T. Bergstrom. 2003. "The role of evolution in the emergence of infectious diseases." *Nature* 426(6967):658–661.

Ashworth, Scott, Ethan Bueno de Mesquita and Amanda Friedenberg. 2018. "Learning about Voter Rationality." *American Journal of Political Science* 62(1):37–54.

Autesserre, Séverine. 2010. *The Trouble with the Congo: Local Violence and the Failure of International Peacebuilding*. Cambridge: Cambridge University Press.

Autesserre, Séverine. 2014. *Peaceland: Conflict Resolution and the Everyday Politics of International Intervention*. New York / Cambridge: Cambridge University Press.

Baddeley, Adrian. 2015. *Spatial Point Patterns: Methodology and Applications with R*. Interdisciplinary statistics first edition. ed. Boca Raton, FL: Chapman and Hall/CRC, an imprint of Taylor and Francis.

Baddeley, Adrian, Rolf Turner, Jesper Møller and Martin Hazelton. 2005. "Residual Analysis for Spatial Point Processes." *Journal of the Royal Statistical Society: Series B* 67(5):617–666.

Bagozzi, Benjamin E. 2016. "On Malaria and the Duration of Civil War." *Journal of Conflict Resolution* 60(5):813–839.

Balcells, Laia. 2017. *Rivalry and Revenge: the Politics of Violence During Civil War*. Cambridge, United Kingdom: Cambridge University Press.

Barks, Patrick M., Anton Camacho, Trish Newport, Filipe Ribeiro, Steve Ahuka-Mundeke, Regis Kitenge, Justus Nsio, Rachel M. Coulborn and Emmanuel Grellety. 2025. "Evaluation of a Decentralised Model of Care on Case Isolation and Patient Outcomes During the 2018–20 Ebola Outbreak in the Democratic Republic of the Congo: a Retrospective Observational Study." *The Lancet Global Health* 13(5):e931–e941.

Bautista, Edgar, Tawee Chotpitayasunondh, Zhancheng Gao, Scott A Harper, Michael Shaw, Timothy M Uyeki, Sherif R Zaki, Frederick G Hayden, David S Hui, John D Kettner et al. 2010. "Clinical aspects of pandemic 2009 influenza A (H1N1) virus infection." *New England Journal of Medicine* 362(18):1708–1719.

Bazzi, Samuel and Christopher Blattman. 2014. "Economic Shocks and Conflict: Evidence from Commodity Prices." *American Economic Journal: Macroeconomics* 6(4):1–38.

Berman, Eli, Jacob N. Shapiro and Joseph H. Felter. 2011. "Can Hearts and Minds Be Bought? The Economics of Counterinsurgency in Iraq." *Journal of Political Economy* 119(4):766–819.

Berman, Nicolas, Mathieu Couttenier, Nathalie Monnet and Rohit Ticku. 2022. "Shutdown Policies and Conflict Worldwide." *Journal of Comparative Economics* 50(1):240–255.

Blattman, Christopher and Edward Miguel. 2010. "Civil War." *Journal of Economic Literature* 48(1):3–57.

Bloem, Jeffrey R. and Colette Salemi. 2021. "COVID-19 and Conflict." *World Development* 140:105294.

Bompangue, Didier, Patrick Giraudoux, Pascal Handschumacher, Martine Piarroux, Bertrand Sudre, Mosiana Ekwanzala, Ilunga Kebela and Renaud Piarroux. 2008. "Lakes as Source of Cholera Outbreaks, Democratic Republic of Congo." *Emerging Infectious Diseases* 14(5):798–800.

Boone, Catherine. 2003. *Political Topographies of the African State: Territorial Authority and Institutional Choice*. Cambridge studies in comparative politics Cambridge, U.K. ; New York: Cambridge University Press.

Boulding, Kenneth E. 1962. *Conflict and Defense: A General Theory*. New York: Harper and Brothers.

Brancati, Dawn, Jóhanna Birnir and Qutaiba Idlbi. 2023. "Locking Down Violence: The COVID-19 Pandemic's Impact on Non-State Actor Violence." *American Political Science Review* pp. 1–17.

Buhaug, Halvard. 2010. "Dude, Where's My Conflict? LSG, Relative Strength, and the Location of Civil War." *Conflict Management and Peace Science* 27(2):107–128.

Buhaug, Halvard and Jan Ketil Rød. 2006. "Local determinants of African civil wars, 1970–2001." *Political Geography* 25(3):315–335.

Buhaug, Halvard and Scott Gates. 2002. "The Geography of Civil War." *Journal of Peace Research* 39(4):417–433.

Burke, Marshall, Solomon M Hsiang and Edward Miguel. 2015. "Climate and Conflict." *Annual Review of Economics* 7(1):577–617.

Caldas de Castro, M, R.L Monte-Mor, D.O Sawyer and B.H Singer. 2006. "Malaria Risk on the Amazon Frontier." *PNAS* 103(7):2452–2457.

Cambon, Jesse, Diego Hernangomez, Christopher Belanger and Daniel Possenriede. 2021. "tidygeocoder: An R Package for Geocoding." *Journal of Open Source Software* 6(65):3544.

Carter, David B., Andrew C. Shaver and Austin L. Wright. 2019. "Places to Hide: Terrain, Ethnicity, and Civil Conflict." *Journal of Politics* 81(4):1446–1465.

CDC. 2006. *Principles of Epidemiology in Public Health Practice*. 3rd ed. Cambridge, United Kingdom: US Department of Health and Human Services.

Cervellati, Matteo, Elena Esposito, Uwe Sunde and Simona Valmori. 2018. "Long-term Exposure to Malaria and Violence in Africa." *Economic Policy* 33(95):403–446.

Cervellati, Matteo, Uwe Sunde and Simona Valmori. 2017. "Pathogens, Weather Shocks and Civil Conflicts." *The Economic Journal* 127(607):2581–2616.

Clemens, John D, G Balakrish Nair, Tahmeed Ahmed, Firdausi Qadri and Jan Holmgren. 2017. "Cholera." *The Lancet* 390(10101):1539–1549.

Clements, Robert Alan, Frederic Paik Schoenberg and Alejandro Veen. 2012. "Evaluation of Space-time Point Process Models Using Super-thinning." *Environmetrics (London, Ont.)* 23(7):606–616.

Crost, Benjamin, Joseph Felter and Patrick Johnston. 2014. "Aid Under Fire: Development Projects and Civil Conflict." *American Economic Review* 104(6):1833–1856.

Cuomo-Dannenburg, Gina, Kelly McCain, Ruth McCabe, H Juliette T Unwin, Patrick Doohan, Rebecca K Nash, Joseph T Hicks, Kelly Charniga, Cyril Geismar, Ben Lambert, Dariya Nikitin, Janetta Skarp, Jack Wardle, Mara Kont, Sangeeta Bhatia, Natsuko Imai, Sabine van Elsland, Anne Cori, Christian Morgenstern, Aaron Morris, Alpha Forna, Amy Dighe, Anne Cori, Arran Hamlet, Ben Lambert, Charlie Whittaker, Christian Morgenstern, Cyril Geismar, Dariya Nikitin, David Jorgensen, Ed Knock, Ettie Unwin, Gina Cuomo-Dannenburg, Hayley Thompson, Isobel Routledge, Janetta Skarp, Joseph Hicks, Keith Fraser, Kelly Charniga, Kelly McCain, Lily Geidelberg, Lorenzo Cattarino, Mara Kont, Marc Baguelin, Natsuko Imai, Nima Moghaddas, Patrick Doohan, Rebecca Nash, Ruth McCabe, Sabine van Elsland, Sangeeta Bhatia, Sreejith Radhakrishnan, Zulma Cucunuba Perez and Jack Wardle. 2024. "Marburg Virus Disease Outbreaks, Mathematical Models, and Disease Parameters: a Systematic Review." *The Lancet Infectious Diseases* 24(5):e307–e317.

Dipoppa, Gemma, Guy Grossman and Stephanie Zonszein. 2022. "Locked Down, Lashing Out: COVID-19 Effects on Asian Hate Crimes in Italy." *The Journal of Politics* .

Dube, Oeindrila and Juan F. Vargas. 2013. "Commodity Price Shocks and Civil Conflict: Evidence from Colombia." *Review of Economic Studies* 80(4):1384–1421.

Ergönül, Önder. 2006. "Crimean-Congo haemorrhagic fever." *The Lancet Infectious Diseases* 6(4):203–214.

Farzanegan, Mohammad Reza and Hassan F. Gholipour. 2023. "COVID-19 Fatalities and Internal Conflict: Does Government Economic Support Matter?" *European Journal of Political Economy* 78:102368.

Fazal, Tanisha M. 2020. "Health Diplomacy in Pandemical Times." *International Organization* 74(S1):E78–E97.

Fearon, James D. 1995. "Rationalist Explanations for War." *International Organization* 49(3):379–414.

Fearon, James D. and David D. Laitin. 2003. "Ethnicity, Insurgency, and Civil War." *American Political Science Review* 97(1):75–90.

Feldmann, Heinz, Armand Sprecher and Thomas W. Geisbert. 2020. "Ebola." *New England Journal of Medicine* 382(19):1832–1842.

GADM. 2024. "Global Administrative Areas Database (GADM), Version 4.1.". Accessed: 2025. **URL:** *https://gadm.org/*

Galula, David. 1964. *Counterinsurgency Warfare*. New York: Praeger.

GBD 2021 Causes of Death Collaborators. 2024. "Global Burden of 288 Causes of Death and Life Expectancy Decomposition in 204 Countries and Territories and 811 Subnational Locations, 1990–2021: a Systematic Analysis for the Global Burden of Disease Study 2021." *The Lancet* 403(10440):2100–2132.

Ge, Zoe. forthcoming. "Empowered by Information: Disease Outbreak Reporting at the World Health Organization." *Journal of Politics* . DOI: 10.1086/740814.

Gessain, Antoine, Emmanuel Nakoune and Yazdan Yazdanpanah. 2022. "Monkeypox." *New England Journal of Medicine* 387(19):1783–1793.

Ghobarah, Hazem Adam, Paul Huth and Bruce Russett. 2003. "Civil Wars Kill and Maim People—Long After the Shooting Stops." *American Political Science Review* 97(2):189–202.

Gleditsch, Nils Petter, Peter Wallensteen, Mikael Eriksson, Margareta Sollenberg and Håvard Strand. 2002. "Armed Conflict 1946–2001: A New Dataset." *Journal of Peace Research* 39(5):615–637.

Goldfien, Michael, Michael Joseph and Roseanne McManus. 2023. "The Domestic Sources of International Reputation." *American Political Science Review* 117(2):609–628.

Gonzalez-Torres, Ada and Elena Esposito. 2016. Epidemics and Conflict: Evidence from the Ebola Outbreak in Western Africa. SSRN Scholarly Paper ID 3544606.

Grasse, Donald, Melissa Pavlik, Hilary Matfess and Travis B. Curtice. 2021. "Opportunistic Repression: Civilian Targeting by the State in Response to COVID-19." *International Security* 46(2):130–165.

Gregg, Michael, ed. 2008. *Field Epidemiology*. 3rd ed. ed. Oxford; New York: Oxford University Press.

GRID3 and OCHA. 2022. "DRC Health Zone and Health Area Boundaries.". Humanitarian Data Exchange. Accessed: 2025.
URL: *https://data.humdata.org/dataset/drc-health-data*

Gurr, Ted Robert. 2010. *Why Men Rebel*. 40th anniversary ed. Boulder, Colo.: Paradigm Publishers.

Harris, J. Andrew and Daniel N. Posner. 2019. "(Under What Conditions) Do Politicians Reward Their Supporters? Evidence from Kenya's Constituencies Development Fund." *American Political Science Review* 113(1):123–139.

Hendrix, Cullen S. 2010. "Measuring State Capacity: Theoretical and Empirical Implications for the Study of Civil Conflict." *Journal of Peace Research* 47(3):273–285.

Herbst, Jeffrey. 2014. *States and Power in Africa: Comparative Lessons in Authority and Control*. Princeton Studies in International History and Politics 2nd ed. Princeton, NJ: Princeton University Press.

Hoover Green, Amelia and Dara Kay Cohen. 2021. "Centering Human Subjects: The Ethics of "Desk Research" on Political Violence." *Journal of Global Security Studies* 6(2):ogaa029.

Huff, Connor. 2024. "Counterinsurgency Tactics, Rebel Grievances, and Who Keeps Fighting." *American Political Science Review* 118(1):475–480.

Ide, Tobias. 2021. "COVID-19 and Armed Conflict." *World Development* 140:105355.

Ilunga Kalenga, Oly, Matshidiso Moeti, Annie Sparrow, Vinh-Kim Nguyen, Daniel Lucey and Tedros A Ghebreyesus. 2019. "The Ongoing Ebola Epidemic in the Democratic Republic of Congo, 2018–2019." *New England Journal of Medicine* 381(4):373–383.

International Medical Corps. 2020. "716 Days: How We Helped End DRC's Largest Ebola Outbreak.".
URL: *https://internationalmedicalcorps.org/story/716-days/*

Jaro, Matthew A. 1989. "Advances in Record-Linkage Methodology as Applied to Matching the 1985 Census of Tampa, Florida." *Journal of the American Statistical Association* 84(406):414–420.

Kalyvas, Stathis N. 2006. *The Logic of Violence in Civil War*. Cambridge studies in comparative politics Cambridge ; New York: Cambridge University Press.

Kennedy, Edward H. 2019. "Nonparametric Causal Effects Based on Incremental Propensity Score Interventions." *Journal of the American Statistical Association* 114(526):645–656.

King, Gary and Mitsuru Mukaigawara. 2025. "Survey Estimates of Wartime Mortality." Working Paper.
URL: *https://gking.harvard.edu/sibs*

Knuth, Donald E. 1973. *The Art of Computer Programming, Volume 3: Sorting and Searching*. Reading, MA: Addison-Wesley.

Koehnlein, Britt and Ore Koren. 2022. "COVID-19, State Capacity, and Political Violence by Non-state Actors." *Journal of Peace Research* 59(1):90–104.

Koos, Carlo and Richard Traunmüller. 2025. "The Gendered Costs of Stigma: How Experiences of Conflict-Related Sexual Violence Affect Civic Engagement for Women and Men." *American Journal of Political Science* 69(2):763–778.

Koren, Ore and Kaderi Noagah Bukari. 2024. "(Re)Emerging Disease and Conflict Risk in Africa, 1997–2019." *Nature Human Behaviour* 8(8):1506–1513.

Koren, Ore and Nils B. Weidmann. 2025. "Infectious Disease Outbreaks Drive Political Mistrust." *PNAS* 122(29):e2506093122.

Koubi, Vally. 2019. "Climate Change and Conflict." *Annual Review of Political Science* 22:343–360.

Kustra, Tyler. 2017. "HIV/AIDS, Life Expectancy, and the Opportunity Cost Model of Civil War." *Journal of Conflict Resolution* 61(10):2130–2157.

Lee, Melissa M. 2020. *Crippling Leviathan: How Foreign Subversion Weakens the State*. Ithaca, New York: Cornell University Press.

Lee, Melissa M. and Nan Zhang. 2017. "Legibility and the Informational Foundations of State Capacity." *The Journal of Politics* 79(1):118–362.

Lindsey, Summer. 2022. "Conflict, Protection, and Punishment: Repercussions of Violence in Eastern DR Congo." *American Journal of Political Science* 66(1):187–204.

Longdon, Ben, Michael A. Brockhurst, Colin A. Russell, John J. Welch and Francis M. Jiggins. 2014. "The Evolution and Genetics of Virus Host Shifts." *PLoS Pathogens* 10(11):e1004395.

Lyall, Jason. 2019. "Civilian Casualties, Humanitarian Aid, and Insurgent Violence in Civil Wars." *International Organization* 73(4):901–926.

Mackenzie, John S., Patrick Drury, Ray R. Arthur, Michael J. Ryan, Thomas Grein, Raphael Slattery, Sameera Suri, Christine Tiffany Domingo and Armand Bejtullahu. 2014. "The Global Outbreak Alert and Response Network." *Global Public Health* 9(9):1023–1039.

Médecins Sans Frontières. 2019. "Crisis Update — Ebola Outbreak in DRC.". Multiple updates, 2018–2020.
URL: *https://www.msf.org/drc-ebola-outbreak-crisis-update*

Medley, Alexandra M, Oscar Mavila, Issa Makumbi, Felicien Nizeyemana, Angela Umutoni, Hélène Balisanga, Yona Kenyi Manoah, Aimee Geissler, Sudhir Bunga, Gene MacDonald, Jaco Homsy, Joseph Ojwang, Raimi Ewetola, Pratima L Raghunathan, Amanda MacGurn, Kimberly Singler, Sarah Ward, Shahrokh Roohi, Vance Brown, Trevor Shoemaker, Richard Lako, Adeline Kabeja, Allan Muruta, Leopold Lubula and Rebecca Merrill. 2020. "Case Definitions Used During the First 6 Months of the 10th Ebola Virus Disease Outbreak in the Democratic Republic of the Congo - Four Neighboring Countries, August 2018–February 2019." *Morbidity and Mortality Weekly Report* 69(1):14–19.

Michaud, Joshua, Kellie Moss, Derek Licina, Ron Waldman, Adam Kamradt-Scott, Maureen Bartee, Matthew Lim, Jamie Williamson, Frederick Burkle, Christina S Polyak, Nicholas Thomson, David L Heymann and Louis Lillywhite. 2019. "Militaries and Global Health: Peace, Conflict, and Disaster Response." *The Lancet* 393(10168):276–286.

Monath, Thomas P. 2001. "Yellow fever: an update." *The Lancet Infectious Diseases* 1(1):11–20.

Monogan, James E., David M. Konisky and Neal D. Woods. 2017. "Gone with the Wind: Federalism and the Strategic Location of Air Polluters." *American Journal of Political Science* 61(2):257–270.

Moore, Sean M., Andrew S. Azman, Benjamin F. Zaitchik, Eric D. Mintz, Joan Brunkard, Dominique Legros, Alexandra Hill, Heather McKay, Francisco J. Luquero, David Olson and Justin Lessler. 2017. "El Niño and the shifting geography of cholera in Africa." *Proceedings of the National Academy of Sciences* 114(17):4436–4441.

MPSMRM/Congo, MSP/Congo and ICF International. 2014. "Enquête Démographique et de Santé en République Démocratique du Congo 2013-2014.".

Mukaigawara, Mitsuru, Amanda Smith and Christopher Murray. 2026. "The Scourge of War: Health Forecasts for Nuclear War, Conventional War, and Political Violence, 2026–2100." Working Paper.

Mukaigawara, Mitsuru, Georgia Papadogeorgou, Jason Lyall and Kosuke Imai. 2023. "geocausal: An R Package for Spatio-temporal Causal Inference." Working Paper.

Mukaigawara, Mitsuru, Kosuke Imai, Jason Lyall and Georgia Papadogeorgou. 2025. "Spatiotemporal Causal Inference with Arbitrary Spillover and Carryover Effects: Airstrikes and Insurgent Violence in the Iraq war." arXiv Preprint.
URL: *https://arxiv.org/abs/2504.03464*

Mulangu, Sabue, Lori E. Dodd, Richard T. Davey, Olivier Tshiani Mbaya, Michael Proschan, Daniel Mukadi, Mariano Lusakibanza Manzo, Didier Nzolo, Antoine Tshomba Oloma, Augustin Ibanda et al. 2019. "A Randomized, Controlled Trial of Ebola Virus Disease Therapeutics." *New England Journal of Medicine* 381(24):2293–2303.

Murray, Christopher J.L and Alan D Lopez. 2013. "Measuring the Global Burden of Disease." *New England Journal of Medicine* 369(5):448–457.

Narang, Neil. 2015. "Assisting Uncertainty: How Humanitarian Aid can Inadvertently Prolong Civil War." *International Studies Quarterly* 59(1):184–195.

Nathan, Noah L. 2023. *The Scarce State: Inequality and Political Power in the Hinterland*. Cambridge studies in comparative politics Cambridge ; New York, NY: Cambridge University Press.

Neumayer, Eric, Katharina Gabriela Pfaff and Thomas Plümper. 2023. "Protest against COVID-19 Containment Policies in European Countries." *Journal of Peace Research* 61(3):398–412.

Nielsen, Richard A., Michael G. Findley, Zachary S. Davis, Tara Candland and Daniel L. Nielson. 2011. "Foreign Aid Shocks as a Cause of Violent Armed Conflict." *American Journal of Political Science* 55(2):219–232.

Novaes, Lucas M. and Luis Schiumerini. 2022. "Commodity Shocks and Incumbency Effects." *British Journal of Political Science* 52(4):1689–1708.

OpenStreetMap Contributors. 2024. "Nominatim: Open-Source Search Engine for OpenStreetMap Data.". Accessed: 2025.
URL: *https://nominatim.org/*

Papadogeorgou, Georgia, Kosuke Imai, Jason Lyall and Fan Li. 2022. "Causal Inference with Spatio-temporal Data: Estimating the Effects of Airstrikes on Insurgent Violence in Iraq." *Journal of the Royal Statistical Society. Series B, Statistical methodology* 84(5):1969–1999.

Pebesma, Edzer. 2018. "Simple Features for R: Standardized Support for Spatial Vector Data." *The R Journal* 10(1):439–446.

Petersen, Lyle R, Denise J Jamieson, Ann M Powers and Margaret A Honein. 2016. "Zika virus." *New England Journal of Medicine* 374(16):1552–1563.

Petersen, Roger Dale. 2002. *Understanding Ethnic Violence: Fear, Hatred, and Resentment in Twentieth-century Eastern Europe*. Cambridge studies in comparative politics Cambridge: Cambridge University Press.

Pigott, David M, Aniruddha Deshpande, Ian Letourneau, Chloe Morozoff, Robert C Reiner, Moritz U G Kraemer, Shannon E Brent, Isaac I Bogoch, Kamran Khan, Molly H Biehl, Roy Burstein, Lucas Earl, Nancy Fullman, Jane P Messina, Adrian Q N Mylne, Catherine L Moyes, Freya M Shearer, Samir Bhatt, Oliver J Brady, Peter W Gething, Daniel J Weiss, Andrew J Tatem, Luke Caley, Tom De Groeve, Luca Vernaccini, Nick Golding, Peter Horby, Jens H Kuhn, Sandra J Laney, Edmond Ng, Peter Piot, Osman Sankoh, Christopher J L Murray and Simon I Hay. 2017. "Local, National, and Regional Viral Haemorrhagic Fever Pandemic Potential in Africa: a Multistage Analysis." *The Lancet* 390(10113):2662–2672.

Pigott, David M, Nick Golding, Adrian Mylne, Zhi Huang, Andrew J Henry, Daniel J Weiss, Oliver J Brady, Moritz UG Kraemer, David L Smith, Catherine L Moyes, Samir Bhatt, Peter W Gething, Peter W Horby, Isaac I Bogoch, John S Brownstein, Sumiko R Mekaru, Andrew J Tatem, Kamran Khan and Simon I Hay. 2014. "Mapping the Zoonotic Niche of Ebola Virus Disease in Africa." *eLife* 3:e04395.

Post, Jerrold M. 2005. "When Hatred is Bred in the Bone: Psycho-cultural Foundations of Contemporary Terrorism." *Political Psychology* 26(4):615–636.

Powell, Robert. 2006. "War as a Commitment Problem." *International Organization* 60(1):169–203.

Prentice, Michael B and Lila Rahalison. 2007. "Plague." *The Lancet* 369(9568):1196–1207.

Price-Smith, Andrew T. 2008. *Contagion and Chaos: Disease, Ecology, and National Security in the Era of Globalization*. Cambridge, MA: The MIT Press.

Racaniello, Vincent R. 2006. "One hundred years of poliovirus pathogenesis." *Virology* 344(1):9–16.

Raleigh, Clionadh, Andrew Linke, Håvard Hegre and Joakim Karlsen. 2010. "Introducing ACLED: an Armed Conflict Location and Event Dataset." *Journal of Peace Research* 47(5):651–660.

Rosenbaum, Paul R. 2002. *Observational Studies*. 2nd ed. New York: Springer.

Sauter, Melanie. 2024. "Politicized Health Emergencies and Violent Resistance Against Healthcare Responders." *Journal of Peace Research* 61(4):513–528.

Savun, Burcu and Daniel C. Tirone. 2011. "Foreign Aid, Democratization, and Civil Conflict: How Does Democracy Aid Affect Civil Conflict?" *American Journal of Political Science* 55(2):233–246.

Sawyer, Donald R. 1987. *Malaria on the Amazon Frontier: Economic and Social Aspects of Transmission and Control*. Relatorio de pesquisa Belo Horizonte: Centro de Desenvolvimento e Planejamento Regional, Faculdade de Ciencias Economicas-UFMG.

Schoenberg, Frederic P. 2003. "Multidimensional Residual Analysis of Point Process Models for Earthquake Occurrences." *Journal of the American Statistical Association* 98(464):789–795.

Schroeder, Wilfrid, Patricia Oliva, Louis Giglio and Ivan A. Csiszar. 2014. "The New VIIRS 375m Active Fire Detection Data Product: Algorithm Description and Initial Assessment." *Remote Sensing of Environment* 143:85–96.

Scott, James C. 1998. *Seeing Like a State: How Certain Schemes to Improve the Human Condition Have Failed*. 1 ed. New Haven: Yale University Press.

Sexton, Renard. 2016. "Aid as a Tool against Insurgency: Evidence from Contested and Controlled Territory in Afghanistan." *American Political Science Review* 110(4):731–749.

Stanton, Jessica A. 2016. *Violence and Restraint in Civil War: Civilian Targeting in the Shadow of International Law*. Cambridge University Press.

Stephens, David S, Brian Greenwood and Petter Brandtzaeg. 2007. "Epidemic meningitis, meningococcaemia, and *Neisseria meningitidis*." *The Lancet* 369(9580):2196–2210.

Taty, Nadège, Didier Bompangue, Sandra Moore, J. J. Muyembe and Nancy Meschinet de Richemond. 2024. "Spatiotemporal dynamics of cholera hotspots in the Democratic Republic of the Congo from 1973 to 2022." *BMC Infectious Diseases* 24(1):360–14.

Tilly, Charles. 1990. *Coercion, Capital, and European States, AD 990-1990*. Studies in social discontinuity Oxford, UK : Cambridge, Mass., USA: B. Blackwell.

Trinquier, Roger. 1964. *Modern Warfare*. New York: Praeger.

UNICEF. 2019. "DR Congo Ebola Situation Reports.". Multiple situation reports, 2018–2020.
URL: *https://www.unicef.org/drcongo/en/reports/situation-reports-ebola*

Uyeki, Timothy M, David S Hui, Maria Zambon, David E Wentworth and Arnold S Monto. 2022. "Influenza." *The Lancet* 400(10353):693–706.

van der Loo, Mark P. J. 2014. "The Stringdist Package for Approximate String Matching." *The R Journal* 6(1):111–122.

Voigtländer, Nico and Hans-Joachim Voth. 2012. "Persecution Perpetuated: The Medieval Origins of Anti-Semitic Violence in Nazi Germany." *Quarterly Journal of Economics* 127(3):1339–1392.

Weinstein, Jeremy M. 2007. *Inside Rebellion: the Politics of Insurgent Violence*. Cambridge studies in comparative politics Cambridge ; New York: Cambridge University Press.

Wiersinga, W Joost, Andrew Rhodes, Allen C Cheng, Sharon J Peacock and Hallie C Prescott. 2020. "Pathophysiology, transmission, diagnosis, and treatment of coronavirus disease 2019 (COVID-19): a review." *JAMA* 324(8):782–793.

Winkler, William E. 1990. String Comparator Metrics and Enhanced Decision Rules in the Fellegi-Sunter Model of Record Linkage. Technical report U.S. Bureau of the Census, Statistical Research Division. Research Report RR-93/07.

Wood, Reed, Gina Yannitell Reinhardt, Babak RezaeeDaryakenari and Leah C Windsor. 2022. "Resisting Lockdown: The Influence of COVID-19 Restrictions on Social Unrest." *International Studies Quarterly* 66(2):sqac015.

Wood, Reed M. 2014. "Opportunities to Kill or Incentives for Restraint? Rebel Capabilities, the Origins of Support, and Civilian Victimization in Civil War." *Conflict Management and Peace Science* 31(5):461–480.

World Health Organization. 2014. Case Definition Recommendations for Ebola or Marburg Virus Diseases. Technical report WHO/EVD/CaseDef/14.1 World Health Organization. Accessed: 2025-10-19.
URL: *https://www.who.int/publications/i/item/WHO-EVD-CaseDef-14.1*

World Health Organization. 2020. "Ebola Virus Disease — Democratic Republic of the Congo: External Situation Reports.". Reports 1–79, August 2018 – February 2020.
URL: *https://www.who.int/emergencies/diseases/ebola/drc-2019/situation-reports*

World Health Organization. 2024. "Health System in the Democratic Republic of the Congo: Current Situation and Challenges.". Health zones are the primary operational unit of DRC disease surveillance.
URL: *https://www.who.int/countries/cod*

Zhou, Lingxiao, Kosuke Imai, Jason Lyall and Georgia Papadogeorgou. 2024. "Estimating Heterogeneous Treatment Effects for Spatio-Temporal Causal Inference." arXiv Preprint.
URL: *https://arxiv.org/abs/2412.15128*

Zhukov, Yuri M. 2012. "Roads and the diffusion of insurgent violence: The logistics of conflict in Russia's North Caucasus." *Political Geography* 31(3):144–156.

Zumla, Alimuddin, David S Hui and Stanley Perlman. 2015. "Middle East respiratory syndrome." *The Lancet* 386(9997):995–1007.

Supplementary Information for

"The Containment Trap: How Efforts to Contain Epidemics Intensify Civil Conflict"

Mitsuru Mukaigawara

A Spatiotemporal Causal Inference Design

In this section, I introduce formal definitions of the causal estimands, assumptions, and estimators for average treatment effects (ATE), heterogeneous treatment effects, and causal mediation analysis. In so doing, I closely follow Mukaigawara et al. (2025). Full technical details of the ATE, heterogeneity, mediation framework are provided in Papadogeorgou et al. (2022), Zhou et al. (2024), and Mukaigawara et al. (2025), respectively. This appendix closely follows Mukaigawara et al. (2025).

A.1 Average Treatment Effects

Causal estimands The causal estimands for the ATE represent the difference in the expected number of political violence events in a given region and time period under two different stochastic interventions. In the patient-level setting, one such estimand is the expected daily counts of lethal violence against civilians when Ebola cases are concentrated in frontier regions, compared with when they are concentrated in central regions. Rather than assigning a binary treatment to discretized spatial units, I employ a stochastic intervention framework in which treatment is represented as a time series of density maps (e.g., density maps of Ebola patient locations).

Formally, I first define the expected number of political violence events in a certain region B and time period t under a certain stochastic intervention F as follows (Papadogeorgou et al., 2022),

$$\boldsymbol{N}_{Bt}(F, L) = \int_{\mathcal{W}} \cdots \int_{\mathcal{W}} N_B\left(Y_t(\overline{\boldsymbol{W}}_{t-L}, w_{t-L+1}, \cdots, w_t)\right) \mathrm{d}F(w_{t-L+1}) \cdots \mathrm{d}F(w_t), \tag{1}$$

where B is the region of interest (e.g., northeast DRC) within the full geographic space Ω (entire DRC); F is a stochastic intervention (e.g., a distribution placing more patients in the frontier, encoded as a time series of maps); L is the number of intervened periods (e.g., days); $N_B(\cdot)$ is the count of outcome events in region B; $\overline{\boldsymbol{W}}_{t-L}$ is the observed treatment history during the pre-intervention period up to $t-L$; and w_t denotes the intervention at time t. In words, $\boldsymbol{N}_{Bt}(F, L)$ is the expected number of political violence events observed in region B at time t after L periods of exposure to the stochastic intervention F.[41]

Notice that $\boldsymbol{N}_{Bt}(F, L)$ is defined for a single time period $t \in \{1, \ldots, T\}$ under a single intervention F. To obtain a causal effect, we take the temporal average of these period-specific quantities and then compare the resulting averages across interventions. Formally, the temporal average of

[41] The integral yields an expected count measure because we employ a Poisson point process. See Papadogeorgou et al. (2022) and Mukaigawara et al. (2025) for details.

$\boldsymbol{N}_{Bt}(F, L)$ is defined as

$$\boldsymbol{N}_B(F, L) = \frac{1}{T - L + 1} \sum_{t=L}^{T} \boldsymbol{N}_{Bt}(F, L) \tag{2}$$

and the comparison between two interventions F' and F'' is defined as,

$$\tau_B(F', F'', L) = \boldsymbol{N}_B(F', L) - \boldsymbol{N}_B(F'', L). \tag{3}$$

For example, F' represents a stochastic intervention that shifts more patients into frontier regions, while F'' represents one that shifts patients into central regions. Equation (3) therefore captures the effect of epidemics in the frontier relative to epidemics in the center.

Causal assumptions The identification strategy relies on unconfoundedness and overlap assumptions. The unconfoundedness assumption requires that the treatment point pattern at each time period is conditionally independent of all potential outcomes, given the observed history of past treatments. In practice, it means that the treatment assignment is random given observed covariates. Formally, the following equation should hold:

$$f(W_t \mid \overline{\boldsymbol{W}}_{t-1}, \overline{\mathcal{Y}}_T, \overline{\mathcal{X}}_T) \;=\; f(W_t \mid \overline{H}_{t-1})$$

where $\overline{\mathcal{Y}}_T$ represents the collection of potential outcomes for all time periods and treatment sequences; $\overline{\mathcal{X}}_T$ denotes the collection of potential values of covariates for all time periods and treatment sequences; and $\overline{H}_{t-1} = \{\overline{\boldsymbol{W}}_{t-1}, \overline{\boldsymbol{Y}}_{t-1}, \overline{\boldsymbol{X}}_t\}$.

The overlap assumption states that the probability of observing hypothetical treatment patterns under the stochastic intervention is non-zero, and thus the counterfactual interventions that we design are realistic. Formally, there exists a positive constant δ such that

$$\frac{f(w \mid \overline{H}_{t-1})}{e_t(w)} > \delta$$

for all $w \in \mathcal{W}$, where $e_t(w) = f(W_t = w \mid \overline{H}_{t-1})$ represents the propensity score at time t.

Estimators Under these assumptions, the estimand is identified by an inverse probability of treatment weighting (IPW) estimator with two components: weights and spatially smoothed outcomes. The weights quantify how likely the realized treatment pattern is under the intervention F relative to its propensity under the observed data-generating process. Formally, the weight assigned to time

period t under intervention F is

$$\zeta_t(F, L) = \prod_{t'=t-L+1}^{t} \frac{f(W_{t'})}{e_{t'}(W_{t'})}. \tag{4}$$

In words, the overall weight is the product of time-specific weights, each of which reflects how likely the realized treatment pattern would be under the hypothetical intervention relative to its likelihood under the observed data (the propensity score).

Additionally, using kernel smoothing, the spatially-smoothed outcome at time t is given by,

$$\widetilde{Y}_t(\omega) = \sum_{s \in S_{Y_t}} K_b(||\omega - s||),\ \omega \in \Omega,$$

with $K_b(u) = b^{-1}K(u/b)$ being a kernel; b representing a bandwidth parameter b; and $||\cdot||$ representing the Euclidean norm.

A combination of weights and spatially-smoothed outcomes defines the weighted smoothed outcome surface $\widehat{Y}_t : \Omega \to \mathbb{R}^+$ as $\widehat{Y}_t(F, L; \omega) = \zeta_t(F, L)\widetilde{Y}_t(\omega)$. Integrating the weighted smoothed outcome surface over region B gives us the estimators of $\boldsymbol{N}_{Bt}(F, L)$, its temporal average $\boldsymbol{N}_B(F, L)$, and $\tau_B(F', F'', L)$:

$$\widehat{\boldsymbol{N}}_{Bt}(F, L) = \int_B \widehat{Y}_t(F, L; \omega) \mathrm{d}\omega, \tag{5}$$

$$\widehat{\boldsymbol{N}}_B(F, L) = \frac{1}{T - L + 1} \sum_{t=L}^{T} \widehat{\boldsymbol{N}}_{Bt}(F, L), \tag{6}$$

$$\widehat{\tau}(F', F'', L) = \widehat{\boldsymbol{N}}_B(F', L) - \widehat{\boldsymbol{N}}_B(F'', L). \tag{7}$$

Because the IPW estimator might become unstable when propensity scores are small, I employ its normalized analog, the Hájek estimator, throughout this article.

A.2 Heterogeneous Treatment Effects

Causal estimands To examine effect heterogeneity, I estimate causal effects at the pixel level. The pixel-level conditional ATE (CATE) is then aggregated by averaging within levels of the moderator. I characterize the relationship between pixel-level CATEs and the moderator using a linear projection and then average these effects across time periods (Zhou et al., 2024).

Formally, I first partition the entire space of interest Ω into p disjoint pixels: $\boldsymbol{Q} = \{Q_1, \cdots, Q_p\}$. Then, the pixel-level CATE of pixel $i \in \{1, 2, \cdots, p\}$ and the comparison between two interventions

are defined as,

$$\boldsymbol{N}_{it}(F, L) = \int_{\mathcal{W}} \cdots \int_{\mathcal{W}} N_{Q_i}\Big(Y_t(\overline{\boldsymbol{W}}_{t-L}, w_{t-L+1}, \cdots, w_t)\Big) \mathrm{d}F(w_{t-L+1}) \cdots \mathrm{d}F(w_t),$$
$$\tau_{it}(F', F'', L) = \boldsymbol{N}_{it}(F', L) - \boldsymbol{N}_{it}(F'', L).$$

I then take the average of $\tau_{it}(F', F'', L)$ for each moderator value. Let $\boldsymbol{R}_{it} \in \mathcal{R}$ be the vector-value of the potential moderator in pixel Q_i at time t. Then, the average of pixel-level CATEs for a given moderator value $\boldsymbol{r} \in \mathcal{R}$ is defined as,

$$\tau_t(F', F'', L; \boldsymbol{r}) = \frac{1}{\sum_{i=1}^{p} I(\boldsymbol{R}_{i,t-L+1} = \boldsymbol{r})} \sum_{i=1}^{p} \tau_{it}(F', F'', L) I(\boldsymbol{R}_{i,t-L+1} = \boldsymbol{r}), \tag{8}$$

where I denotes the indicator function.

The next step is to regress the average pixel-level CATEs on moderator values, which yields the time-specific projection estimand, $\tilde{\tau}_t(F', F'', L; \boldsymbol{R}_{t-L+1}, \boldsymbol{\beta}_t^*)$, where

$$\boldsymbol{\beta}_t^* = \arg\min_{\boldsymbol{\beta}_t} \sum_{i=1}^{p} \left(\tau_t(F', F'', L; \boldsymbol{R}_{i,t-L+1}) - \tilde{\tau}_t(F', F'', L; \boldsymbol{R}_{i,t-L+1}, \boldsymbol{\beta}_t)\right)^2$$

with the following projection model that minimizes the mean square error,

$$\tilde{\tau}_t(F', F'', L; \boldsymbol{r}, \boldsymbol{\beta}_t) = \sum_{k=1}^{K} \beta_{tk} z_k(\boldsymbol{r}) = \boldsymbol{z}(\boldsymbol{r})^\top \boldsymbol{\beta}_t$$

with known functions $\boldsymbol{z}(\boldsymbol{r}) = [z_1(\boldsymbol{r}), \cdots, z_K(\boldsymbol{r})]^\top$. The temporal average is then given by,

$$\tilde{\tau}(F', F'', L; \boldsymbol{r}, \boldsymbol{\beta}_L^*, \cdots \boldsymbol{\beta}_T^*) = \frac{1}{T - L + 1} \sum_{t=L}^{T} \tilde{\tau}_t(F', F'', L; \boldsymbol{R}_{i,t-L+1} = \boldsymbol{r}, \boldsymbol{\beta}_t^*).$$

Causal assumptions and estimators To estimate heterogeneous treatment effects, I rely on the unconfoundedness and overlap assumptions for the ATE. Under these assumptions, I apply Equations (5) and (7) to pixel Q_i as follows,

$$\widehat{\boldsymbol{N}}_{it}(F, L) = \int_{Q_i} \widehat{Y}_t(F, L; \omega) \mathrm{d}\omega, \quad \text{and} \quad \widehat{\tau}_{it}(F', F'', L) = \widehat{\boldsymbol{N}}_{it}(F', L) - \widehat{\boldsymbol{N}}_{it}(F'', L).$$

Then the coefficient estimates are obtained by,

$$\widehat{\boldsymbol{\beta}}_t = \arg\min_{\boldsymbol{\beta}_t} \big(\widehat{\boldsymbol{\tau}}_t - \boldsymbol{Z}_t\boldsymbol{\beta}_t\big)^\top \big(\widehat{\boldsymbol{\tau}}_t - \boldsymbol{Z}_t\boldsymbol{\beta}_t\big),$$

with $\widehat{\boldsymbol{\tau}}_t = (\widehat{\tau}_{1t}(F', F'', L), \cdots \widehat{\tau}_{pt}(F', F'', L))^\top$ representing the vector of causal effect estimators; and $\boldsymbol{Z}_t = [\boldsymbol{z}(\boldsymbol{R}_{1,t-L+1}), \cdots, \boldsymbol{z}(\boldsymbol{R}_{p,t-L+1})]^\top$ denoting the matrix of p moderators. The projection CATE estimator is then obtained as follows:

$$\widehat{\tau}^{\text{Proj.}}_{F',F''}(\boldsymbol{r}; \boldsymbol{\beta}^*_L, \cdots \boldsymbol{\beta}^*_T) = \boldsymbol{z}(\boldsymbol{r})^\top \Big(\frac{1}{T-L+1}\sum_{t=L}^{T} \widehat{\boldsymbol{\beta}}_t\Big).$$

Normalizing the weights produces Hájek estimators.

A.3 Causal Mediation Analysis

Causal estimands Causal estimands for mediation analysis are defined analogously to those for the ATE, with the key difference that the mediator is now incorporated. Let $M_t(s)$ denote the mediator at location $s \in \Omega$. For simplicity, I consider a binary mediator $M_t(s) \in \mathcal{M} = \{0, 1\}$ indicating the presence of a symptom (e.g., hemorrhage). Let $M_t = \{M_t(s) : s \in \Omega\}$ denote the collection of mediator values across all locations, with its realization m_t, and let the mediator history be $\overline{\boldsymbol{M}}_t = (M_1, M_2, \ldots, M_t)$ with realized history $\overline{\boldsymbol{m}}_t$. With these definitions, Equations (1), (2), and (3) can be redefined to incorporate the mediator as follows,

$$\begin{aligned}
\boldsymbol{N}^{\text{med}}_{Bt}(F, L) = &\int_{(\mathcal{W},\mathcal{M})} \cdots \int_{(\mathcal{W},\mathcal{M})} N_B\Big(Y_t(\overline{\boldsymbol{W}}_{t-L}, \overline{\boldsymbol{M}}_{t-L}, w_{t-L+1}, m_{t-L+1}, \ldots, w_t, m_t)\Big) \\
&\qquad \mathrm{d}F(w_{t-L+1}, m_{t-L+1}) \cdots \mathrm{d}F(w_t, m_t), \\
\boldsymbol{N}^{\text{med}}_{B}(F, L) = &\frac{1}{T-L+1}\sum_{t=L}^{T} \boldsymbol{N}^{\text{med}}_{Bt}(F, L), \\
\tau^{\text{med}}_{B}(F', F'', L) = &\boldsymbol{N}^{\text{med}}_{B}(F', L) - \boldsymbol{N}^{\text{med}}_{B}(F'', L),
\end{aligned}$$

where two stochastic interventions, $F' = (F'_W, F'_{M|w})$ and $F'' = (F''_W, F''_{M|w})$, jointly specify both the treatment and mediator distributions. These definitions allow us to decompose the total effect into a direct effect, given by changing the treatment distribution while holding the mediator distribution fixed, and an indirect effect, given by changing the mediator distribution while keeping the treatment distribution unchanged.

Causal assumptions and estimators To perform causal mediation analysis, the identification assumptions should change by incorporating the presence of the mediator. In this setup, a stochastic intervention F is redefined as $F = (F_W, F_{M|w})$, with the second element $F_{M|w}$ representing the conditional distribution of the mediator given treatment. Then, the unconfoundedness assumption is equivalent to stating both the treatment and mediator assignment are independent of any potential outcomes and potential values of time-varying confounders given the observed history. Formally, the following two equations should hold:

$$
\begin{aligned}
f(W_t \mid \overline{\boldsymbol{W}}_{t-1}, \overline{\boldsymbol{M}}_{t-1}, \overline{\boldsymbol{y}}_T, \overline{\boldsymbol{X}}_T) &= f(W_t \mid \overline{H}_{t-1}), \\
f(M_t \mid \overline{\boldsymbol{W}}_t, \overline{\boldsymbol{M}}_{t-1}, \overline{\boldsymbol{y}}_T, \overline{\boldsymbol{X}}_T) &= f(M_t \mid W_t, \overline{H}_{t-1}).
\end{aligned}
$$

Next, the overlap assumption is restated by considering the distribution of the mediator. Similarly to the propensity score, let $\rho_t(m) = f(m \mid \overline{H}_{t-1}, W_t)$ represent the mediator score. Then, the assumption states that there exist positive constants δ_W, δ_M such that

$$
\frac{f(w \mid \overline{H}_{t-1})}{e_t(w)} > \delta_W \quad \text{and} \quad \frac{f(m \mid \overline{H}_{t-1}, W_t = w)}{\rho_t(m)} > \delta_M.
$$

for all $w \in \mathcal{W}$ and $m \in \mathcal{M}$.

With the restated assumptions, the causal estimators are defined by incorporating the density ratio of mediators. Formally, consider an intervention $F = (F_W, F_{M|w})$ with corresponding densities $f_W, f_{M|w}$. Then, the weight at time period t is defined as

$$
\xi_t(F, L) = \prod_{t'=t-L+1}^{t} \frac{f_W(W_{t'}) f_{M|W_{t'}}(M_{t'})}{e_{t'}(W_{t'}) \rho_{t'}(M_{t'})}.
$$

Finally, the estimators with mediators are defined by replacing $\zeta_t(F, L)$ in the estimators for ATE by $\xi_t(F, L)$:

$$
\widehat{Y}_t^{\text{med}}(F, L; \omega) = \xi_t(F, L) \widetilde{Y}_t(\omega), \quad \widehat{\boldsymbol{N}}_{Bt}^{\text{med}}(F, L) = \int_B \widehat{Y}_t^{\text{med}}(F, L; \omega) \mathrm{d}\omega,
$$

$$
\widehat{\boldsymbol{N}}_B^{\text{med}}(F, L) = \frac{1}{T - L + 1} \sum_{t=L}^{T} \widehat{\boldsymbol{N}}_{Bt}^{\text{med}}(F, L), \quad \widehat{\tau}_B^{\text{med}}(F', F'', L) = \widehat{\boldsymbol{N}}_B^{\text{med}}(F', L) - \widehat{\boldsymbol{N}}_B^{\text{med}}(F'', L).
$$

I use the Hájek estimator throughout this article, which are asymptotically normal and more efficient than the IPW estimators (Zhou et al., 2024; Mukaigawara et al., 2025).

B Microlevel Data and Context

B.1 Outbreak-level Data

I collect all reliable and available evidence regarding the locations of Ebola, Marburg, cholera, and meningococcal meningitis outbreaks in sub-Saharan Africa. Figure S1 summarizes the literature search strategies. I first collect spatiotemporal information about Ebola, Marburg, cholera, and meningococcal meningitis outbreaks in sub-Saharan Africa from 2011 to 2020 using key published literature (Moore et al., 2017; Cuomo-Dannenburg et al., 2024; Pigott et al., 2014) and the Emergency Events (EM-DAT) Database (see www.emdat.be). The information obtained from the literature is then extended and confirmed by reviewing official sources of the US CDC and WHO, as well as EM-DAT database and published literature.

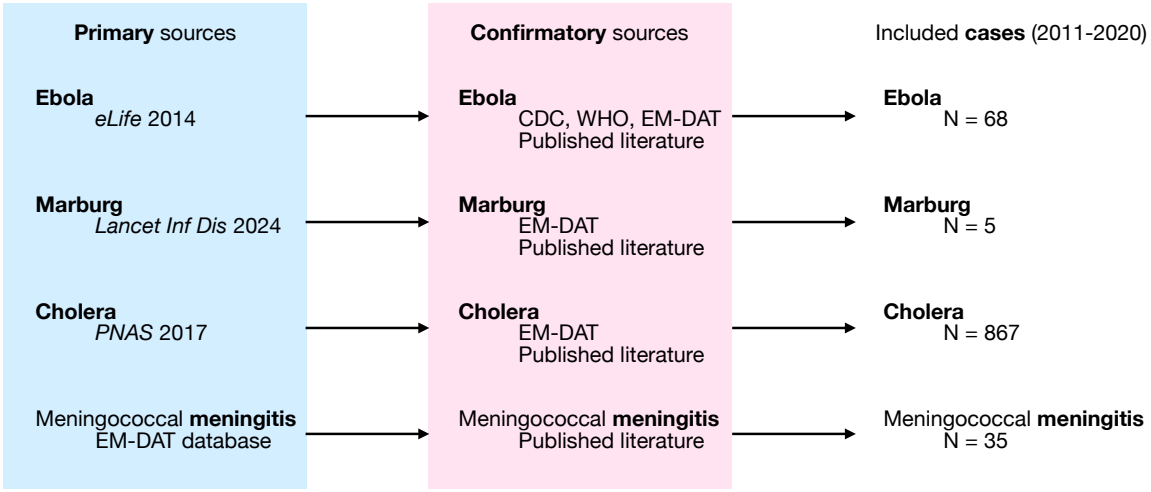

Figure S1: **Search strategies for the outbreak-level data**. Spatiotemporal information about epidemics in sub-Saharan Africa is confirmed by official sources by the US Centers for Disease Control and Prevention (CDC), WHO, EM-DAT database, and published literature.

B.2 Patient-level Line List

Table S1: **Characteristics of Ebola and non-Ebola Patients**. A total of 44,331 Ebola cases and 42,597 non-Ebola cases during the 2018-2020 Ebola outbreak is summarized after excluding cases with no or unreliable geolocation information. Patients determined not to be Ebola cases are also excluded from analyses. Bleeding refers to any internal or external bleeding symptoms. Case definitions follow the WHO's standard case definitions, with confirmed cases requiring laboratory confirmation (positive IgM antibody, positive PCR or viral isolation) (World Health Organization, 2014; Medley et al., 2020).

	All (Ebola) $n = 44,331$	**Confirmed** $n = 3,163$ (7.1%)	**Probable** $n = 136$ (0.3%)	**Suspected** $n = 41,032$ (93%)	**Not Ebola** $n = 42,597$
Age group (years)					
0-9	13,724 (31%)	631 (20%)	41 (30%)	13,052 (32%)	11,637 (28%)
10-19	7,959 (18%)	410 (13%)	15 (11%)	7,534 (18%)	7,825 (19%)
20-29	8,679 (20%)	748 (24%)	22 (16%)	7,909 (19%)	8,871 (21%)
30-39	5,495 (12%)	554 (18%)	17 (13%)	4,924 (12%)	5,325 (13%)
40-49	3,110 (7.1%)	368 (12%)	12 (8.8%)	2,730 (6.7%)	3,112 (7.4%)
50-59	1,960 (4.4%)	240 (7.6%)	13 (9.6%)	1,707 (4.2%)	1,981 (4.7%)
60-69	1,630 (3.7%)	147 (4.6%)	10 (7.4%)	1,473 (3.6%)	1,524 (3.6%)
70-79	924 (2.1%)	52 (1.6%)	3 (2.2%)	869 (2.1%)	983 (2.3%)
80-89	441 (1.0%)	12 (0.4%)	1 (0.7%)	428 (1.1%)	600 (1.4%)
90+	133 (0.3%)	0 (0%)	2 (1.5%)	131 (0.3%)	237 (0.6%)
Gender					
Female	22,605 (51%)	1,805 (57%)	65 (48%)	20,735 (51%)	20,621 (49%)
Male	21,647 (49%)	1,358 (43%)	71 (52%)	20,218 (49%)	21,813 (51%)
Status					
Alive	35,437 (80%)	1,140 (36%)	0 (0%)	34,297 (84%)	34,372 (81%)
Dead	8,793 (20%)	2,023 (64%)	136 (100%)	6,634 (16%)	8,045 (19%)
Symptoms					
Fever	27,621 (67%)	1,940 (68%)	90 (85%)	25,591 (67%)	17,846 (46%)
Bleeding	4,317 (11%)	535 (19%)	58 (49%)	3,724 (9.8%)	3,441 (8.6%)
Headache	22,268 (56%)	1,698 (62%)	59 (66%)	20,511 (56%)	21,696 (58%)
Myalgia	8,655 (23%)	1,025 (40%)	22 (31%)	7,608 (22%)	8,881 (25%)
Dyspnea	5,173 (14%)	428 (17%)	23 (32%)	4,722 (14%)	4,920 (14%)

B.3 Ethical Considerations

The patient-level Ebola data analyzed in this article are operational surveillance records originally compiled by the Democratic Republic of the Congo Ministry of Health, the World Health Organization, and humanitarian medical organizations during the 2018–2020 outbreak response. Harvard University's Institutional Review Board reviewed and approved the study (IRB 23-0440) and granted a waiver of individual consent because the records were collected for public health response, reconsent across 44,331 records from an active conflict zone would be impracticable, and secondary analysis poses minimal incremental risk relative to the original data collection.

The study follows the American Political Science Association's *Principles and Guidance for Human*

Subjects Research, with particular attention to consent, confidentiality, and harm. The records concern a vulnerable population: Ebola patients in a region of protracted civil conflict. Re-identification could expose individuals or households to stigma, retaliation, or denial of services (Hoover Green and Cohen, 2021). To mitigate these risks, direct identifiers, including names and exact addresses, were removed before analysis. No attempt was made to re-identify individuals or households from the surveillance records. Geographic information is reported only as smoothed kernel-density surfaces, and all spatial outputs were reviewed to ensure that maps do not reveal exact case locations. The manuscript and appendix include no individual case narratives or identifying combinations of covariates. The de-identified working dataset is stored on a secure hardware drive and is available only to personnel listed on the IRB protocol.

For replication, I will deposit the materials on the APSR Dataverse, including code, propensity-score specifications, counterfactual definitions, and aggregated outcome counts. The underlying patient-level records and the hyperframes generated from them cannot be publicly redistributed because public release would violate the data-sharing agreement and create unjustifiable re-identification risks. Researchers with appropriate ethical approval may request access through the data-stewarding institution. These protections preserve transparency while limiting risks to individuals and households represented in the surveillance records.

B.4 ACLED Dataset

One key concern for newspaper-based datasets is that reporting frequency may decline during exogenous shocks, including disease epidemics. However, inspection of temporal trends from 1997 to 2020 shows no observable change in the reporting of political violence in Ituri, North Kivu, or South Kivu between 1997–2017 and 2018–2020 (Figure S2).

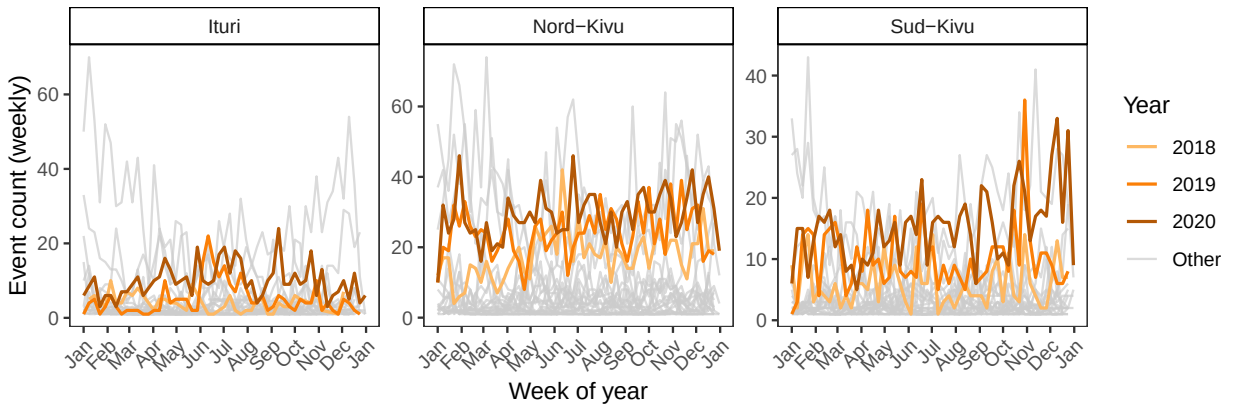

Figure S2: **Trends in ACLED reports in northeast DRC, 1997-2020**. Gray lines show trends for years 1997-2020. All counts are aggregated at the weekly level.

C Data-Generating Process

C.1 Geolocations of Ebola Patients

The line-list data record each patient's residence, location of onset, and locations of hospitals using at most five text fields (country, province (district), health zone (*sous-coordination*), parish (*aire de santé*), and village) but contain no geographic coordinates. I therefore build a geocoding pipeline that assigns latitude–longitude pairs to all patient records. The pipeline proceeds in five stages.

Stage 1. Text normalization. All five location fields are converted to uppercase, trimmed of leading and trailing whitespace, stripped of diacritics and stray special characters (e.g., ?, £, ^{2}), and standardized so that hyphens and slashes are consistently formatted. Literal string "NA" entries are converted to missing values. Compound village names separated by "/" are split into primary and secondary components.

Stage 2. Column misplacement repair. Because the data contain frequent column misplacements,[42] I detect such errors by checking whether values in each column match canonical name sets from the reference gazetteer described below (i.e., the 26 DRC province names from GADM and the 519 health zone names from the GRID3/OCHA shapefile). When a misplacement is detected, the value is shifted to the appropriate column and the source column is corrected (e.g., the country field is set to "RDC"). Missing province values are inferred from the patient's matched health zone using a health zone–to–province lookup derived from the same shapefile, where available.

Stage 3. Hierarchical fuzzy matching. After normalization and repair, each location field is matched against a reference gazetteer. The gazetteer combines two sources: (i) administrative boundary centroids from the Database of Global Administrative Areas (GADM, version 4.1; GADM, 2024) at the province level (26 provinces), and (ii) health zone polygon centroids from the GRID3/OCHA shapefile of 519 DRC health zones (GRID3 and OCHA, 2022). Matching proceeds top-down (i.e., province, then health zone, then parish, then village) so that each resolved level constrains the candidate set for the next (e.g., once a record is matched to province Nord-Kivu, health zone matching is restricted to health zones within Nord-Kivu).

For each level, I apply a matching cascade in the following order.

1. *Exact match* against the canonical name set after text normalization.

[42] For example, province names are entered in the country field, or health zone names are in the province field.

2. *Optimal string alignment* (OSA) distance (van der Loo, 2014), which counts the minimum number of insertions, deletions, substitutions, and transpositions of adjacent characters needed to transform one string into another. I set a maximum edit distance of 3, meaning that a misspelling with up to three character-level errors (e.g., "MABALAKOO" → "MABALAKO," distance 1; "NOORD-KIVU" → "NORD-KIVU," distance 1) is accepted as a match. The threshold of 3 accommodates the most common data-entry errors observed in the line list (single-character duplications, omissions, and transpositions). Because matching at each level is constrained by the parent level already resolved (e.g., health zone candidates are restricted to those within the matched province), the risk of false matches between similarly named health zones in different provinces is mitigated by the hierarchical structure of the pipeline.
3. *Jaro–Winkler similarity* (Winkler, 1990; Jaro, 1989), a normalized measure that gives additional weight to matching prefixes. I require a Jaro–Winkler distance below 0.25 (equivalently, similarity above 0.75).
4. *Soundex phonetic coding* (Knuth, 1973), which maps names to four-character codes based on their English-language pronunciation, capturing phonetically similar variants that may differ substantially in spelling (e.g., "COMANDA" and "KOMANDA" share the same Soundex code).

If all four steps fail, the record is left unmatched at that level and falls back to a coarser geographic resolution in the coordinate assignment step. Health zone matching is the most consequential step because health zones are the primary administrative unit for DRC disease surveillance (World Health Organization, 2024). Each of the 519 health zones belongs to exactly one province, providing a one-to-many mapping that anchors the entire hierarchy.

Stage 4. Coordinate assignment. Coordinates are assigned using a hierarchical fallback: (1) village-level coordinates from the OpenStreetMap/Nominatim geocoding service (OpenStreetMap Contributors, 2024), queried via the `tidygeocoder` R package (Cambon et al., 2021), constrained by health zone and province; (2) health zone polygon centroids from the GRID3/OCHA shapefile (GRID3 and OCHA, 2022); (3) province centroids from GADM (GADM, 2024); and (4) a country-level centroid for records with no subnational information. To avoid redundant API calls, the pipeline first deduplicates queries by unique village–health zone combinations and caches all results for reuse across runs. Importantly, no patient-identifiable information is transmitted to the geocoding API. Queries consist solely of the combinations of village, health zone, and province names that are matched with the existing, publicly-available datasets.

Table S2: **Geographic resolution levels and confidence levels for residence, symptom onset, and current hospital locations.** No data indicates that both village and district names are missing for onset and residence data, or that both hospital and village names are missing for hospital data.

Category		Residence	Onset	Hospital	Past hospital (1)	Past hospital (2)
Level	Village	35,243 (39.8%)	35,339 (40.0%)	35,245 (39.8%)	530 (0.6%)	148 (0.2%)
	Health zone	52,714 (59.6%)	50,994 (57.6%)	11,578 (13.1%)	213 (0.2%)	35 (0.04%)
	Province	235 (0.3%)	360 (0.4%)	1,045 (1.2%)	48,198 (54.5%)	6,156 (7.0%)
	Country	54 (0.06%)	147 (0.2%)	127 (0.1%)	465 (0.5%)	110 (0.1%)
	No data	212 (0.2%)	1,618 (1.8%)	40,463 (45.7%)	39,052 (44.1%)	82,009 (92.7%)
Confidence	High	87,597 (99.0%)	85,424 (96.6%)	46,413 (52.5%)	713 (0.8%)	176 (0.2%)
	Medium	359 (0.4%)	904 (1.0%)	408 (0.5%)	30 (0.03%)	7 (0.008%)
	Low	1 (0.001%)	5 (0.006%)	1,047 (1.2%)	48,198 (54.4%)	6,156 (7.0%)
	Very low	0 (0%)	0 (0%)	127 (0.14%)	465 (0.5%)	110 (0.1%)
	No data	501 (0.6%)	2,125 (2.4%)	40,463 (45.7%)	39,052 (44.1%)	82,009 (92.7%)

Stage 5. Confidence scoring and validation. Each geocoded record receives a composite confidence score (0–100) that summarizes four dimensions of geocoding quality. The *geographic resolution* component (40% of the total score) awards 40 points for village-level coordinates, 20 for health zone centroids, 10 for province centroids, and 0 for the country centroid, reflecting the order-of-magnitude differences in spatial precision across levels (approximately 1 km, 20 km, 100 km, and 500 km, respectively). The *match quality* component (30%) awards 30 points for an exact string match after normalization, 25 for an OSA match at edit distance $\leq$1, 20 for an OSA match at edit distance $\leq$2, 20 for an API-geocoded result, and 5 for a Soundex-only match. The *hierarchy consistency* component (15%) awards 15 points when all resolved administrative levels are mutually consistent (e.g., the matched health zone belongs to the matched province) and 0 when they conflict. The *data completeness* component (15%) awards 3 points for each non-missing location field (out of five), reflecting the amount of information available for geocoding. Records are classified as HIGH ($\geq$75), MEDIUM ($\geq$50), LOW ($\geq$25), or VERY LOW ($<$25). I verify spatial consistency by checking whether each assigned coordinate falls within a DRC health zone polygon using the `sf` R package (Pebesma, 2018).

Results. Three types of location information are transformed by the pipeline described above: patient residences, onset locations, and hospital locations. Hospital locations have up to three inputs, including the current location and at most two past locations.

Residence and onset locations are recorded at high geographic precision, whereas current hospital locations are much coarser (Table S2). Residence and onset locations are overwhelmingly high confidence (99.0% and 96.6%), whereas only 52.5% of current hospital locations are high confidence. Throughout this paper, I only use the high-confidence locations. For hospital data, I construct a combined hospital-location dataset by retaining high-confidence current locations and replacing lower-

confidence observations with high-confidence values from past datasets, first from past hospital (1) and then from past hospital (2).

C.2 Ebola Treatment Centers (ETC)

I compile the coordinates of all 42 Ebola treatment facilities operated during the 2018-2020 Kivu outbreak from Figure S1 of Barks et al. (2025). The facilities comprise three types located across the provinces of Ituri, Nord-Kivu, and Sud-Kivu:

- 21 *centres de transit décentralisés* (CTD; decentralized transit centers mainly in remote areas, with small units embedded within existing healthcare facilities);
- 9 *centres de transit* (CT; transit centers for triage, initial isolation, and stabilization before transfer to CTEs); and
- 12 *centres de traitement Ebola* (CTE; full treatment centers with isolation and treatment capacity and lab testing).

I geocode each facility using OpenStreetMap/Nominatim, GeoNames, and WHO Ebola situation reports. I then cross-validate all coordinates against OpenStreetMap health area boundaries (originally sourced from MSF) and correct cases where the initial geocode fell more than 10 km from the named health area (e.g., Mangina, Butsiri, Makeke). Notably, the CT "Komanda" (a 20-bed MSF transit center) was located at Bwana-Sura health area on the RN4, approximately 35 km south of Komanda town, and is therefore recorded at a distinct location from the CTE at Komanda. After deduplication by unique latitude-longitude pairs, I retain 37 unique locations from the 42 entries (some facilities share sites across types).

Operational dates. To identify when each facility opened and closed, I systematically extract dates from publicly available sources: MSF crisis updates and press releases (Médecins Sans Frontières, 2019), ALIMA operational updates (ALIMA, 2019), WHO External Situation Reports (World Health Organization, 2020), UNICEF Ebola Situation Reports (UNICEF, 2019), IMC operational reports (International Medical Corps, 2020), and academic publications including the PALM trial (Mulangu et al., 2019). For each facility, I record the opening date, closing date, bed capacity, and operating organization where available, and assign a confidence level (high, medium, or low) based on source specificity. High-confidence dates come from sources that explicitly name a facility with a specific date (e.g., "MSF opened a 60-bed transit center in Beni on November 14, 2018"). Medium-confidence dates come from sources that mention a facility in a date-specific context but without an exact opening or closing date (e.g., a facility described as operational in a monthly situation report). Low-confidence entries lack

Table S3: **Coverage of ETC operational dates by facility type and confidence level.** High- and medium-confidence dates are sourced from named references to specific facilities. Low-confidence entries have no facility-specific date information and are recorded as missing.

	Dates available			
Facility type	High	Medium	Low (missing)	Total
CTE (*centres de traitement Ebola*)	6	5	1	12
CT (*centres de transit*)	4	3	2	9
CTD (*centres de transit décentralisés*)	0	4	17	21
Total	10	12	20	42

any source that names the specific facility with a date; I leave their dates blank rather than impute from the general outbreak timeline. Table S3 summarizes the coverage of operational dates by facility type.

Of the 42 facilities, 22 (52%) have operational dates at medium or higher confidence. The main gap concerns the 17 CTD decentralized transit centers (small units integrated into existing health structures beginning in early 2019) whose individual opening and closing dates were not systematically documented in public reports. The total first-admission counts for all 42 facilities are available from Table S1 of Barks et al. (2025).

Spatial processing. I construct a continuous proximity surface over our study window (DRC extended to include border areas of Uganda and Rwanda). Specifically, I project all ETC coordinates onto the ESRI:102022 (Albers Equal Area) coordinate reference system, rasterize the study window at 128×128 pixels, and compute for each pixel the Euclidean distance d_i (in kilometers) to the nearest ETC. To convert distances into a bounded proximity measure, I apply a negative exponential transformation:

$$\text{ETC proximity}_i = \exp\left(-\frac{d_i}{50}\right)$$

where d_i is the distance in kilometers from pixel i to the nearest ETC, and 50 km is the decay parameter. This yields values in $(0, 1]$: pixels at an ETC receive a value near 1, while pixels far from any ETC approach 0. The same transformation with a 50 km decay parameter is applied to other facility types (public hospitals, public clinics, private clinics) for comparability.

C.3 Moderators for Heterogeneity Analyses

I construct spatial moderators to conduct heterogeneity analyses (Figure S3): proximity to ETCs (Panel A), poverty (Panel B), and infant mortality (Panel C). ETC locations are drawn from Barks

et al. (2025) and transformed using a negative exponential decay function to assign higher values to areas closer to ETCs (Panel A, orange shades).[43] Poverty is defined as households in the bottom two wealth quintiles (poorest 40%) based on the DHS wealth index from the DRC Demographic and Health Survey 2013-14 (MPSMRM/Congo, MSP/Congo and ICF International, 2014).[44] Infant mortality is computed from the DHS birth history module as the proportion of births resulting in death before 12 months of age, restricted to births within five years of the survey. Both poverty and infant mortality are aggregated to the admin-2 level.

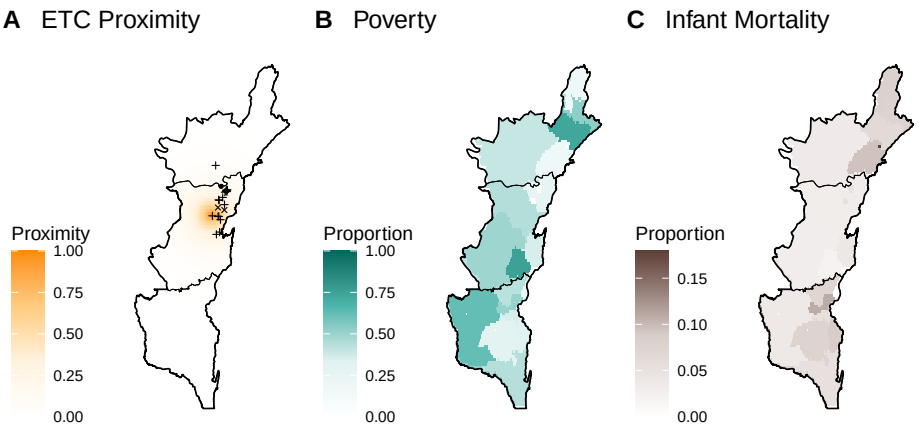

Figure S3: **Moderators for heterogeneity analyses**. Panel A displays proximity to Ebola Treatment Centers (ETCs), measured as $\exp(-d_i/50)$ where d_i is the distance in kilometers; values near 1 (darker orange) indicate locations close to an ETC and values near 0 (white) indicate distant locations. Symbols mark the locations of ETCs operational on the snapshot date (May 29, 2019): filled circles denote *centres de traitement Ebola* (CTEs, tertiary treatment facilities), × marks denote *centres de transit* (CTs, intermediate triage facilities), and + marks denote *centres de transit décentralisés* (CTDs, decentralized triage points). Panel B shows the proportion classified as poor (bottom two DHS wealth quintiles) and Panel C shows the infant mortality rates, both aggregated to the admin-2 level. Province boundaries for Ituri, North Kivu, and South Kivu are shown in black. Data from northeastern DRC are displayed for visualization, yet analyses use full data from the DRC and neighboring regions.

[43] See Appendix C.2 for further information.

[44] Variable `v190` assigns each household to a wealth quintile (1 = poorest, 2 = poorer, 3 = middle, 4 = richer, 5 = richest). Households with `v190` ≤ 2 are coded as poor.

D State Capacity: Descriptive Evidence

To examine shifts in state administrative, coercive, and informational capacity, I conduct a qualitative literature review of two epidemic responses in the DRC. The first case is the outbreak of Ebola from 2018 to 2020, and the second case is the cholera outbreak from 2017 to 2018. Both epidemics hit provinces in northeastern DRC, where state capacity is weak. The comparison illustrates how states respond to epidemics and shifts its capacity through healthcare service provision, disease surveillance, and the deployment of its police and military force. Below I provide a summary of each epidemic and the search strategy.

D.1 Context

As described in the main text, the 2018–2020 Ebola epidemic hit the northeastern provinces of the DRC (Ituri, North Kivu, and South Kivu). It was the largest Ebola epidemic recorded in the DRC and the second-largest globally after West Africa Ebola outbreak in 2014-16. The outbreak resulted in 3,470 officially-confirmed and probable cases and 2,287 deaths, with a case fatality ratio of 66 percent.

The cholera epidemic in 2017 and 2018 affected most regions of the DRC, including the northeast. It was the most severe cholera epidemic in history. The epidemic affected 21 of the 26 provinces, and official reports documented more than 55,000 cases. The number of deaths was 1,190, with the case fatality ratio of two percent. The first major rise in cases took place in South Kivu and then spread across the rest of the country.

D.2 Search Strategy

To examine the state response to Ebola and cholera in the DRC, I conducted a literature review and compile evidence on the creation of treatment centers for both diseases, the expansion of diagnostic laboratories, and the deployment of police and military forces during each crisis. These three dimensions correspond to the administrative, informational, and coercive capacity of the state.

Ebola The primary sources for shifts in administrative and informational capacity include daily situation reports from the DRC Ministry of Health, and official documents from the WHO (including Disease Outbreak News, Strategic Response Plans, and formal situation reports). I also use operational records from humanitarian organizations that took part in the response, including Médecins Sans Frontières, ALIMA, the International Medical Corps (MSF), the International Committee of the Red Cross, and the United Nations Childrens Fund (UNICEF). These sources allow a reconstruction of the time, the location, and the facility-level capacity of each treatment center that opened during the epidemic.

To identify the deployment of coercive force, I rely on material from the United Nations Security Council, records of troop redeployment from MONUSCO, and public statements from the DRC government. I validate these records with reports from Reuters, the New Humanitarian, and France24, which documented the presence of soldiers at treatment sites, the use of force for public health control, and the use of armed escorts for burial teams and vaccination teams.

Cholera For the cholera epidemic, I rely on records from MSF, the UNICEF, and the WHO to trace shifts in administrative and informational capacity. I also use epidemiological bulletins from the DRC Ministry of Health to identify the rise in case numbers in each province that led to the creation of treatment units in public hospitals. To identify the use of coercive force, I rely on humanitarian reports from the United Nations Office for the Coordination of Humanitarian Affairs (UN OCHA), archival reports from major news agencies, and summaries of peacekeeping activity from the United Nations.

D.3 Treatment Centers

Table S4: **Ebola treatment centers in the DRC, 2018-2020**. ETC: Ebola Treatment Centers; MoH: Ministry of Health (DRC); MSF: Médecins Sans Frontières; WHO: World Health Organization; IMC: International Medical Corps.

Name	Province	Second admin region	Health zone	Managing organization
Makeke ETC	Ituri	Mandima area	Mandima	MoH and IMC
Tchomia ETC	Ituri	Djugu Territory	Tchomia	MoH and MSF
Komanda ETC	Ituri	Irumu Territory	Komanda	MoH and WHO
Bunia ETC	Ituri	Bunia City	Bunia	MoH and MSF
Mambasa ETC	Ituri	Mambasa Territory	Mambasa	MoH and MSF
Mangina ETC	North Kivu	Beni Territory	Mabalako	MSF → MoH and IMC
Beni ETC	North Kivu	Beni City	Beni	ALIMA and MoH
Butembo ETC	North Kivu	Butembo City	Butembo	MSF → MoH and WHO
Katwa ETC	North Kivu	Butembo City	Katwa	MSF → MoH and WHO
Munigi ETC (Goma)	North Kivu	Goma City	Karisimbi	MoH and MSF
Mwenga ETC	South Kivu	Mwenga Territory	Mwenga	MoH and MSF

Table S5: **Cholera Treatment Centers in the DRC, 2017-2018**. CTC/CTU: Cholera Treatment Centers/Units; MoH: Ministry of Health (DRC); MSF: Médecins Sans Frontières; WHO: World Health Organization.

Name	Province	Second admin region	Health zone	Managing organization
Goma CTC	North Kivu	Goma City	Goma	MSF
Virunga CTC	North Kivu	Goma City	Karisimbi	MSF
Minova CTC	South Kivu	Kalehe Territory	Minova	MSF
Katana CTC	South Kivu	Kabare Territory	Katana	MSF
Idjwi Island CTC	South Kivu	Idjwi Territory	Idjwi	MSF
Camp Luka CTU	Kinshasa	Kinshasa City	Binza Ozone	MSF and MoH
Pakadjuma CTU	Kinshasa	Kinshasa City	Limete	MSF
Bumbu CTU	Kinshasa	Kinshasa City	Bumbu	MSF
Liziba CTU	Kinshasa	Kinshasa City	Lingwala	MSF Spain
Maluku I CTC	Kinshasa	Kinshasa City	Maluku I	MoH and WHO

D.4 Diagnostic Laboratories

Table S6: **Laboratory infrastructure for the Ebola response in the DRC, 2018-20**. NIBMR: National Institute for Bio Medical Research.

Name	Province	Second admin region	Health zone	Managing organization
Beni field lab	North Kivu	Beni City	Beni	NIBMR / WHO
Mangina field lab	North Kivu	Beni Territory	Mabalako	NIBMR / WHO
Butembo field lab	North Kivu	Butembo City	Butembo	NIBMR / Africa CDC
Katwa field lab	North Kivu	Butembo City	Katwa	NIBMR / WHO
Goma field lab	North Kivu	Goma City	Karisimbi	NIBMR / WHO
Bunia field lab	Ituri	Bunia City	Bunia	NIBMR / WHO
Komanda field lab	Ituri	Irumu Territory	Komanda	NIBMR / WHO
Mambasa field lab	Ituri	Mambasa Territory	Mambasa	NIBMR / ALIMA
Makeke field lab	Ituri	Mandima area	Mandima	NIBMR / IMC
Bukavu field lab	South Kivu	Bukavu City	Ibanda	NIBMR
Kinshasa national lab	Kinshasa	Kinshasa City	Lingwala	NIBMR

Table S7: **Laboratory infrastructure for the Ebola response in the DRC, 2017-18**. Only laboratories in northeast DRC are summarized.

Name	Province	Second admin region	Health zone	Managing organization
Goma provincial ref.	North Kivu	Goma City	Goma	MoH
Bukavu provincial hosp.	South Kivu	Bukavu City	Ibanda	MoH

D.5 Coercive Capacity

Table S8: **Use of force during the Ebola response in the DRC, 2018-20**. MONUSCO: The UN Organization Stabilization Mission in the Democratic Republic of the Congo.

Date	Province	Admin 2	Purpose	Security actor
Oct 2018	North Kivu	Beni	Escort of safe burial teams	Police and army
Feb to Mar 2019	North Kivu	Butembo	Guard of treatment centers	Police, army, MONUSCO
Apr 2019	North Kivu	Butembo	Guard of hospitals	Police and army
May 2019	North Kivu	Beni	Support for field teams	Police with MONUSCO
Nov 2019	Ituri	Mambasa, Biakato	Guard of health workers	Army with UN
Jun 2020	Ituri	Bunia	Guard of triage sites	Police

Table S9: **Use of force during the cholera response in the DRC, 2017-18**. No formal troop deployment was observed during the cholera outbreak from 2017 to 2018.

Date	Province	Admin 2	Purpose	Security actor
Late 2017	South Kivu	Bukavu City	No direct force, support role for safe access	No deployment
Early 2018	North Kivu	Goma City	No direct force, normal public order only	No deployment

E Estimation: Cholera

In this section, I describe the model specification, assess its performance, and detail the counterfactual densities.

E.1 Model Specification

I model the locations of cholera outbreaks using an inhomogeneous Poisson point process, which allows the intensity to vary across space and the expected number of events to be obtained by integrating the intensity surface over a region of interest (Mukaigawara et al., 2025; Baddeley, 2015). The outbreak-level dataset records the location and timing of the index patient for each cholera outbreak. After conditioning on the spatiotemporal covariates described below, the model is expected to capture the underlying spatiotemporal trend of cholera occurrence.

Because the borders between the DRC, Uganda, and Rwanda are porous and insurgents might operate across international boundaries, I define the spatial domain of interest (Ω in Section A) to include the entire DRC as well as adjacent districts in Rwanda and Uganda.

Covariates. The spatiotemporal trends of cholera outbreaks can be affected by histories of outbreaks and political violence events, exposure to environmental reservoirs (water sources including lakes and rivers), and population density. Thus, I include as covariates histories of cholera (4 weeks); histories of all violence (4 weeks); population density; inverted distances from rivers (the Congo River), Lake Kivu, Lake Tanganyika, Lake Albert, and Lake Edward; exponentiated distances from all cities; and three time splines (Figure S4). Locations of the rivers in the DRC are obtained from the World Bank. The population density data is obtained from Africa High Resolution Population Density Maps by the Center for International Earth Science Information Network (CIESIN), Columbia University.

Distances from water sources are inverted to capture potentially elevated risks near water by subtracting each distance from the maximum distance and dividing by the full range. Histories of cholera outbreaks and violence are first computed as distances[45] from past events and then transformed using $\exp(-0.25 \times \text{distance})$ to capture spatial decay and local clustering. For distances from all cities, varying coefficients are used to reflect the population size (see Mukaigawara et al. (2025) for details).

Coefficients. Table S10 summarizes the coefficients from the inhomogeneous Poisson point process model. Several covariates, most notably histories of cholera outbreaks over the past 12 weeks, population density, the proportion of people using unimproved water sources, and proximity to major lakes, are strongly associated with higher outbreak intensity, which is in keeping with my expectation. The dispersion parameter (1.73) also indicates a reasonable fit.

[45] I use the `distmap` function in the `spatstat` package.

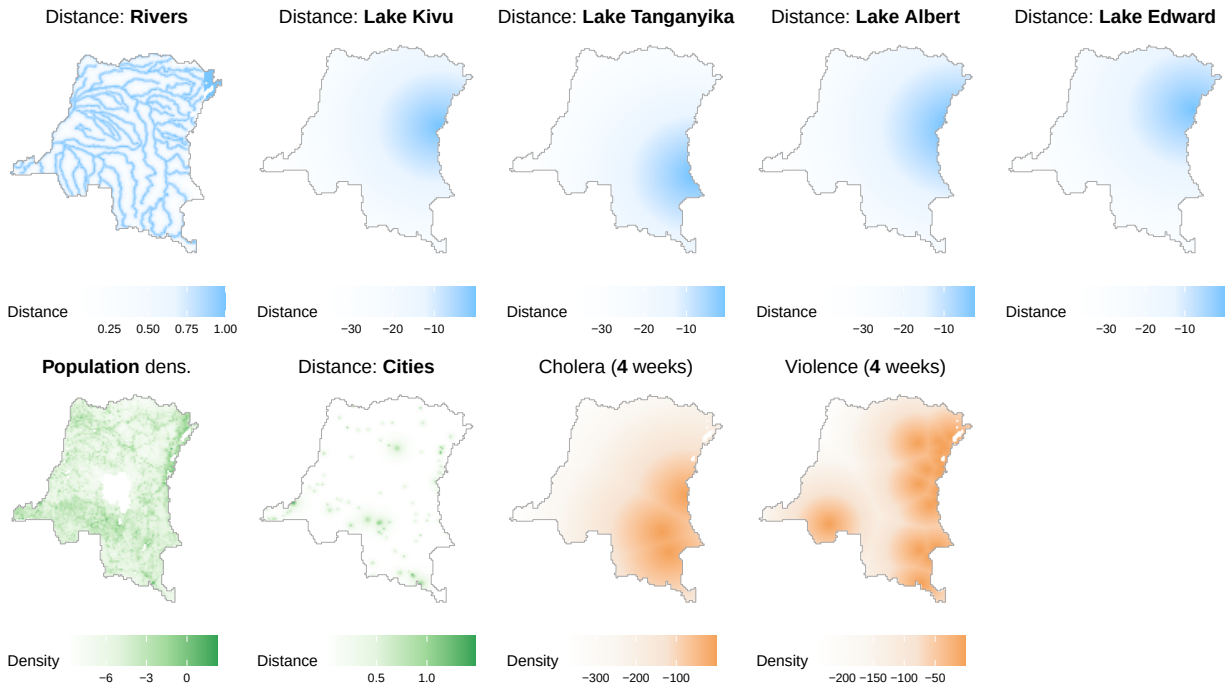

Figure S4: **Covariates (cross-epidemic, cholera)**. Covariates included in the propensity score model are summarized. For population density, log-transformation is used for visualization purposes.

Table S10: **Coefficients for the propensity score model (cholera)**. Coefficients for spatiotemporal covariates (images and scalers) are summarized. Deviance dropped from 1910.37 to 1630.13 (dispersion = 1.73).

	Estimate	Std. Error	t value	Pr(>|t|)
(Intercept)	-13.98	0.76	-18.32	0.00
History of cholera (4 weeks)	1.69	5.38	0.31	0.75
History of violence (4 weeks)	-2.46	3.00	-0.82	0.41
Distance (all cities, exponentiated)	3.66	0.50	7.39	0.00
Distance (Lake Kivu, inverted)	5.24	1.32	3.97	0.00
Distance (Lake Albert, inverted)	24.32	22.33	1.09	0.28
Distance (Lake Tanganyika, inverted)	6.45	4.57	1.41	0.16
Distance (rivers, inverted)	2.26	2.66	0.85	0.40
Distance (Lake Edward, inverted)	-0.31	0.62	-0.50	0.62
Population density	0.63	0.12	5.31	0.00
Time spline (1)	-0.69	0.52	-1.33	0.18
Time spline (2)	-6.20	1.68	-3.69	0.00
Time spline (3)	-1.91	0.66	-2.91	0.00

E.2 Model Performance

To assess whether the fitted point process model makes treatment patterns random, I perform three diagnostic tests. First, I examine the superimposed Pearson residual field obtained by averaging the raw residual surfaces across all weekly point patterns. In spatial statistics, residual maps provide a direct visual test of unexplained spatial structure (Baddeley et al., 2005). With an appropriate model, the residual surface should exhibit no systematic patterns beyond stochastic noise.

Second, I conduct a superthinning residual test, which is regarded as one of the most powerful diagnostic for spatial point process models (Schoenberg, 2003; Clements, Schoenberg and Veen, 2012). Superthinning transforms the observed pattern into a residual point process by randomly removing points where the fitted intensity is high and randomly adding simulated points where the fitted intensity is low. The resulting process should look like a homogeneous Poisson process if and only if the model is specified correctly (Schoenberg, 2003). After superthinning, I employ the K-function (Baddeley, 2015), which measures the number of points that lie within a given distance of a certain observation and compares it to the expected number of points under complete spatial randomness.

Third, as a supplementary diagnostic, I compare the expected versus observed temporal counts of treatment events. Comparing the model-implied counts with observed counts is a standard model validation strategy in spatiotemporal point processes. I also conduct an out-of-sample forecasting test, using 80% of the patterns for estimation and predicting case counts and spatial intensities in the remaining 20%. I also visualize the densities as maps to visually investigate the propensity score model.

Average residual fields. The average residual fields (Figure S5, Panel A) indicate that the inhomogeneous Poisson point process model provides a good fit to the cholera outbreak data. Deviations are small throughout the DRC and its neighboring regions.

Super-thinning residual tests. I next apply the superthinning tests (Schoenberg, 2003; Clements, Schoenberg and Veen, 2012). Formally, let $z \in \Omega$, which represents a location (point) within the entire space. I first obtain the model-predicted intensity surfaces for all time periods. For each time-specific intensity, I then select a cutoff c equal to the (across-time) mean of the mean values of intensities from each time period (Clements, Schoenberg and Veen, 2012) and thin each observed point z_i independently with probability $\min\{1,\ c/\hat{\lambda}(z_i)\}$. This removes more points where the model predicts high intensity and keeps most points in low-intensity regions. Contrarily, in low-intensity regions, I simulate a Poisson point process with an intensity $\max\{c - \hat{\lambda}(z),\ 0\}$ and add points. Finally, I sum all the superthinned points to form a single combined intensity. This resulting superthinned pattern should be a homogeneous Poisson process if the propensity score model is specified well.

The superthinned pattern aligns with the theoretical expectation of complete spatial randomness.

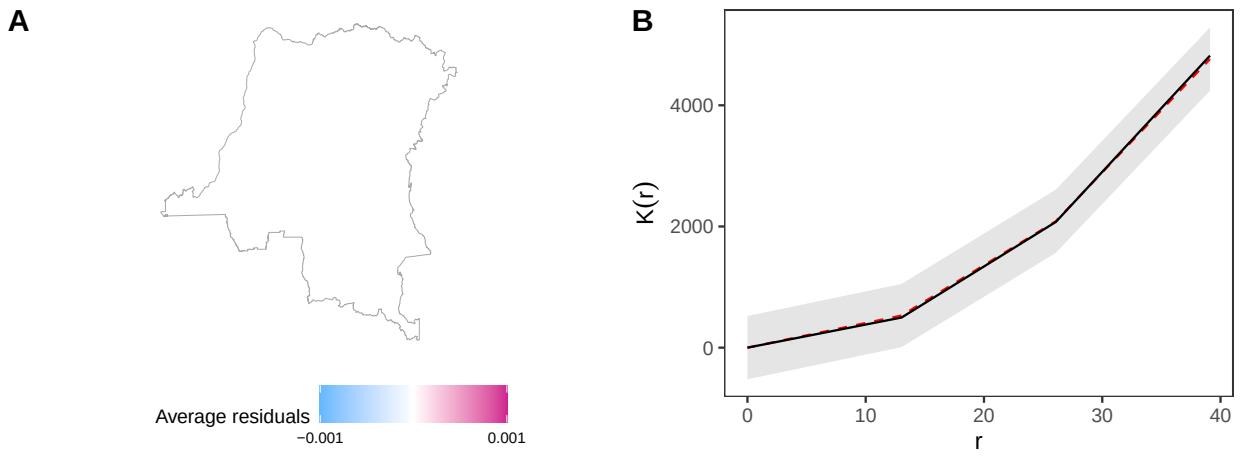

Figure S5: **Average residual fields and super-thinning test results (cholera)**. Panel A: The map shows the average residual field across all time periods. Panel B: The gray region represents the range of $K(r)$ values based on 1,000 simulated homogeneous Poisson paterns. The black line is the empirical K-function and the red dashed line is the theoretical $K(r)$ values. The x-axis represents the distance from points.

As shown in the envelope plot (Figure S5, Panel B), the observed K-function (black) lies entirely within the global simulation envelope across the full range of distances (gray shades), which suggests that the propensity model is well specified to account for spatiotemporal trends of cholera outbreaks.

Out-of-sample prediction and visual inspection. The out-of-sample predictions (Figure S6) indicate that the model captures the overall temporal trends of cholera outbreaks. Visual inspection (Figure S7) also suggests that the model reproduces the major spatial patterns of cholera incidence, particularly the higher intensities in the eastern part of the DRC.

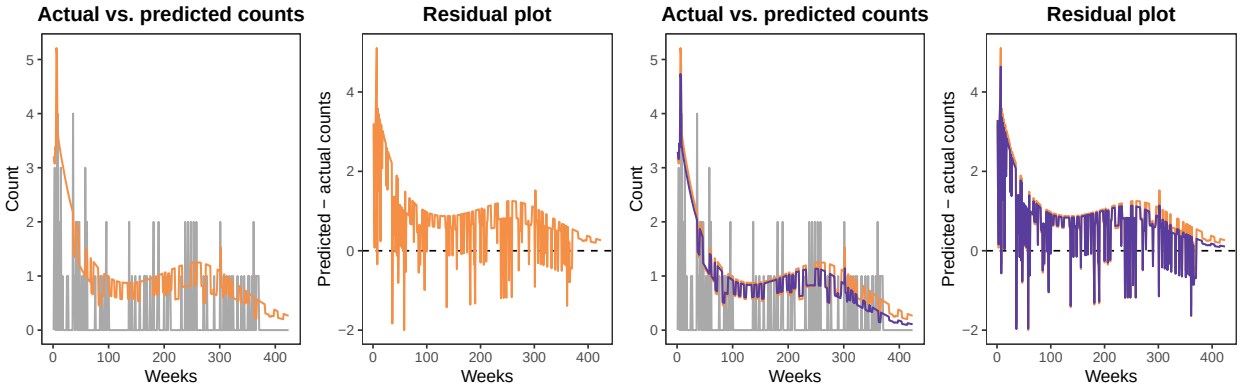

Figure S6: **Predicted and actual counts**. Panel A (left) compares actual (gray) and predicted (orange) counts, indicating that the model reproduces the observed temporal dynamics. Panel B (left) shows the out-of-sample performance, using the first 80 percent of data as a training set, with purple lines displaying predicted counts. For both panels, the subpanels on the right display residuals.

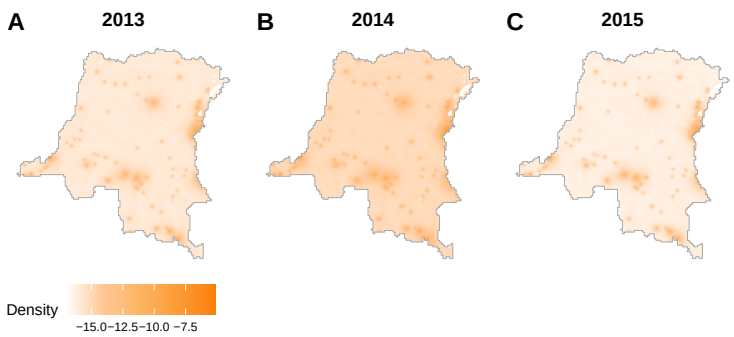

Figure S7: **Observed densities as maps**. Observed densities from weeks 30, 83, and 136 (corresponding to years 2013–5) are displayed (log-transformed for visualization purposes).

E.3 Counterfactuals

I construct counterfactual interventions using the baseline density, which reflects the out-of-sample distribution of cholera outbreaks, and power densities that encode spatial prioritization. Intuitively, I obtain counterfactuals as maps using the baseline density re-weighted by power densities.

Formally, a power density is defined as $d_\alpha(\omega) = \prod_{i=1}^{k} d_i(\omega)^{\alpha_i} / \int_\Omega \prod_{i=1}^{k} d_i(\omega)^{\alpha_i}$, where $d_i(\omega)$ denotes the distributions of spatial objects prioritized and α_i represents the prioritization parameter. For power densities that move outbreaks toward the central regions, I set $k = 2$ and $\alpha_i \in \{1.5, 1.6, 1.7, \cdots, 2.0\}$, and use the density of public hospitals and public clinics, since these healthcare facilities are concentrated in Kinshasa and its neighboring regions. For the frontier regions, I set $k = 1$ and use the density of private hospitals, which are concentrated more toward the northeast. I set $\alpha = 1.5$ to make the spatial distributions of Ebola and cholera comparable, since Ebola cases during the 2018–2020 outbreak are already concentrated in the frontier region, and further increases in α might violate the overlap assumption. As shown in Figure S8, these counterfactuals move outbreak locations either toward the central or frontier regions.

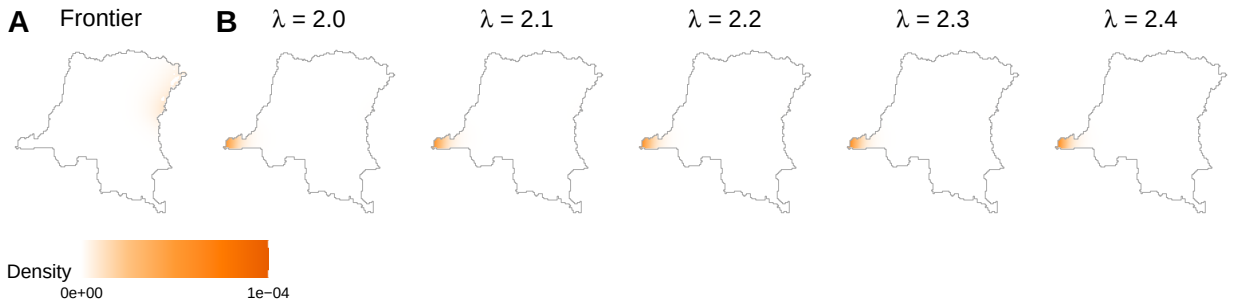

Figure S8: **Counterfactual interventions (cholera)**. Panel A shows the coutnerfactual density that move cholera outbreaks toward the frontier. Panel B shows the counterfactuals for the center.

F Estimation: Ebola

I model the spatiotemporal distribution of Ebola patients separately for the hospital, onset, and residence location datasets.

F.1 Model Specification: Hospital Locations

Covariates. I include as covariates 2- and 10-day histories of confirmed, probable, and suspected Ebola cases to reflect the minimum and mean incubation periods; 1-, 2-, and 4-week histories of all violence, VAC, and battles to capture the recent trends of violence; Ebola index case potentials derived from the distribution of reservoir animals (fruit bats) (Pigott et al., 2017); indicators for surges in all cases (February 18—May 28, 2019), decline in confirmed cases (December 16, 2019–); and indicators for six admin-2 regions in the northeast with clustering of patients. Histories of Ebola cases are transformed using $\exp(-0.25 \times \text{distance}/10^5)$ (Figure S9).

Coefficients. Coefficients of the model with confirmed cases, all cases, and non-Ebola cases are summarized in Tables S11, S12, and Table S13), respectively. For the non-Ebola model, I exclude histories of suspected cases and also use the provincial indicators due to model instability.

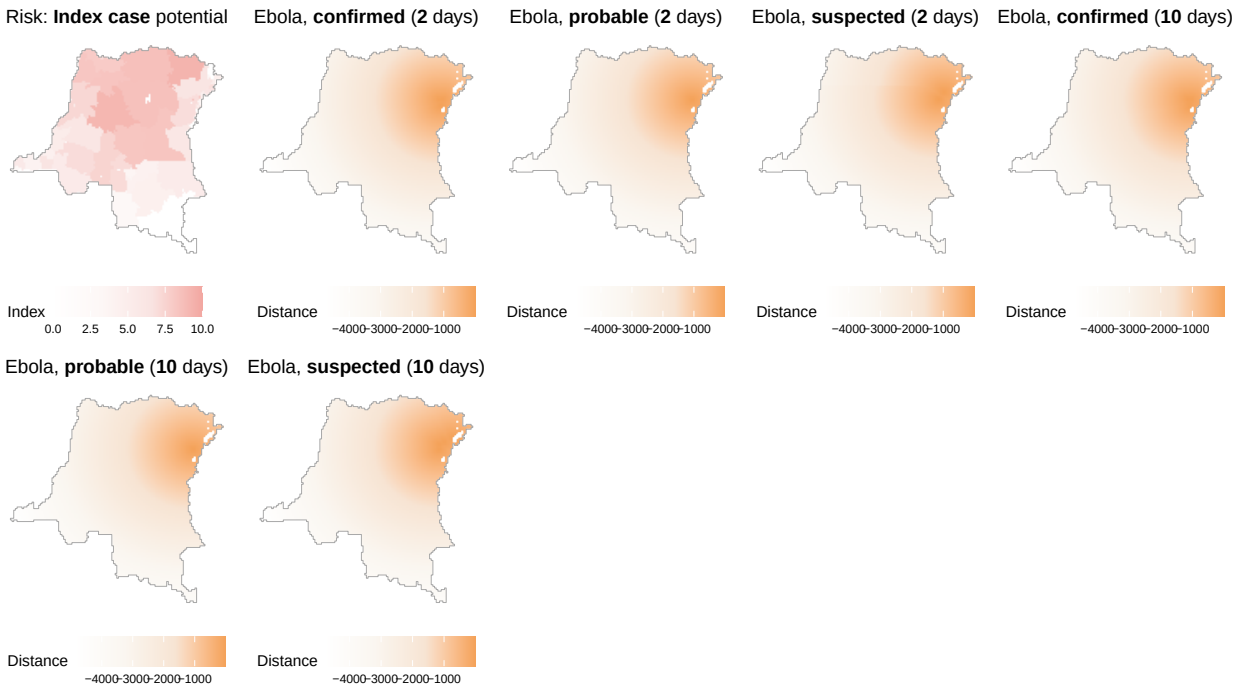

Figure S9: **Spatial covariates in the propensity score model (Ebola)**. Histories of Ebola cases are log-transformed and then multiplied by 10^6 only for visualization purposes. Data from days 50 and 100 are shown for histories of Ebola cases.

Table S11: **Coefficients for the propensity score model (Ebola, hospital locations, confirmed cases)**. Coefficients for spatiotemporal covariates (images and scalers) are summarized. Deviance dropped from 26,779.38 to 3,609.43 (dispersion = 16.82).

	Estimate	Std. Error	t value	Pr(>|t|)
(Intercept)	-30.94	4.22	-7.34	0.00
History of confirmed cases (2 days)	0.40	0.71	0.56	0.57
History of probable cases (2 days)	0.01	0.43	0.02	0.99
History of suspected cases (2 days)	0.05	0.57	0.09	0.93
History of confirmed cases (10 days)	1.28	3.19	0.40	0.69
History of probable cases (10 days)	0.13	0.29	0.45	0.65
History of suspected cases (10 days)	0.48	0.94	0.51	0.61
Time spline (1)	0.96	0.68	1.42	0.15
Time spline (2)	-1.54	3.14	-0.49	0.62
Time spline (3)	-3.47	2.92	-1.19	0.23
History of all violence (1 week)	-0.65	1.51	-0.43	0.67
History of violence against civilians (1 week)	0.16	1.26	0.12	0.90
History of battles (1 week)	0.25	1.28	0.20	0.84
History of all violence (2 week)	0.19	1.57	0.12	0.90
History of violence against civilians (2 week)	-0.21	1.25	-0.17	0.86
History of battles (2 week)	-0.11	1.30	-0.08	0.93
History of all violence (4 week)	1.27	1.44	0.88	0.38
History of violence against civilians (4 week)	0.99	0.99	1.00	0.32
History of battles (4 week)	0.09	1.24	0.07	0.94
Risk for initial cases of Ebola	1.40	0.29	4.88	0.00
Surge of patients (indicator)	0.10	0.33	0.30	0.76
Decline in confirmed cases (indicator)	0.30	0.98	0.31	0.76
Bunia, Ituri (indicator)	11.58	1.90	6.09	0.00
Mambasa, Ituri (indicator)	7.30	0.98	7.48	0.00
Beni, North Kivu (indicator)	8.19	0.75	10.99	0.00
Butembo, North Kivu (indicator)	21.05	2.59	8.12	0.00
Lubero, North Kivu (indicator)	4.72	1.56	3.02	0.00
Oicha, North Kivu (indicator)	9.49	0.80	11.84	0.00

Table S12: **Coefficients for the propensity score model (Ebola, hospital locations, all cases)**. Coefficients for spatiotemporal covariates (images and scalers) are summarized. Deviance dropped from 210,535.24 to 69,734.38 (dispersion = 5.45).

	Estimate	Std. Error	t value	Pr(>|t|)
(Intercept)	-15.97	0.45	-35.76	0.00
History of confirmed cases (2 days)	-0.16	0.06	-2.84	0.00
History of probable cases (2 days)	-0.06	0.16	-0.40	0.69
History of suspected cases (2 days)	0.35	0.28	1.27	0.20
History of confirmed cases (10 days)	-0.09	0.06	-1.50	0.13
History of probable cases (10 days)	-0.10	0.09	-1.16	0.25
History of suspected cases (10 days)	1.40	0.50	2.81	0.00
Time spline (1)	2.18	0.14	16.07	0.00
Time spline (2)	0.88	0.50	1.75	0.08
Time spline (3)	0.26	0.16	1.63	0.10
History of all violence (1 week)	0.52	0.28	1.84	0.07
History of violence against civilians (1 week)	-0.65	0.23	-2.82	0.00
History of battles (1 week)	-0.67	0.22	-3.08	0.00
History of all violence (2 week)	0.62	0.30	2.10	0.04
History of violence against civilians (2 week)	-0.17	0.21	-0.80	0.42
History of battles (2 week)	-0.06	0.22	-0.28	0.78
History of all violence (4 week)	2.18	0.34	6.42	0.00
History of violence against civilians (4 week)	0.71	0.24	2.94	0.00
History of battles (4 week)	-0.10	0.25	-0.41	0.68
Risk for initial cases of Ebola	0.02	0.01	1.18	0.24
Surge of patients (indicator)	0.67	0.09	7.66	0.00
Decline in confirmed cases (indicator)	0.99	0.08	11.98	0.00
Bunia, Ituri (indicator)	6.10	0.17	35.99	0.00
Mambasa, Ituri (indicator)	4.36	0.05	80.56	0.00
Beni, North Kivu (indicator)	6.20	0.10	59.24	0.00
Butembo, North Kivu (indicator)	6.14	0.14	45.19	0.00
Lubero, North Kivu (indicator)	1.01	0.27	3.81	0.00
Oicha, North Kivu (indicator)	5.16	0.07	70.59	0.00

Table S13: **Coefficients for the propensity score model (hospital locations, non-Ebola cases)**. Coefficients for spatiotemporal covariates (images and scalers) are summarized. Deviance dropped from 351,044.12 to 55,537.04 (dispersion = 2.58).

	Estimate	Std. Error	t value	Pr(>|t|)
(Intercept)	-17.55	0.29	-60.55	0.00
History of confirmed cases (2 days)	0.16	0.04	3.96	0.00
History of probable cases (2 days)	-0.16	0.06	-2.53	0.01
History of confirmed cases (10 days)	0.72	0.08	9.40	0.00
History of probable cases (10 days)	0.24	0.03	6.88	0.00
Time spline (1)	1.55	0.06	25.12	0.00
Time spline (2)	-0.15	0.22	-0.67	0.50
Time spline (3)	-2.13	0.15	-13.90	0.00
History of all violence (1 week)	-0.52	0.15	-3.52	0.00
History of violence against civilians (1 week)	1.12	0.13	8.59	0.00
History of battles (1 week)	0.15	0.13	1.18	0.24
History of all violence (2 week)	-0.81	0.16	-5.22	0.00
History of violence against civilians (2 week)	1.26	0.13	9.78	0.00
History of battles (2 week)	1.17	0.13	8.78	0.00
History of all violence (4 week)	2.49	0.13	18.87	0.00
History of violence against civilians (4 week)	2.62	0.11	24.59	0.00
History of battles (4 week)	0.79	0.11	6.91	0.00
Risk for initial cases of Ebola	-0.30	0.00	-91.55	0.00
Surge of patients (indicator)	0.09	0.04	2.21	0.03
Decline in confirmed cases (indicator)	0.84	0.06	14.59	0.00
North Kivu (indicator)	8.98	0.27	33.88	0.00
Ituri (indicator)	7.35	0.27	27.44	0.00

F.2 Model Performance: Hospital Locations

Average residual fields and super-thinning test results. Figures S10, S11, and S12 confirm the performance of the propensity score models.

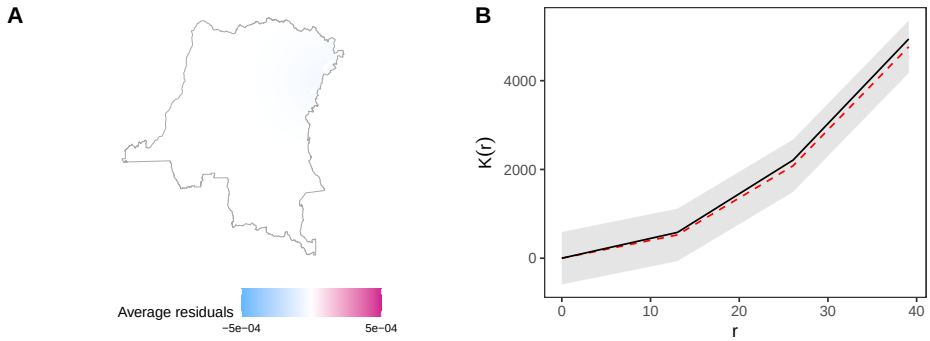

Figure S10: **Average residual fields and super-thinning test results (Ebola, hospital locations, confirmed cases)**.

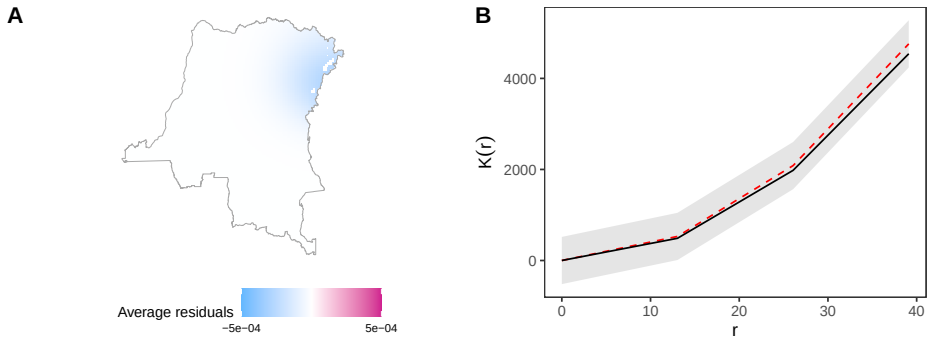

Figure S11: **Average residual fields and super-thinning test results (Ebola, hospital locations, all cases)**.

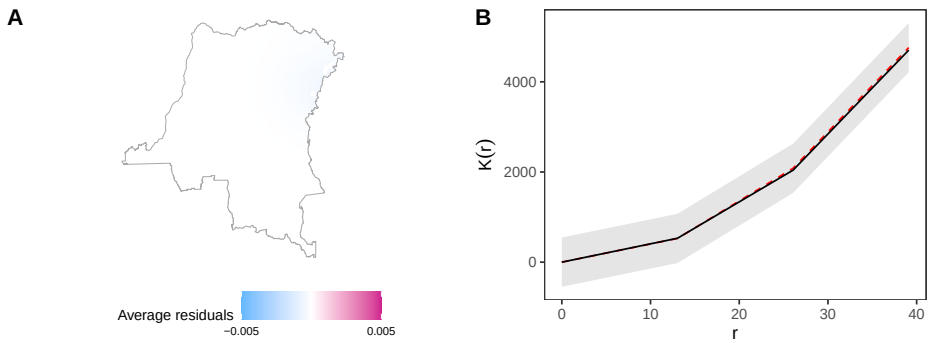

Figure S12: **Average residual fields and super-thinning test results (Ebola, hospital locations, non-Ebola cases)**.

Out-of-sample prediction and visual inspection. The out-of-sample prediction performance confirms that the model performs well in predicting the frequencies of confirmed Ebola cases (Figures S13, S14, and S15). For non-Ebola cases, a spike arises in the out-of-sample model primarily due to the use of time splines. Observed densities as maps are shown in Figures S16, S17, and S18.

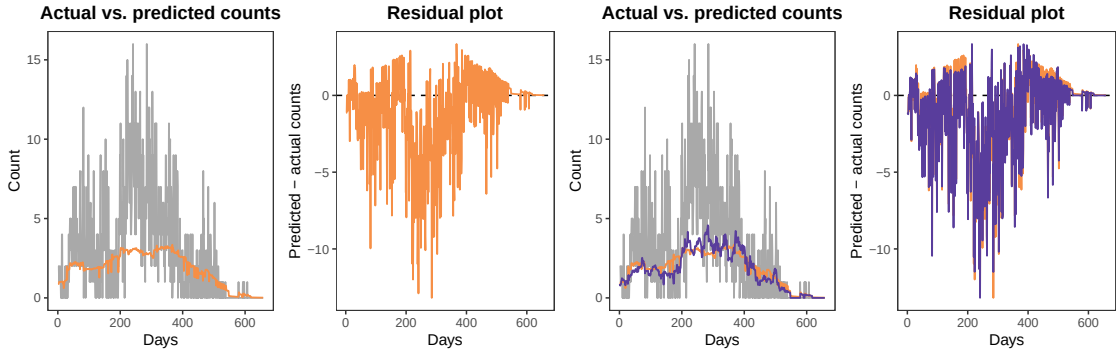

Figure S13: **Predicted and actual counts (Ebola, hospital locations, confirmed cases)**.

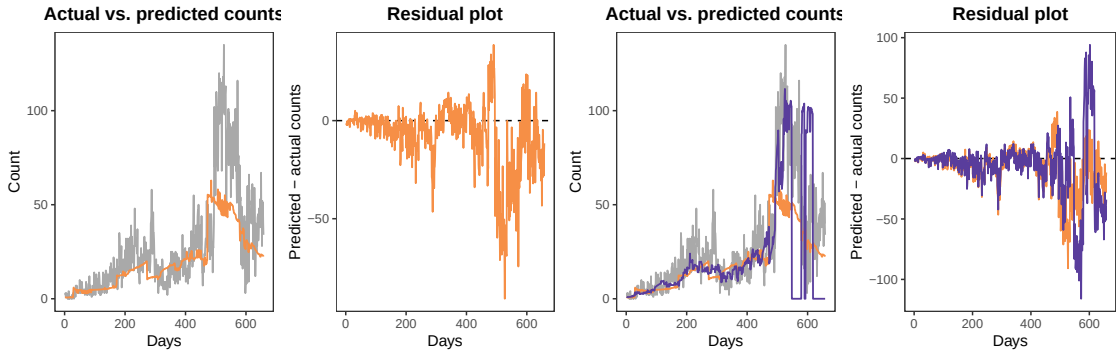

Figure S14: **Predicted and actual counts (Ebola, hospital locations, all cases)**.

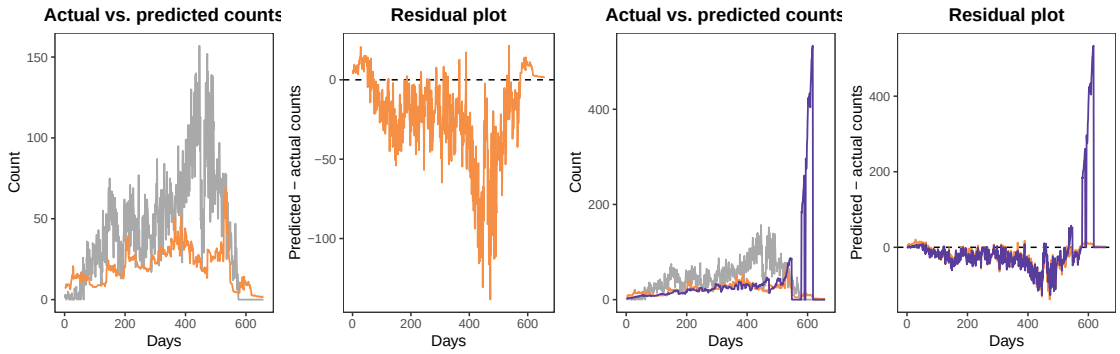

Figure S15: **Predicted and actual counts (Ebola, hospital locations, non-Ebola cases)**.

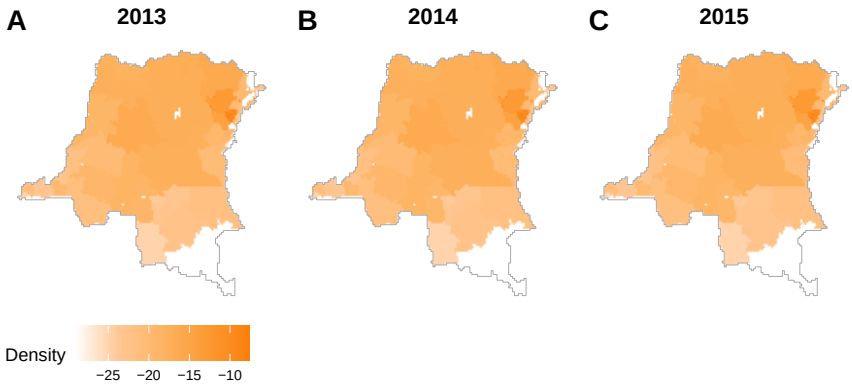

Figure S16: **Observed densities as maps (Ebola, hospital locations, confirmed cases)**. Observed densities from days 50, 300, and 500 are displayed (log-transformed for visualization purposes).

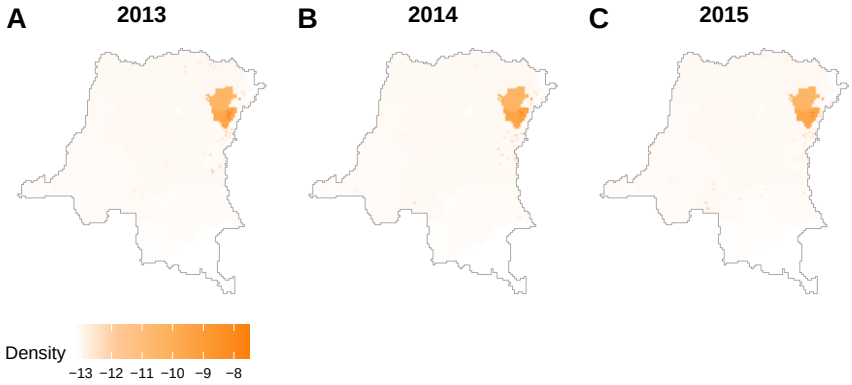

Figure S17: **Observed densities as maps (Ebola, hospital locations, all cases)**.

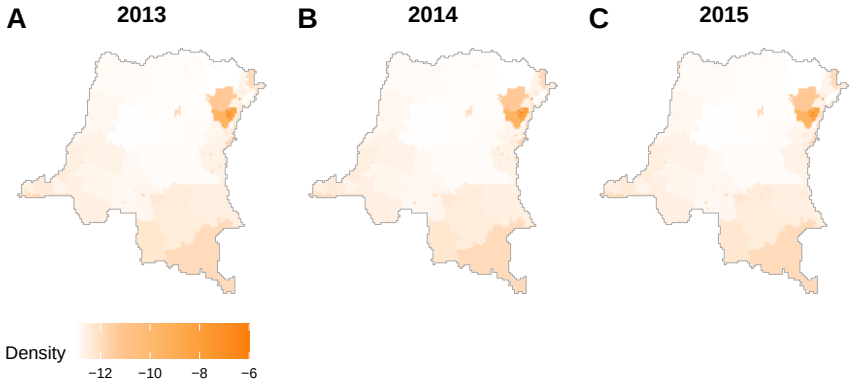

Figure S18: **Observed densities as maps (Ebola, hospital locations, non-Ebola cases)**.

F.3 Model Specification: Onset Locations

Table S14: **Coefficients for the propensity score model (Ebola, onset locations, confirmed cases)**. Coefficients for spatiotemporal covariates (images and scalers) are summarized. Deviance dropped from 38,019.74 to 8,127.05 (dispersion = 10.37).

	Estimate	Std. Error	t value	Pr(>|t|)
(Intercept)	-28.19	4.21	-6.70	0.00
History of confirmed cases (2 days)	0.09	0.73	0.12	0.91
History of probable cases (2 days)	-0.01	0.13	-0.08	0.93
History of suspected cases (2 days)	-0.18	1.16	-0.16	0.87
History of confirmed cases (10 days)	1.57	3.85	0.41	0.68
History of probable cases (10 days)	0.24	0.19	1.27	0.20
History of suspected cases (10 days)	0.93	1.31	0.71	0.48
Time spline (1)	1.96	0.48	4.09	0.00
Time spline (2)	-3.34	2.30	-1.45	0.15
Time spline (3)	-7.36	2.27	-3.25	0.00
History of all violence (1 week)	-0.65	1.16	-0.56	0.57
History of violence against civilians (1 week)	0.25	0.99	0.26	0.80
History of battles (1 week)	0.69	0.97	0.71	0.48
History of all violence (2 week)	0.25	1.21	0.20	0.84
History of violence against civilians (2 week)	-0.17	1.03	-0.16	0.87
History of battles (2 week)	-0.08	1.01	-0.08	0.94
History of all violence (4 week)	1.01	0.97	1.04	0.30
History of violence against civilians (4 week)	1.06	0.78	1.36	0.18
History of battles (4 week)	-0.61	0.88	-0.70	0.49
Risk for initial cases of Ebola	1.06	0.18	5.96	0.00
Surge of patients (indicator)	0.17	0.20	0.85	0.40
Decline in confirmed cases (indicator)	0.88	0.67	1.33	0.18
Bunia, Ituri (indicator)	9.99	1.15	8.69	0.00
Mambasa, Ituri (indicator)	7.41	0.54	13.71	0.00
Beni, North Kivu (indicator)	7.80	0.48	16.39	0.00
Butembo, North Kivu (indicator)	17.71	1.58	11.19	0.00
Lubero, North Kivu (indicator)	7.01	0.48	14.48	0.00
Oicha, North Kivu (indicator)	9.28	0.46	20.11	0.00

Table S15: **Coefficients for the propensity score model (Ebola, onset locations, all cases)**. Coefficients for spatiotemporal covariates (images and scalers) are summarized. Deviance dropped from 467,449.98 to 158,158.92 (dispersion = 10.91).

	Estimate	Std. Error	t value	Pr(>|t|)
(Intercept)	-16.25	0.72	-22.64	0.00
History of confirmed cases (2 days)	-0.27	0.05	-4.96	0.00
History of probable cases (2 days)	0.07	0.06	1.26	0.21
History of suspected cases (2 days)	0.27	0.93	0.29	0.77
History of confirmed cases (10 days)	-0.12	0.06	-2.05	0.04
History of probable cases (10 days)	-0.12	0.05	-2.33	0.02
History of suspected cases (10 days)	2.17	1.16	1.87	0.06
Time spline (1)	3.03	0.13	22.86	0.00
Time spline (2)	1.07	0.48	2.21	0.03
Time spline (3)	-0.28	0.16	-1.78	0.07
History of all violence (1 week)	0.93	0.39	2.38	0.02
History of violence against civilians (1 week)	-0.64	0.33	-1.94	0.05
History of battles (1 week)	-0.85	0.32	-2.68	0.01
History of all violence (2 week)	0.03	0.37	0.09	0.93
History of violence against civilians (2 week)	-0.23	0.29	-0.80	0.43
History of battles (2 week)	0.15	0.30	0.49	0.62
History of all violence (4 week)	-0.05	0.38	-0.13	0.89
History of violence against civilians (4 week)	1.06	0.33	3.24	0.00
History of battles (4 week)	-0.00	0.28	-0.01	0.99
Risk for initial cases of Ebola	-0.02	0.02	-1.27	0.20
Surge of patients (indicator)	0.57	0.09	6.27	0.00
Decline in confirmed cases (indicator)	1.39	0.07	19.51	0.00
Bunia, Ituri (indicator)	6.00	0.17	36.15	0.00
Mambasa, Ituri (indicator)	4.57	0.05	83.50	0.00
Beni, North Kivu (indicator)	6.89	0.11	61.18	0.00
Butembo, North Kivu (indicator)	6.63	0.13	49.34	0.00
Lubero, North Kivu (indicator)	5.10	0.06	88.00	0.00
Oicha, North Kivu (indicator)	6.32	0.05	115.80	0.00

Table S16: **Coefficients for the propensity score model (Ebola, onset locations, all cases)**. Coefficients for spatiotemporal covariates (images and scalers) are summarized. Deviance dropped from 472,004.86 to 102,765.15 (dispersion = 3.27).

	Estimate	Std. Error	t value	Pr(>|t|)
(Intercept)	-17.04	0.23	-75.23	0.00
History of confirmed cases (2 days)	0.23	0.05	4.87	0.00
History of probable cases (2 days)	-0.04	0.02	-1.60	0.11
History of confirmed cases (10 days)	0.07	0.07	1.06	0.29
History of probable cases (10 days)	0.22	0.02	8.96	0.00
Time spline (1)	2.11	0.05	39.32	0.00
Time spline (2)	0.09	0.20	0.47	0.64
Time spline (3)	-2.81	0.14	-20.40	0.00
History of all violence (1 week)	0.09	0.14	0.63	0.53
History of violence against civilians (1 week)	0.88	0.12	7.40	0.00
History of battles (1 week)	-0.36	0.12	-3.11	0.00
History of all violence (2 week)	-0.29	0.15	-1.93	0.05
History of violence against civilians (2 week)	0.98	0.12	8.02	0.00
History of battles (2 week)	0.76	0.12	6.17	0.00
History of all violence (4 week)	-0.22	0.13	-1.62	0.11
History of violence against civilians (4 week)	3.69	0.12	32.00	0.00
History of battles (4 week)	2.31	0.10	22.46	0.00
Risk for initial cases of Ebola	-0.21	0.00	-68.01	0.00
Surge of patients (indicator)	-0.10	0.04	-2.62	0.01
Decline in confirmed cases (indicator)	1.03	0.05	21.24	0.00
North Kivu (indicator)	8.84	0.20	43.88	0.00
Ituri (indicator)	7.44	0.20	36.66	0.00

F.4 Model Performance: Onset Locations

Average residual fields and super-thinning test results. Figures S19, S20, and S21 confirm the performance of the propensity score models.

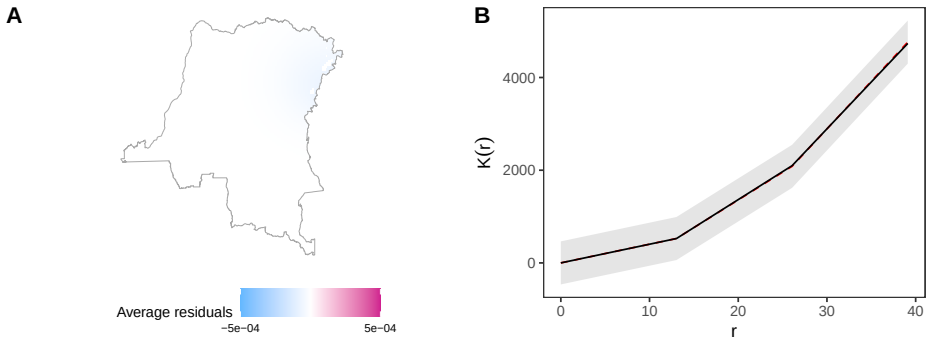

Figure S19: **Average residual fields and super-thinning test results (Ebola, onset locations, confirmed cases)**.

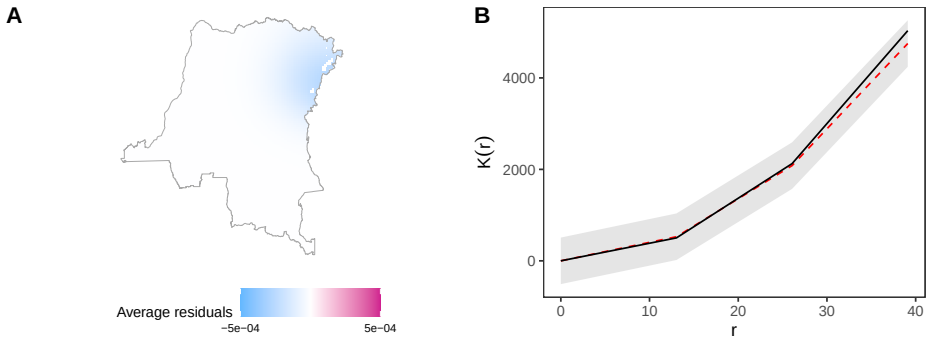

Figure S20: **Average residual fields and super-thinning test results (Ebola, onset locations, all cases)**.

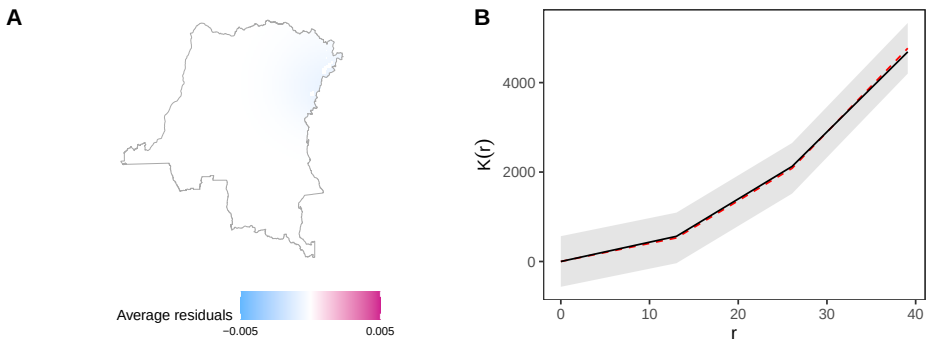

Figure S21: **Average residual fields and super-thinning test results (Ebola, onset locations, non-Ebola cases)**.

Out-of-sample prediction and visual inspection. The out-of-sample prediction performance confirms that the model performs well in predicting the frequencies of confirmed Ebola cases (Figures S22, S23, and S24). For all cases and non-Ebola cases, a spike arises in the out-of-sample model primarily due to the use of time splines. Observed densities as maps are shown in Figures S25, S26, and S27.

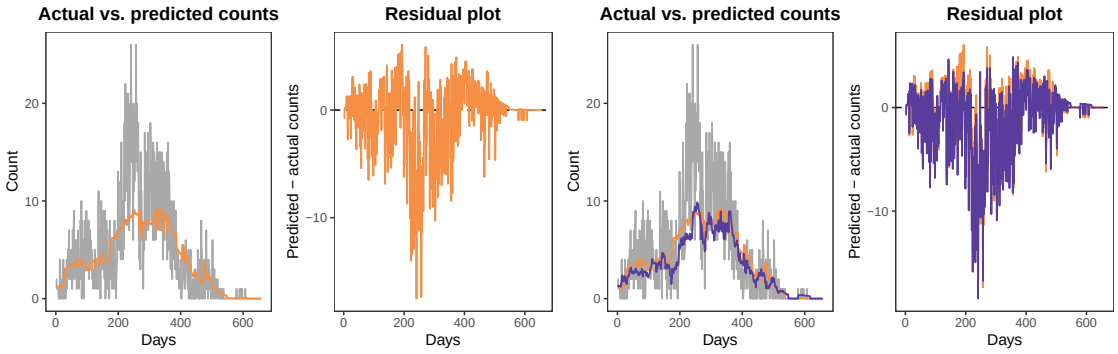

Figure S22: **Predicted and actual counts (Ebola, onset locations, confirmed cases)**.

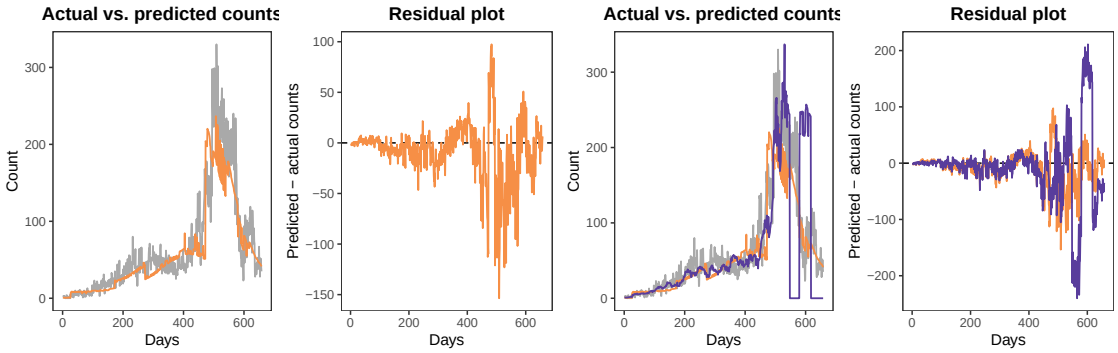

Figure S23: **Predicted and actual counts (Ebola, onset locations, all cases)**.

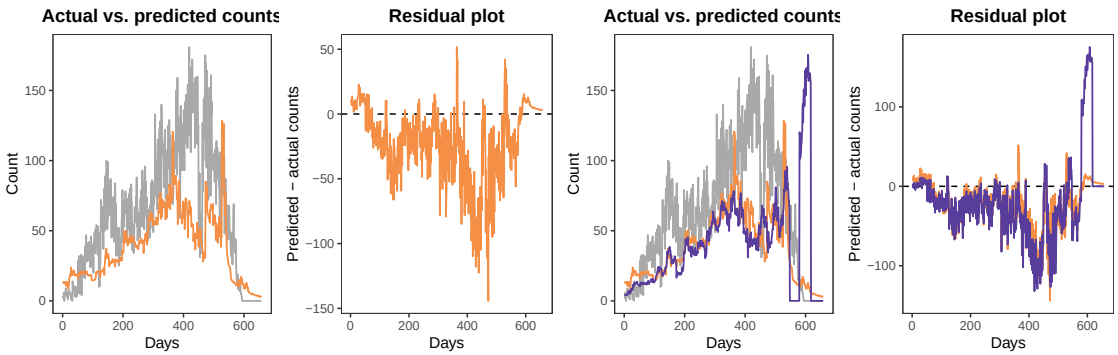

Figure S24: **Predicted and actual counts (Ebola, onset locations, non-Ebola cases)**.

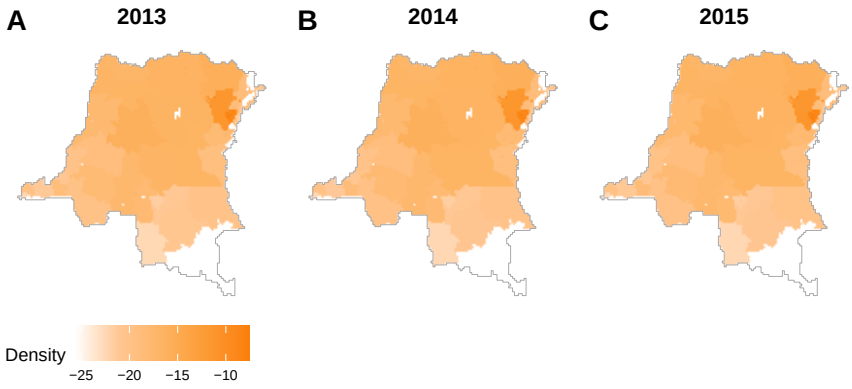

Figure S25: **Observed densities as maps (Ebola, onset locations, confirmed cases)**. Observed densities from days 50, 300, and 500 are displayed (log-transformed for visualization purposes).

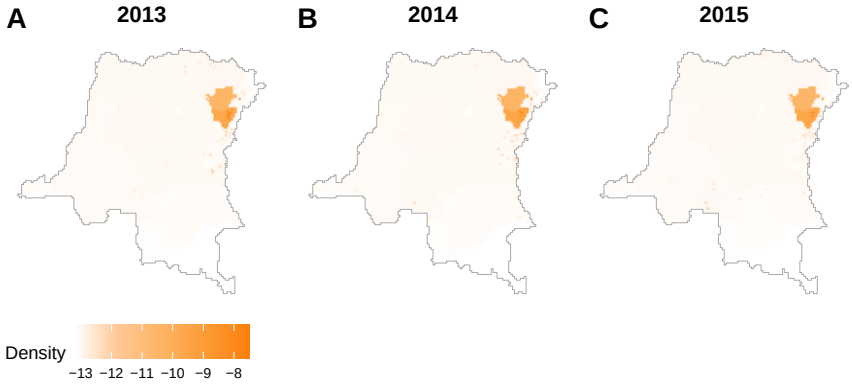

Figure S26: **Observed densities as maps (Ebola, onset locations, all cases)**.

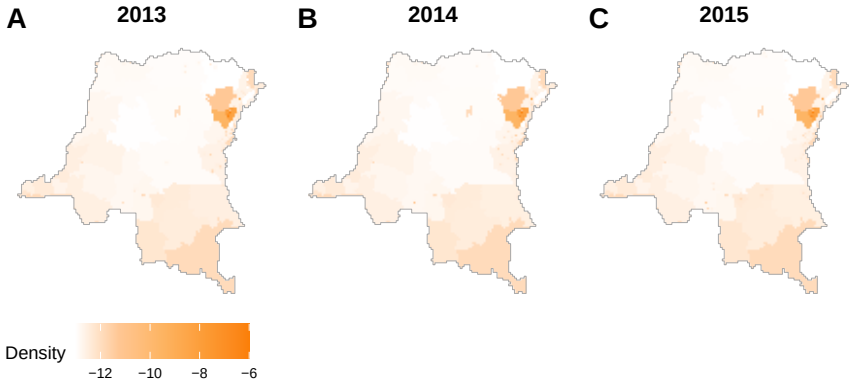

Figure S27: **Observed densities as maps (Ebola, onset locations, non-Ebola cases)**.

F.5 Counterfactuals

For the cross-epidemic analyses, I construct counterfactuals in the same way as for cholera, with different values of α that generate outbreaks concentrated in the center or the frontier. For the center, I vary α from 1.5 to 2.0 in increments of 0.1. For the frontier, I set $\alpha = 1.5$ because the observed outbreak is already concentrated there. Figure S28 presents these counterfactuals. Panel B shows that shifts toward the center correspond to scenarios in which Ebola occurs not only in the northeast but also in the northwest and southwest.

For the within-epidemic analyses (Figure S29), I examine outbreak intensification without location shifts, from 1 daily case to 7 daily cases. The spatial distribution remains unchanged, but pixel values in the frontier increase as the outbreak intensifies.

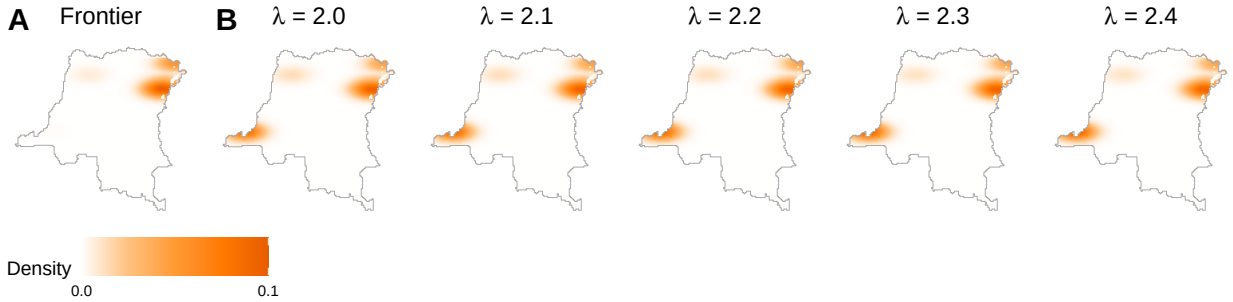

Figure S28: **Counterfactual interventions (Ebola, hospital locations, cross-epidemic)**. Panel A shows the coutnerfactual densities that move Ebola patients toward the frontier with varying degrees of α parameters. Panel B shows the counterfactual densities that move Ebola patients toward the center. Pixel values are raised to the power of 0.2 for visualization purposes.

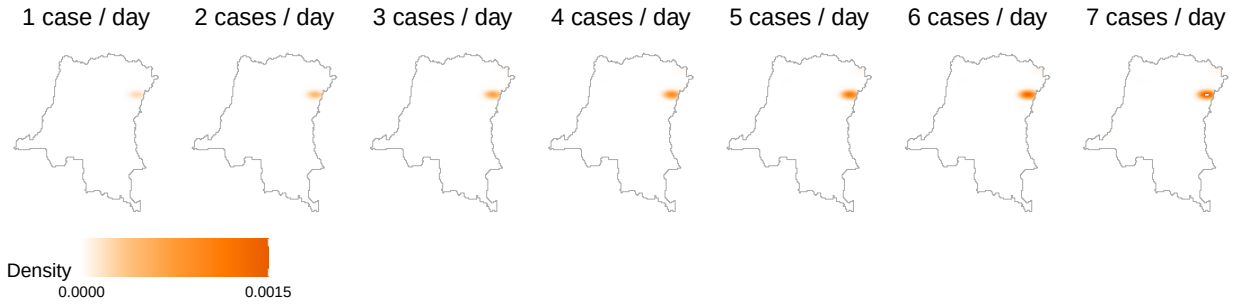

Figure S29: **Counterfactual interventions (Ebola, hospital locations, within-epidemic)**. For the within-epidemic analyses, I maintain the spatial distribution of patients and increase the daily number of patients.

F.6 Causal Mediation Analysis

Following Kennedy (2019) and Mukaigawara et al. (2025), I model the conditional mediator distribution and vary an incremental parameter $\delta \in (0, \infty)$ to construct counterfactual mediator densities. Because the proportion of patients with severe symptoms depends on healthcare access and infection risk, I include distances to cities and hospitals, log population density, elevation, slope, terrain ruggedness, and geographic coordinates as covariates.

Table S17 summarizes the parametric and smooth components of the binary GAM. The three distance covariates use exponential-decay transformations. Distance to major cities captures large urban centers, while distance to cities captures towns of all sizes. The Gaussian-process spline on (lon, lat) absorbs residual spatial structure. The model AUC is 0.657.

Table S17: **Coefficients.** Left and right panels show parametric and smooth-term coefficients, respectively.

Term	Estimate	Std. Error
(Intercept)	-1.11	0.06

Smooth terms	edf	Ref.df	Chi.sq	Pr(>F)
Distance to major cities	1.00	1.00	4.87	0.03
Distance to cities	1.00	1.00	4.22	0.04
Distance to hospitals	1.00	1.00	10.55	0.00
Population density (log transformed)	1.12	1.22	4.22	0.04
Elevation	1.00	1.00	5.95	0.01
Slope	1.00	1.00	20.59	0.00
Terrain ruggedness index	0.00	0.00	0.00	1.00
s(lon,lat)	6.38	8.24	86.98	0.00

Figure S30 plots the conditional mediator distribution given covariates and treatment, separately for patients with bleeding (orange) and without bleeding (gray), at baseline and under shifts of $\delta = 2, 4, 6$. Higher values of δ shift the bleeding density rightward and the non-bleeding density leftward, which indicates a higher proportion of patients with bleeding.

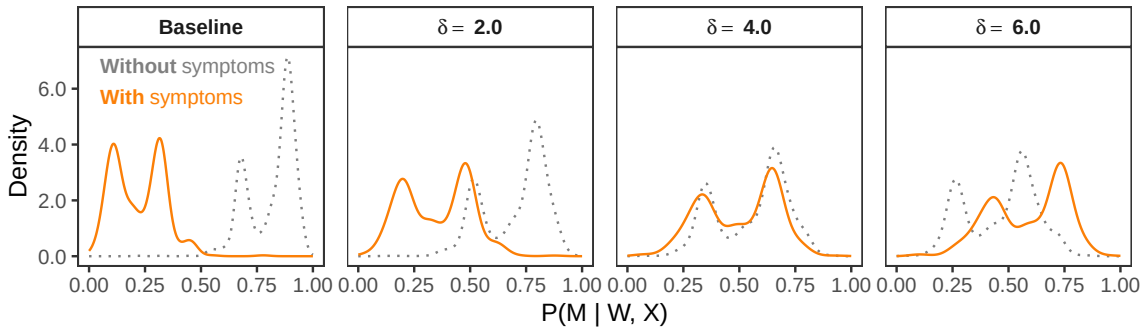

Figure S30: **Mediator densities.** As the δ parameter increases, the proportion of patients with bleeding increases, as shown by the orange lines shifting to the right.

G Full Results

G.1 Cross-Epidemic Comparison

Because the outbreak-level data collects onset location of confirmed cases, the main analysis is conducted with the onset location data of confirmed Ebola patients. Interaction effects (Table S18) suggest fewer battles in regions with higher α and more violence against civilians at the outbreak epicenter. Incomplete statistical significance likely reflects heterogeneity. For non-Ebola cases (Table S19), except for sporadic significant results, all results are insignificant.

Table S18: **Full results (interaction effects, onset locations)**. The value α defines counterfactual specifications. The columns with region names report interaction effects with 95% CIs. VAC: violence against civilians.

Outcome	α	DRC/UGA/RWA	Northeast	Ituri	North Kivu	South Kivu
Battles	1.50	1.475 [0.184, 2.766]	1.364 [0.364, 2.364]	0.229 [-0.001, 0.459]	0.756 [0.212, 1.3]	0.379 [-0.012, 0.769]
	1.60	1.444 [0.279, 2.61]	1.342 [0.437, 2.246]	0.228 [0.011, 0.444]	0.756 [0.239, 1.272]	0.358 [-0.008, 0.724]
	1.70	1.406 [0.231, 2.581]	1.312 [0.386, 2.238]	0.226 [0.01, 0.443]	0.753 [0.204, 1.301]	0.333 [-0.036, 0.702]
	1.80	1.359 [0.044, 2.674]	1.275 [0.218, 2.331]	0.224 [-0.006, 0.454]	0.747 [0.117, 1.376]	0.303 [-0.097, 0.704]
	1.90	1.321 [-0.236, 2.879]	1.25 [-0.017, 2.517]	0.224 [-0.034, 0.483]	0.748 [0.001, 1.494]	0.278 [-0.177, 0.733]
VAC (lethal)	1.50	1.152 [0.249, 2.054]	0.893 [0.198, 1.587]	0.13 [-0.044, 0.304]	0.5 [0.109, 0.891]	0.263 [0.061, 0.464]
	1.60	1.142 [0.344, 1.94]	0.888 [0.281, 1.494]	0.126 [-0.032, 0.284]	0.5 [0.167, 0.833]	0.261 [0.064, 0.458]
	1.70	1.125 [0.345, 1.904]	0.878 [0.28, 1.476]	0.121 [-0.032, 0.274]	0.498 [0.173, 0.823]	0.259 [0.055, 0.463]
	1.80	1.1 [0.249, 1.951]	0.864 [0.194, 1.535]	0.114 [-0.046, 0.275]	0.493 [0.125, 0.862]	0.257 [0.034, 0.479]
	1.90	1.099 [0.105, 2.092]	0.87 [0.068, 1.672]	0.109 [-0.072, 0.289]	0.498 [0.049, 0.947]	0.263 [0.014, 0.511]
VAC (non-lethal)	1.50	1.283 [0.264, 2.302]	0.893 [0.139, 1.647]	0.173 [0.058, 0.288]	0.446 [-0.051, 0.944]	0.274 [0.043, 0.505]
	1.60	1.249 [0.295, 2.202]	0.863 [0.161, 1.566]	0.172 [0.06, 0.284]	0.428 [-0.034, 0.89]	0.263 [0.036, 0.491]
	1.70	1.209 [0.264, 2.155]	0.83 [0.131, 1.528]	0.17 [0.058, 0.282]	0.408 [-0.048, 0.864]	0.252 [0.018, 0.486]
	1.80	1.165 [0.168, 2.163]	0.793 [0.05, 1.535]	0.167 [0.051, 0.283]	0.386 [-0.095, 0.867]	0.24 [-0.009, 0.488]
	1.90	1.138 [0.039, 2.237]	0.78 [-0.047, 1.607]	0.167 [0.043, 0.29]	0.375 [-0.157, 0.906]	0.239 [-0.033, 0.51]

Table S19: **Full results (interaction effects, non-Ebola cases)**. Full results for non-Ebola cases are shown.

Outcome	α	DRC/UGA/RWA	Northeast	Ituri	North Kivu	South Kivu
Battles	1.50	1.1 [-290.02, 292.22]	0.94 [-221.87, 223.74]	0.24 [-44.24, 44.72]	0.36 [-112.88, 113.61]	0.33 [-64.75, 65.42]
	1.60	1.05 [-340.18, 342.27]	0.9 [-260.25, 262.04]	0.24 [-51.95, 52.44]	0.32 [-132.29, 132.94]	0.33 [-76, 76.67]
	1.70	0.99 [-382.55, 384.53]	0.85 [-292.67, 294.37]	0.24 [-58.47, 58.95]	0.28 [-148.7, 149.26]	0.33 [-85.51, 86.16]
	1.80	0.93 [-414.34, 416.19]	0.8 [-316.99, 318.6]	0.25 [-63.36, 63.85]	0.23 [-160.99, 161.45]	0.32 [-92.65, 93.29]
	1.90	0.88 [-438.08, 439.83]	0.77 [-335.15, 336.69]	0.25 [-67.03, 67.53]	0.19 [-170.14, 170.52]	0.33 [-97.98, 98.64]
VAC (lethal)	1.50	1.08 [-224.93, 227.09]	0.77 [-166.75, 168.3]	0.13 [-44.88, 45.14]	0.44 [-90.39, 91.27]	0.2 [-31.49, 31.88]
	1.60	1.06 [-263.92, 266.04]	0.75 [-195.64, 197.15]	0.12 [-52.58, 52.81]	0.44 [-106.05, 106.92]	0.2 [-37.01, 37.41]
	1.70	1.04 [-296.86, 298.93]	0.73 [-220.04, 221.5]	0.1 [-59.09, 59.28]	0.42 [-119.29, 120.13]	0.21 [-41.67, 42.08]
	1.80	1 [-321.58, 323.59]	0.7 [-238.35, 239.76]	0.08 [-63.95, 64.11]	0.41 [-129.22, 130.04]	0.21 [-45.18, 45.6]
	1.90	1 [-340.04, 342.04]	0.69 [-252.02, 253.41]	0.06 [-67.58, 67.7]	0.41 [-136.64, 137.45]	0.23 [-47.81, 48.26]
VAC (non-lethal)	1.50	1.3 [-206.91, 209.51]	0.92 [-147.67, 149.52]	0.19 [-19.56, 19.94]	0.5 [-80.5, 81.5]	0.23 [-47.62, 48.08]
	1.60	1.26 [-242.72, 245.24]	0.9 [-173.24, 175.03]	0.19 [-22.97, 23.35]	0.49 [-94.45, 95.43]	0.21 [-55.82, 56.25]
	1.70	1.21 [-272.98, 275.41]	0.87 [-194.84, 196.57]	0.19 [-25.85, 26.23]	0.48 [-106.24, 107.2]	0.2 [-62.75, 63.14]
	1.80	1.16 [-295.68, 297.99]	0.83 [-211.04, 212.7]	0.19 [-28.02, 28.4]	0.46 [-115.08, 116.01]	0.18 [-67.94, 68.3]
	1.90	1.12 [-312.6, 314.85]	0.82 [-223.12, 224.76]	0.19 [-29.64, 30.02]	0.46 [-121.68, 122.6]	0.17 [-71.8, 72.14]

G.2 Within-Epidemic Comparison

Table S20: **Full results (within-epidemic comparison)**. Full results with hospital locations (all cases) are summarized.

Outcome	Daily cases	Northeast	Ituri	North Kivu	South Kivu
All	2	1.880 [0.446, 3.314]	0.059 [-0.205, 0.324]	1.185 [0.236, 2.135]	0.635 [0.145, 1.125]
	3	3.354 [1.360, 5.347]	0.042 [-0.292, 0.375]	2.229 [0.859, 3.598]	1.083 [0.384, 1.783]
	4	4.504 [2.078, 6.929]	-0.051 [-0.459, 0.358]	2.969 [1.389, 4.549]	1.585 [0.624, 2.547]
	5	5.326 [2.759, 7.892]	-0.082 [-0.545, 0.381]	3.577 [1.904, 5.249]	1.831 [0.834, 2.828]
	6	6.274 [3.219, 9.329]	-0.120 [-0.633, 0.393]	4.203 [2.295, 6.111]	2.191 [1.014, 3.367]
	7	6.669 [3.503, 9.834]	-0.173 [-0.703, 0.357]	4.481 [2.497, 6.465]	2.361 [1.155, 3.566]
Battles	2	0.212 [-0.667, 1.090]	-0.109 [-0.305, 0.088]	0.427 [-0.256, 1.110]	-0.107 [-0.398, 0.183]
	3	0.687 [-0.466, 1.840]	-0.171 [-0.440, 0.098]	0.866 [-0.013, 1.745]	-0.007 [-0.489, 0.474]
	4	0.995 [-0.469, 2.458]	-0.293 [-0.634, 0.048]	1.231 [0.233, 2.228]	0.057 [-0.580, 0.694]
	5	1.239 [-0.261, 2.738]	-0.366 [-0.744, 0.012]	1.466 [0.461, 2.470]	0.139 [-0.525, 0.803]
	6	1.547 [-0.096, 3.190]	-0.422 [-0.816, -0.028]	1.645 [0.623, 2.667]	0.324 [-0.484, 1.131]
	7	1.744 [0.019, 3.469]	-0.452 [-0.854, -0.051]	1.747 [0.705, 2.789]	0.449 [-0.414, 1.312]
VAC (lethal)	2	0.372 [-0.075, 0.819]	0.108 [-0.036, 0.253]	0.112 [-0.147, 0.370]	0.153 [-0.033, 0.339]
	3	0.623 [0.017, 1.229]	0.184 [0.003, 0.366]	0.198 [-0.175, 0.570]	0.241 [-0.022, 0.504]
	4	0.802 [0.070, 1.535]	0.208 [-0.018, 0.435]	0.265 [-0.203, 0.734]	0.329 [-0.013, 0.671]
	5	1.008 [0.220, 1.796]	0.238 [0.004, 0.473]	0.369 [-0.137, 0.875]	0.401 [0.038, 0.764]
	6	1.409 [0.307, 2.511]	0.285 [0.016, 0.554]	0.537 [-0.142, 1.215]	0.588 [0.165, 1.011]
	7	1.478 [0.340, 2.615]	0.271 [0.006, 0.536]	0.559 [-0.154, 1.272]	0.648 [0.217, 1.078]
VAC (non-lethal)	2	1.295 [0.683, 1.906]	0.034 [-0.078, 0.145]	0.678 [0.325, 1.032]	0.583 [0.297, 0.869]
	3	2.043 [1.160, 2.926]	0.002 [-0.143, 0.146]	1.166 [0.535, 1.796]	0.876 [0.514, 1.237]
	4	2.674 [1.569, 3.779]	-0.012 [-0.193, 0.169]	1.446 [0.731, 2.160]	1.241 [0.721, 1.761]
	5	3.035 [1.854, 4.217]	-0.014 [-0.205, 0.177]	1.694 [0.917, 2.472]	1.355 [0.805, 1.905]
	6	3.272 [2.080, 4.464]	-0.039 [-0.249, 0.171]	1.973 [1.164, 2.782]	1.338 [0.793, 1.882]
	7	3.412 [2.206, 4.618]	-0.043 [-0.259, 0.174]	2.126 [1.287, 2.964]	1.329 [0.785, 1.873]

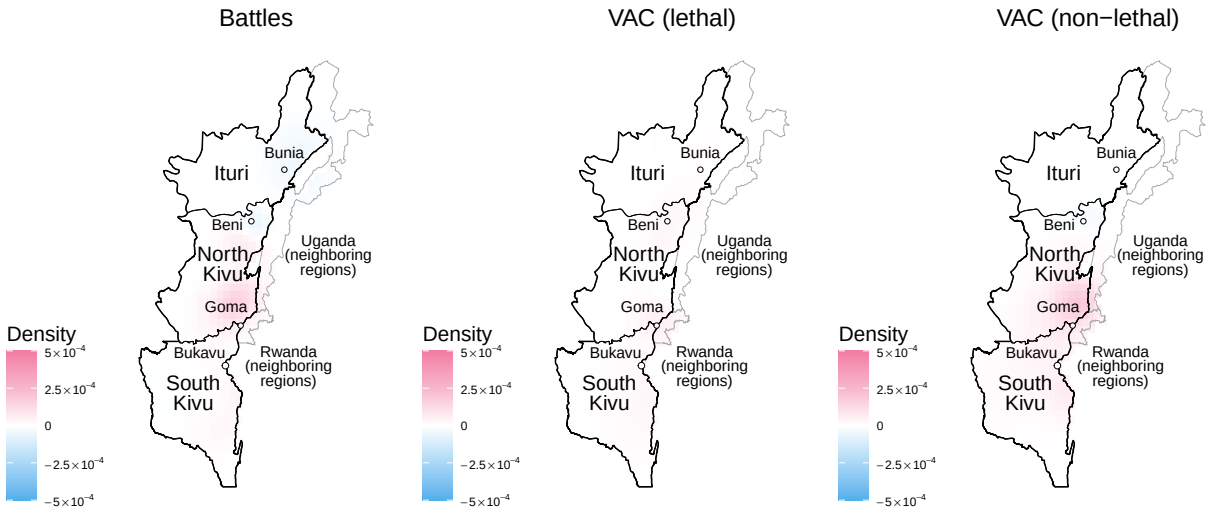

Figure S31: **Outcome surfaces (all cases, cases = 7 vs. 1 per day)**. Blue and red areas show areas with decreased and increased violence.

In the within-epidemic analysis, I use the hospital location data of all cases, which reflect a more complete and accurate picture of the effects of frontier plagues. The effects on lethal violence against civilians exhibit greater heterogeneity than the effects on non-lethal violence against civilians (Ta-

ble S20). However, the outcome surface in Figure S31 reveals that lethal violence against civilians increases in and around major North Kivu cities, consistent with the tactical substitution hypothesis.

Table S21: **Full results (distance decay from insurgent bases)**. Cumulative effects of Ebola intensification on non-lethal violence against civilians. The treatment contrast compares 1 versus 6 daily Ebola cases.

Distance (km)	Point estimate	95% CI	% of total	95% CI (%)
5	0.000	[0.000, 0.000]	0.0	[0.0, 0.0]
10	0.046	[0.028, 0.064]	2.1	[1.3, 2.9]
15	0.085	[0.053, 0.118]	3.9	[2.4, 5.4]
20	0.159	[0.100, 0.217]	7.3	[4.6, 10.0]
25	0.293	[0.180, 0.405]	13.5	[8.3, 18.7]
30	0.413	[0.254, 0.572]	19.1	[11.7, 26.4]
35	0.530	[0.333, 0.727]	24.5	[15.4, 33.6]
40	0.678	[0.420, 0.935]	31.3	[19.4, 43.2]
45	0.851	[0.526, 1.177]	39.3	[24.3, 54.4]
50	0.924	[0.575, 1.273]	42.7	[26.6, 58.8]
55	1.137	[0.707, 1.567]	52.5	[32.6, 72.3]
60	1.319	[0.817, 1.821]	60.9	[37.7, 84.1]
65	1.407	[0.876, 1.938]	65.0	[40.4, 89.5]
70	1.566	[0.979, 2.154]	72.3	[45.2, 99.5]
75	1.689	[1.052, 2.325]	78.0	[48.6, 107.3]
80	1.812	[1.129, 2.494]	83.6	[52.1, 115.1]
85	1.916	[1.195, 2.636]	88.4	[55.2, 121.7]
90	2.023	[1.266, 2.780]	93.4	[58.4, 128.3]
95	2.129	[1.333, 2.926]	98.3	[61.5, 135.1]
100	2.166	[1.359, 2.973]	100.0	[62.7, 137.3]

Table S22: **Full results (heterogeneity by ETC proximity)**. CATE of Ebola intensification on battles as a function of proximity to ETCs.

Daily cases	0.10	0.34	0.52	0.71	0.90
2.00	0.0033 [-0.0003, 0.0068]	0.0018 [-0.0040, 0.0077]	-0.0068 [-0.0150, 0.0014]	-0.0201 [-0.0370, -0.0032]	-0.0361 [-0.0652, -0.0069]
4.00	0.0085 [0.0034, 0.0136]	0.0061 [-0.0027, 0.0148]	-0.0141 [-0.0281, -0.0002]	-0.0457 [-0.0741, -0.0174]	-0.0840 [-0.1318, -0.0363]
6.00	0.0111 [0.0058, 0.0164]	0.0081 [-0.0006, 0.0168]	-0.0182 [-0.0338, -0.0026]	-0.0592 [-0.0918, -0.0267]	-0.1091 [-0.1638, -0.0544]

Table S23: **Full results (heterogeneity by poverty)**. CATE of Ebola intensification on battles as a function of poverty.

Daily cases	0.1	0.3	0.5	0.7	0.9
2.00	-0.0001 [-0.0004, 0.0003]	0.0000 [-0.0005, 0.0005]	-0.0000 [-0.0003, 0.0002]	0.0001 [-0.0000, 0.0003]	0.0000 [-0.0000, 0.0001]
4.00	-0.0005 [-0.0010, 0.0001]	0.0003 [-0.0007, 0.0013]	0.0003 [-0.0001, 0.0007]	0.0001 [-0.0001, 0.0004]	0.0001 [0.0000, 0.0002]
6.00	-0.0006 [-0.0012, 0.0001]	0.0007 [-0.0004, 0.0019]	0.0005 [0.0001, 0.0009]	0.0001 [-0.0001, 0.0004]	0.0001 [0.0000, 0.0002]

Table S24: **Full results (heterogeneity by infant mortality)**. CATE of Ebola intensification on battles as a function of infant mortality rate (IMR).

Daily cases	0.010	0.058	0.105	0.153	0.200
2.00	0.0003 [0.0000, 0.0005]	-0.0001 [-0.0003, 0.0001]	-0.0001 [-0.0003, 0.0002]	0.0002 [-0.0001, 0.0004]	0.0005 [-0.0006, 0.0017]
4.00	0.0006 [0.0003, 0.0010]	-0.0001 [-0.0005, 0.0002]	-0.0002 [-0.0007, 0.0003]	0.0002 [-0.0003, 0.0008]	0.0008 [-0.0016, 0.0033]
6.00	0.0007 [0.0003, 0.0011]	-0.0001 [-0.0005, 0.0003]	-0.0002 [-0.0007, 0.0004]	0.0000 [-0.0006, 0.0006]	0.0003 [-0.0025, 0.0032]

G.3 Alternative Mechanisms

Effects on direct tactics. I classify each event of violence against civilians as either a direct (contact) tactic, an indirect (ranged) tactic, or indeterminate, using a combination of ACLED's sub-event categories and keyword matching on the event's text description. Abductions and sexual violence are coded as contact by definition, since both require physical contact with the victim. For events labeled as attacks, I apply three keyword sets to the description.

- Contact weapon: `machete-d/-s`, `hack-ed/-ing`, `stab-bed/-bing`, `kni-fe/-ves`, `sword`, `panga-/-s`, `slashed`, `behead-ed/-ing`, `decapitat-ed/-ion`, `throats slit`, `butchered`, `slaughtered`, `mutilated`, `tortured`, `strangled`, `drowned`, `burned alive`, `set ablaze`, `set (on) fire`, `torched`, `arson`, `beat-en/-ing`, `clubbed`, and `bludgeoned`
- Ranged weapon: `shot`, `shoot-s/-ing`, `fir-ed/-ing`, `gunfire`, `gun-man/-men`, `gunpoint`, `gunshot`, `bullet-/-s`, `sprayed`, `opened fire`, `drive-by`, `grenade-/-s`, `mortar-/-s`, `bomb-/-ing`, `explos-ive/-ives/-ion`, `rpg`, `landmine`, `sniper`, and `blast`
- Incursion: `raid-/-ed/-ing`, `storm-ed/-ing`, `kidnap-/-ped/-ping`, `abduct-ed/-ion/-ing`, `entered the village/house/home`, `house-to-house`, `brok-e/-en into`, `invaded`, and `incursion`

I apply these keyword sets in priority order. Events are coded as contact if they contain a contact-weapon or incursion keyword, as ranged if they contain a ranged-weapon keyword, and as indeterminate otherwise. Table S25 summarizes the effects of intensifying frontier plagues on the three outcomes. The results provide no evidence of reduced contact or increased use of ranged tactics.

Table S25: **Effects of intensifying frontier plagues on contact, ranged, or intermediate violence against civilians**. I set treatment duration to one day; the pattern remains consistent at longer durations.

Outcome	Daily Ebola cases	Northeast	Ituri	North Kivu	South Kivu
Contact	2	1.375 [0.735, 2.014]	0.096 [-0.040, 0.232]	0.726 [0.356, 1.095]	0.553 [0.273, 0.833]
	3	2.240 [1.338, 3.142]	0.117 [-0.068, 0.302]	1.332 [0.684, 1.980]	0.791 [0.452, 1.131]
	4	2.842 [1.813, 3.871]	0.128 [-0.095, 0.351]	1.690 [0.962, 2.418]	1.024 [0.616, 1.432]
	5	3.120 [2.050, 4.191]	0.127 [-0.104, 0.359]	1.924 [1.137, 2.711]	1.069 [0.661, 1.476]
	6	3.225 [2.134, 4.315]	0.109 [-0.130, 0.347]	2.139 [1.316, 2.962]	0.978 [0.560, 1.395]
	7	3.281 [2.184, 4.377]	0.087 [-0.151, 0.324]	2.246 [1.402, 3.091]	0.948 [0.530, 1.365]
Ranged	2	-0.178 [-0.402, 0.045]	-0.020 [-0.065, 0.025]	-0.097 [-0.221, 0.028]	-0.062 [-0.185, 0.061]
	3	-0.206 [-0.535, 0.124]	-0.031 [-0.087, 0.025]	-0.122 [-0.319, 0.076]	-0.053 [-0.217, 0.112]
	4	-0.197 [-0.594, 0.199]	-0.035 [-0.100, 0.031]	-0.143 [-0.388, 0.102]	-0.020 [-0.211, 0.171]
	5	-0.091 [-0.520, 0.339]	-0.030 [-0.098, 0.038]	-0.093 [-0.355, 0.170]	0.032 [-0.178, 0.241]
	6	0.257 [-0.386, 0.900]	-0.028 [-0.102, 0.047]	0.047 [-0.286, 0.379]	0.238 [-0.102, 0.578]
	7	0.376 [-0.302, 1.055]	-0.029 [-0.106, 0.048]	0.103 [-0.248, 0.454]	0.303 [-0.055, 0.660]
Intermediate	2	0.448 [0.146, 0.750]	0.064 [-0.020, 0.148]	0.181 [0.047, 0.316]	0.203 [0.054, 0.352]
	3	0.587 [0.155, 1.020]	0.088 [-0.037, 0.213]	0.196 [-0.021, 0.413]	0.304 [0.111, 0.496]
	4	0.746 [0.135, 1.357]	0.103 [-0.073, 0.280]	0.228 [-0.069, 0.525]	0.415 [0.149, 0.680]
	5	0.928 [0.257, 1.599]	0.139 [-0.053, 0.332]	0.290 [-0.031, 0.612]	0.499 [0.209, 0.788]
	6	1.128 [0.370, 1.886]	0.187 [-0.044, 0.419]	0.356 [-0.034, 0.746]	0.584 [0.291, 0.877]
	7	1.172 [0.396, 1.947]	0.196 [-0.041, 0.433]	0.363 [-0.055, 0.781]	0.612 [0.318, 0.906]

Effects of reducing the number of Ebola patients. I compare the effects of reducing Ebola cases from the median number (34 per day) to 25, 15, and 5 daily cases. As expected from the main analysis, I observe the opposite pattern of intensifying Ebola cases (see Figure S32). The pattern is consistent across a range of the intervention durations (1–7 days).

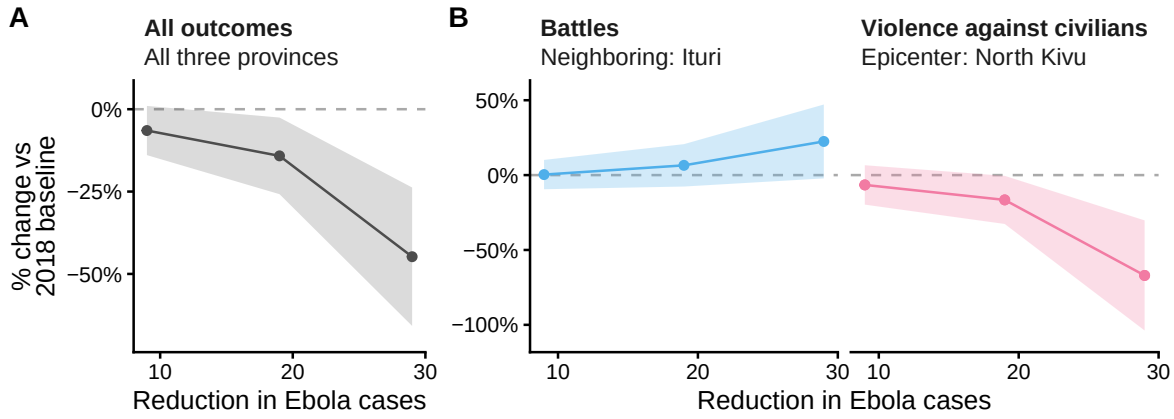

Figure S32: **Reducing the number of Ebola cases does not intensify civil conflict.** The treatment contrast compares 34 daily Ebola cases with counterfactual levels of 25, 15, and 5 cases (duration = one day), corresponding to reductions of 9, 19, and 29 cases.

Mediating effects of clinical symptoms. The indirect effects of increasing the proportion of patients with bleeding (while keeping the number of Ebola patients) are not statistically significant across all regions (Figure S33).

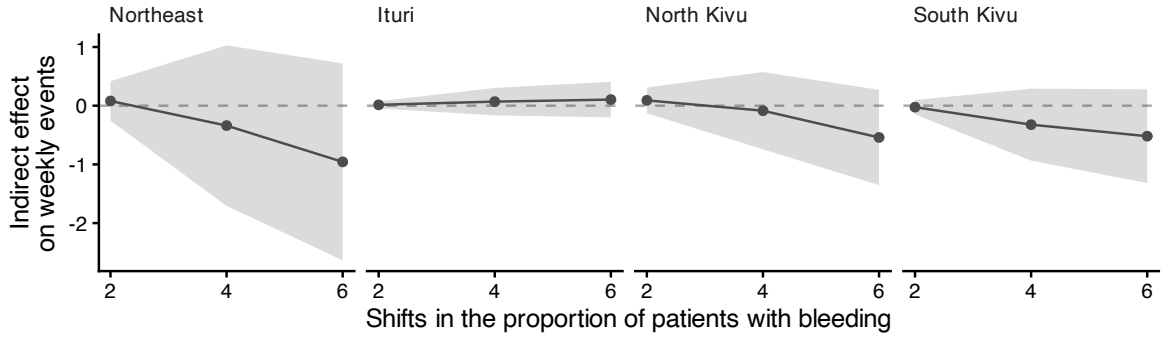

Figure S33: **Effects of increasing the proportion of patients with hemorrhage.** Indirect effects are shown while the number of Ebola patients is held fixed at 6. The x-axis represents the δ parameter, with higher values indicating larger proportions of patients with bleeding.

H Threats to Inference

H.1 Spatial Support Stationarity

A potential concern for the overlap assumption, especially for Ebola given its high case fatality rate, is that the disease permanently removes locations from the spatial support. If individuals at a location die or flee and no new cases arise there, the set of patient-generating locations could shrink over time and reduce overlap between the observed and counterfactual treatment distributions.

I employ a nearest-neighbor diagnostic to examine the validity of spatial support stationarity. For each week in the study period, I compute the distance from every new patient to the nearest patient from all prior weeks and report the share within 1 km, a conservative threshold that approximates the spatial precision of the village-level geocoding (Section C.1). The comparison to all prior weeks rather than only adjacent weeks provides the strongest test because, if any previously affected location still generates patients, the nearest-neighbor distance remains small regardless of week-to-week fluctuations. I conduct this test for all three geocoded location types: symptom onset, patient residence, and hospital (Section C.1).

Figure S34 shows that all three series rise monotonically toward 100%, with median weekly shares of 98.9% (hospital), 99.4% (onset), and 99.6% (residence). At no point do new patients systematically appear farther from previously affected locations.

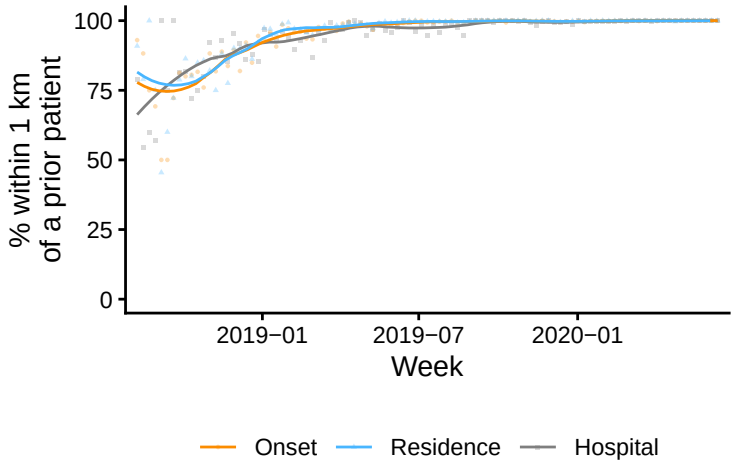

Figure S34: **Spatial support stationarity.** Each point shows the weekly share of new patients within 1 km of a prior patient. Curves are LOESS fits. All three location types converge to 100%, with no downward trend. Thus, the spatial support does not shrink over the course of the epidemic.

H.2 Placebo Outcome Tests

I conduct a placebo test using an outcome that shares the same spatial confounding structure as political violence but has no plausible causal link to Ebola intensification. I replace the violence outcome with the onset of satellite-detected fires from NASA's Visible Infrared Imaging Radiometer Suite (VIIRS) on the Suomi NPP satellite (Schroeder et al., 2014). VIIRS detects active fires at 375-meter resolution with daily global coverage.

Fire onsets serve as a suitable placebo outcome for two reasons. First, fires in the DRC, which are predominantly agricultural slash-and-burn fires, share spatial confounders with political violence. Both cluster in rural, remote, and underserved areas with low state presence. Although slash-and-burn fires are more prevalent in the central and southern savannas than in the forested northeast where Ebola concentrated, fires do occur throughout the study region and their spatial distribution shares the same confounders that could bias the main results. Second, there is no plausible mechanism through which an intensified Ebola outbreak would cause new fires to ignite. Thus, if the main results reflect a genuine causal effect of Ebola intensification on violence rather than a spurious correlation driven by shared spatial confounders, the placebo test should yield null effects for fire onsets across all treatment contrasts, lag structures, and geographic windows.

I obtain VIIRS data from the NASA Fire Information for Resource Management System (FIRMS) (see `firms.modaps.eosdis.nasa.gov`) for the DRC, Uganda, and Rwanda over the study period (August 2, 2018 to June 23, 2020) and retain only high-confidence detections to minimize false positives from sun glint, hot surfaces, or industrial heat sources. Because VIIRS could capture the same fire on consecutive satellite passes, I identify new fire onsets by clustering detections within 1-kilometer grid cells and treating a detection as a new onset only if no fire was detected in the same cell during the preceding seven days. I then construct a hyperframe of weekly fire onset point patterns, smooth the outcomes, and estimate the ATE of Ebola intensification on fire onsets.

Table S26 summarizes the placebo test results. Across all regions and specifications, the effects remain null.

Table S26: **Placebo test results.** The effects of Ebola intensification on satellite-detected fires are summarized. The Ebola column indicates the number of daily cases.

Lag	Ebola	Northeast	Ituri	North Kivu	South Kivu
1	2	0.575 [-1.257, 2.408]	-1.46 [-2.34, -0.579]	-0.191 [-0.328, -0.055]	2.226 [0.434, 4.018]
	3	0.947 [-2.429, 4.322]	-2.398 [-4.009, -0.787]	-0.312 [-0.558, -0.066]	3.657 [0.489, 6.824]
	4	1.521 [-3.654, 6.696]	-2.903 [-5.223, -0.583]	-0.411 [-0.761, -0.061]	4.835 [-0.082, 9.753]
	5	2.317 [-4.411, 9.046]	-3.137 [-5.877, -0.397]	-0.45 [-0.868, -0.031]	5.905 [-0.584, 12.393]
	6	2.738 [-4.823, 10.299]	-3.298 [-6.318, -0.278]	-0.48 [-0.946, -0.015]	6.516 [-0.807, 13.839]
	7	3.111 [-5.036, 11.259]	-3.394 [-6.555, -0.234]	-0.493 [-0.986, -0.001]	6.999 [-0.922, 14.92]
2	2	-0.612 [-3.877, 2.652]	-1.277 [-3.196, 0.642]	-0.092 [-0.415, 0.231]	0.757 [-1.279, 2.792]
	3	0.739 [-8.205, 9.684]	-1.817 [-5.493, 1.859]	-0.052 [-0.87, 0.767]	2.608 [-3.292, 8.508]
	4	2.077 [-9.106, 13.261]	-1.555 [-6.003, 2.893]	0.025 [-0.964, 1.015]	3.607 [-3.798, 11.011]
	5	3.264 [-6.922, 13.45]	-1.046 [-5.524, 3.433]	0.128 [-0.758, 1.014]	4.182 [-2.863, 11.226]
	6	3.041 [-4.455, 10.536]	-1.904 [-6.131, 2.323]	0.134 [-0.517, 0.784]	4.811 [-1.003, 10.625]
	7	3.14 [-4.504, 10.784]	-2.298 [-6.956, 2.36]	0.157 [-0.514, 0.827]	5.282 [-0.435, 10.998]
3	2	-0.143 [-40.134, 39.847]	-1.348 [-13.847, 11.151]	-0.068 [-3.334, 3.198]	1.273 [-23.186, 25.731]
	3	0.867 [-110.379, 112.112]	-1.285 [-35.732, 33.161]	-0.001 [-9.027, 9.024]	2.153 [-65.773, 70.08]
	4	0.697 [-112.628, 114.022]	-2.319 [-31.071, 26.433]	0.007 [-9.326, 9.34]	3.009 [-72.532, 78.55]
	5	0.862 [-94.06, 95.784]	-2.551 [-24.947, 19.844]	-0.006 [-7.666, 7.654]	3.42 [-61.896, 68.736]
	6	1.384 [-36.215, 38.984]	-2.626 [-11.247, 5.994]	0.025 [-2.931, 2.981]	3.985 [-23.457, 31.428]
	7	2.545 [-21.555, 26.645]	-2.672 [-9.132, 3.788]	0.098 [-1.745, 1.941]	5.119 [-13.284, 23.522]
4	2	0.881 [-119.014, 120.776]	-0.722 [-27.686, 26.243]	-0.02 [-10.107, 10.067]	1.623 [-81.27, 84.516]
	3	3.427 [-292.925, 299.779]	-0.046 [-68.789, 68.697]	0.179 [-24.563, 24.921]	3.294 [-199.65, 206.238]
	4	4.069 [-330.329, 338.468]	-0.582 [-66.175, 65.01]	0.238 [-27.776, 28.252]	4.414 [-236.487, 245.314]
	5	4.045 [-166.202, 174.291]	-0.468 [-34.596, 33.66]	0.25 [-14.091, 14.592]	4.262 [-117.731, 126.256]
	6	5.162 [-94.376, 104.7]	-0.056 [-20.811, 20.698]	0.317 [-7.883, 8.516]	4.902 [-66.079, 75.883]
	7	6.048 [-44.136, 56.233]	0.513 [-11.022, 12.049]	0.375 [-3.669, 4.42]	5.16 [-30.285, 40.605]
5	2	0.568 [-403.187, 404.323]	-0.909 [-56.973, 55.155]	0.01 [-33.862, 33.882]	1.467 [-312.411, 315.345]
	3	3.205 [-1895.705, 1902.115]	-0.791 [-242.36, 240.777]	0.131 [-149.152, 149.415]	3.865 [-1504.214, 1511.944]
	4	4.781 [-1459.014, 1468.576]	0.559 [-268.37, 269.488]	0.257 [-114.909, 115.423]	3.965 [-1075.763, 1083.693]
	5	7.647 [-2135.843, 2151.136]	1.137 [-397.707, 399.982]	0.413 [-161.828, 162.654]	6.096 [-1576.33, 1588.522]
	6	8.84 [-905.592, 923.271]	2.081 [-194.779, 198.941]	0.485 [-67.975, 68.946]	6.273 [-642.896, 655.442]
	7	7.086 [-87.977, 102.148]	1.949 [-19.413, 23.311]	0.442 [-6.947, 7.831]	4.695 [-62.125, 71.514]
6	2	-0.253 [-396.521, 396.015]	-0.259 [-26.302, 25.784]	-0.111 [-33.648, 33.426]	0.117 [-336.584, 336.818]
	3	4.56 [-7498.913, 7508.032]	0.693 [-751.209, 752.596]	0.155 [-578.517, 578.826]	3.711 [-6169.189, 6176.612]
	4	6.55 [-5495.272, 5508.371]	0.847 [-538.23, 539.924]	0.266 [-412.677, 413.209]	5.437 [-4544.367, 4555.24]
	5	7.354 [-2120.131, 2134.84]	1.679 [-281.486, 284.844]	0.277 [-154.475, 155.029]	5.398 [-1684.18, 1694.975]
	6	3.952 [-186.779, 194.683]	2.907 [-40.616, 46.43]	0.143 [-14.858, 15.144]	0.902 [-131.433, 133.237]
	7	2.706 [-39.865, 45.276]	4.415 [-10.492, 19.321]	0.115 [-3.369, 3.6]	-1.824 [-27.014, 23.366]
7	2	-0.47 [-1173.101, 1172.162]	-0.292 [-44.689, 44.105]	-0.151 [-96.044, 95.742]	-0.027 [-1032.369, 1032.316]
	3	0.291 [-4146.324, 4146.907]	0.248 [-295.307, 295.803]	-0.118 [-331.485, 331.25]	0.161 [-3519.533, 3519.855]
	4	3.923 [-5119.194, 5127.039]	0.636 [-399.297, 400.569]	0.087 [-386.397, 386.572]	3.199 [-4333.502, 4339.901]
	5	1.1 [-940.392, 942.593]	1.584 [-140.209, 143.377]	-0.104 [-72.31, 72.102]	-0.38 [-727.89, 727.131]
	6	-1.805 [-113.605, 109.996]	2.531 [-26.558, 31.62]	-0.272 [-9.279, 8.736]	-4.064 [-78.034, 69.906]
	7	-1.65 [-26.811, 23.51]	2.777 [-4.486, 10.041]	-0.279 [-2.229, 1.671]	-4.148 [-21.525, 13.228]